TECHNICAL REPORT
NATICK/TR-02/002

AD_____

A CONDUCTING POLYMER-BASED ELECTRONIC NOSE FOR LANDMINE DETECTION

by
Nathan S. Lewis
Rodney M. Goodman
and
Robert H. Grubbs

California Institute of Technology
Pasadena, CA 91125

October 2001

Final Report
April 1997 - September 2000

20011025 054

DISCLAIMERS

DESTRUCTION NOTICE

REPORT DOCUMENTATION PAGE

Form Approved
OMB No. 0704-0188

1. REPORT DATE (DD-MM-YYYY)	2. REPORT TYPE	3. DATES COVERED (From - To)
10-10-2001	Final Report	April 1999 - November 1999

4. TITLE AND SUBTITLE
A CONDUCTING POLYMER-BASED ELECTRONIC NOSE FOR LANDMINE DETECTION

5a. CONTRACT NUMBER
C-DAAK60-97-K-9503

5b. GRANT NUMBER

5c. PROGRAM ELEMENT NUMBER

6. AUTHOR(S)
Nathan S. Lewis, Rodney M. Goodman and Robert H. Grubbs

5d. PROJECT NUMBER

5e. TASK NUMBER

5f. WORK UNIT NUMBER

7. PERFORMING ORGANIZATION NAME(S) AND ADDRESS(ES)
California Institute of Technology
1200 E. California Blvd., M/C 127-72
Pasadena, CA 91125

8. PERFORMING ORGANIZATION REPORT NUMBER

9. SPONSORING/MONITORING AGENCY NAME(S) AND ADDRESS(ES)
Sponsor: Defense Advanced Research Projects Agency (DARPA)
Advanced Technology Office (Regina Dugan)
3701 North Fairfax Drive
Arlington, VA 22203-1714

10. SPONSOR/MONITOR'S ACRONYM(S)

11. SPONSOR/MONITOR'S REPORT NUMBER(S)
NATICK/TR-02/002

12. DISTRIBUTION/AVAILABILITY STATEMENT
Approved for Public Release;
Distribution Unlimited

13. SUPPLEMENTARY NOTES
Monitor: US Army Soldier and Biological Chemical Command, Soldier Systems Center,
ATTN: AMSSB-RSS-D(N) (H. Girolamo), Natick, MA 01760-5020

14. ABSTRACT
This program was part of DARPA's "Dog Nose" initiative to develop landmine detection technology based upon the chemical signature of the mine explosive charge. The focus of this DARPA-sponsored project was to exploit the exciting breakthrough technology developed recently at Caltech that forms the basis for a low power, simple, manufacturable "electronic nose." This nose-on-a-chip involves chemically sensitive resistors, whose signals reveal the identification and concentration of vapors in a fashion analogous to that of the mammalian olfactory system. This technology has been developed into a landmine detection system, based on the characteristic chemical signature of mines, that operates in real-time through a VLSI-compatible Si process.

15. SUBJECT TERMS
ELECTRONIC NOSES, LANDMINES, MINE DETECTION, CHEMICAL SIGNATURES, CHEMICALLY SENSITIVE VAPOR DETECTION, VAPOR SIGNATURES, VAPOR SENSOR, DEMINING, DETECTION TECHNOLOGY, CHEMICAL VAPOR DETECTORS, ODOR RECOGNITION

16. SECURITY CLASSIFICATION OF:

a. REPORT	b. ABSTRACT	c. THIS PAGE
UNCLASSIFIED	UNCLASSIFIED	UNCLASSIFIED

17. LIMITATION OF ABSTRACT
SAR

18. NUMBER OF PAGES
165

19a. NAME OF RESPONSIBLE PERSON
Henry Girolamo, Program Manager

19b. TELEPHONE NUMBER (Include area code)
508-233-5071

Standard Form 298 (Rev. 8/98)
Prescribed by ANSI Std. Z39.18

Contents

Contents (Cont'd)

Contents (Cont'd)

Contents (Cont'd)

Contents (Cont'd)

Contents (Cont'd)

List of Figures

List of Figures (Cont'd)

List of Figures (Cont'd)

List of Figures (Cont'd)

List of Figures (Cont'd)

List of Figures (Cont'd)

List of Tables

PREFACE

This is a report of the main research and development findings of a project performed under the Defense Advanced Research Projects Agency Dog's Nose program under contract number C-DAAK60-97-K-9503 from April 1997 to September 2000. The goal of this program is to develop vapor detection capabilities based on inspiration of the canine olfactory sense, because canines are documented to effectively find land mines with a high search rate and a low false alarm rate. The project involved several team members, including materials chemists, polymer chemists, and electrical engineers at the lead institution, the California Institute of Technology (Caltech), signal processing engineers at the Jet Propulsion Laboratory (JPL), mechanical engineers at Aerovironment, Inc. in Monrovia, CA, system engineers at Cyrano Sciences Inc. in Pasadena, CA and at Draper Laboratories in Cambridge, MA, and polymer chemists at the University of Florida. The goal of this project is to develop, evaluate, and deploy artificial olfactory systems in a field-portable, low power implementation and to use this technology to detect implanted land mines based on their vapor signatures.

A CONDUCTING POLYMER-BASED ELECTRONIC NOSE FOR LANDMINE DETECTION

SUMMARY

The approach pursued in this work to vapor sensing involves construction of an "electronic nose" that does not require development of highly specific recognition chemistries, one for each of the many possible components of a land mine vapor signature (TNT, DNT, plasticizer, and other possible signature compounds that dogs might be clueing on, for example). Instead we have utilized a broadly responsive array of sensors that is trainable to the target signature of interest. The instrumentation then can recognize this signature in the field and deliver it to the sensing electronics in a robust fashion for subsequent processing by target recognition algorithms. The enabling technology for this project involves low power, small vapor sensors that operate at room temperature and atmospheric pressure. The conductive composite chemiresistor technology has several potential advantages over alternative array detection schemes in that a) the sensor films are simple to fabricate (so that large numbers of sensors can be produced in a low cost process), b) are readily made chemically diverse (so that confusion of the target vapors with other background clutter signals can be minimized in at least some channels of the array output and thus sensed as a distinct pattern by the readout electronics), c) are readily miniaturized (enabling large numbers of sensors on chip for improvements in sensitivity, signal averaging, better target discrimination, etc.), and d) yield a very simple, low power readout signal--the film resistance--that is compatible with modern electronic processing.

Combinatorial approaches have been used to prepare libraries of films in order to best evaluate the properties that are needed to discriminate the target odors from those of the background. Analog VLSI circuit designs, modeled after biological sensory functioning, have been utilized to construct electronic circuits that provide adaptation to background changes, low power constraints, adaptive gains in response to local responses on the array, and sophisticated classification and on-chip learning algorithms. All process steps, including that of sensor fabrication, are VLSI-compatible so that the resulting electronic nose device will be low cost and will be manufacturable without constructing special facilities for this application. Detection limits, performance characteristics, and other key features of this technology both in the laboratory and in the field are discussed in this report. Early transition opportunities of this technology could include industrial process control, low cost, compact detectors of chemical warfare production and use, and implanted monitors of the integrity of a soldier's protective masks or clothing.

1. Introduction

The goal of this work is to produce a low power, low cost, lightweight, small volume, sensitive, chemical vapor detection device for use in detecting emplaced land mines. All of these design constraints must be met if a fieldable system is to be developed that can address the problem of locating most of the over 100 million emplaced land mines. The design constraints become even more important when considering that the demining task rests with military and civilian personnel of various training and skill levels. Additionally, demining must be accomplished with a reasonable search rate and on a reasonable time scale in order merely to have the detection rate become equal to the current mine emplacement rate.

A large majority of the currently emplaced anti-tank (AT) and anti-personnel (AP) land mines can be located with metal detectors, and deminers are well-acquainted with the use and operation of these types of instruments. However, when the metal detectors are set to sufficient sensitivity to detect the low metal content AP mines, the false alarm rate becomes prohibitively high. Deminers must treat every hit as if it were a mine, and thus expend enormous amounts of time and effort interrogating false alarms. Although these false alarms share a common feature in that they have at least a certain amount of metal, they do not share a vapor signature with actual mine targets. It is well-known that canines are the most successful detectors of AP land mines, and canines achieve their low false alarm rate by using the vapor signature of the mine as their target signal. The first goal of our chemical vapor detection device is therefore to develop a system that can be integrated into an existing metal detector, so that a "hit" on the metal detector could be interrogated with the integrated vapor detector in order to decide whether the target is actually a land mine as given by its chemical signature. In this fashion, the task of target localization would be performed using the already familiar metal detector technology, while the false alarm rate would be lowered with a seamlessly integrated chemical sensor system. A second goal of this project is to develop even more sophisticated vapor detection devices that would not require cueing from a metal detector but could be used in a stand-alone fashion to cue deminers to the location of emplaced land mines through odor localization and, if necessary, odor tracking algorithms, much as canines lead their handlers to buried mines in the field.

The focus of our project is inspired by the success of the biological olfaction system in conquering this formidable odor detection, identification, tracking, and location problem. We do not attempt to cope with the engineering challenges involved with modifying or miniaturizing traditional laboratory analytical chemical systems that involve high power and high vacuum (mass spectrometers, for example), high pressures and/or gas flows (e.g., gas chromatography) or other operational constraints that present severe mismatches between the optimal instrumental operating conditions and those in the fields of Cambodia, for example. Instead, our approach starts with low power, small vapor sensors that operate at room temperature and atmospheric pressure. This makes the technology inherently compatible with the conditions under which it is intended to be utilized. The individual sensors are broadly responsive and thus mimic the operation of the mammalian olfactory system, so that the sensing system, comprised of an array of individual vapor sensors, can be applied to many different types of target vapor signatures without a redesign of sensors or a fundamental paradigm shift in the detection technology. This is important because it is not clear what vapors canines are actually keying on when they detect land mines, and not all land mines have the same vapor signature. If a detector were developed

2

for TNT, for example, it would not be able to detect RDX or cyclohexanone in the RDX mines, and a separate technology would then have to be developed and fielded in order to detect these other classes of mines. Furthermore, certain types of mines might have more volatile, more readily detectable signatures than RDX, for example, and there is no reason to focus on pushing a technology towards a more difficult target such as, for example, an RDX vapor signature detector, if these RDX-containing mines could more readily be detected by using a signature of a more volatile impurity originating from the RDX itself, from the plastic mine casing, etc. Only a versatile, broadly responsive, chemical detection system can therefore take advantage of the most readily detected, unique signature compounds of the desired targets in order to perform the mine identification task.

Several unique capabilities make the lead institution of this project, Caltech, a uniquely qualified to lead the development of systems based on this type of vapor sensing technology. Work at Caltech by N. Lewis and R. Grubbs has led to a new family of broadly responsive vapor sensors, based on conductor/insulator composites, that have drawn widespread attention from both the popular press[1,2] and the scientific community[3,4] for their promise in a diverse collection of civilian and military applications. R. Goodman and the NSF-funded Caltech Center for Neuromorphic Systems Engineering are leaders in developing analog very large scale integration (AVLSI) circuitry that uses biological signal processing implementations as inspiration for the construction of sensory-type devices (artificial cochleas, retinas, active skins, etc.)[5] and have produced devices that have superior performance and much lower power consumption than can be readily obtained using traditional approaches. Cyrano Sciences, Inc. has the commercial license to manufacture devices based on the Caltech sensor film technology, and is leveraging its manufacturing experience in developing sensors for civilian applications to preparing technologically advanced vapor sensors for use in the demining mission. Another key contribution to the proposed work has come from Caltech's Jet Propulsion Laboratory who, along with the Goodman group's expertise in pattern recognition and neural networks, has contributed expertise in signal processing algorithms to the specific issue of optimizing the detection probability, while minimizing false alarm rates, for signals arising from these vapor sensing devices when operated under actual field conditions.

The enabling technology underlying our approach is a series of conductive polymeric composite vapor sensors that have been developed at Caltech, and which form the basis for an "electronic nose".[3,4] In this very simple implementation of vapor detection, the presence of an odorant is detected through a change in the electrical resistance of a chemically sensitive carbon-based resistor. The sensor films are composed of patented conductor/insulator composites, in which the organic conducting polymer sorbs the vapor and thereby induces a change in the electrical resistivity of the material due to the swelling of the film (Figure 1). When the vapor is removed, the swelling reverses and the resistance returns to its original value. The response of these types of sensors has been shown to be reversible over tens of thousands of vapor exposures as well as to be reproducible over a large number of trials under a variety of ambient atmospheric conditions.

Since the polymer films are broadly responsive and swell in the presence of many odorants, the signal from one sensor film allows detection of a change in the composition of the analyte, but does not allow identification of that analyte. However, an array of such sensing elements

3

produces a reversible, diagnostic pattern of electrical resistance changes upon exposure to different odorants. An example of the diagnostic patterns produced by such an array is illustrated in Figure 2, which shows the excellent separation that can be achieved between the patterns arising from exposure (in air, with no control over the temperature or humidity of the environment) of a relatively simple 17-element sensor array to various organic vapors (including 3-nitrotoluene). This type of broadly responsive, pattern-recognition based approach to vapor sensing not only imitates the biological olfactory response, but affords the opportunity to develop a low power, small size, fieldable, land mine detector that could be trained to recognize the patterns of the various targets and then compare the signature of the vapor that is in the immediate environment of the sensor to that of the library of target compounds that are characteristic of the land mines of interest.

There are other array-based approaches being pursued at present for vapor detection, including surface acoustic wave devices, tin oxide sensors, other conductive polymer sensors, optical sensors, etc..[5-9] The Caltech conductive composite chemiresistor technology has several important potential advantages in that a) the sensor films are simple to fabricate (so that large numbers of sensors can be produced in a low cost process), b) are readily made very chemically diverse (so that confusion of the target vapors with other background clutter signals can be minimized in at least some channels of the array output) , c) are readily miniaturized (enabling large numbers of sensors on chip for improvements in sensitivity, signal averaging, better target discrimination, etc.), d) yield signature patterns for a vapor that are linearly related to the vapor concentration and are largely independent of the nature of the background clutter, and e) yield a very simple, low power readout signal--the film resistance--that is compatible with modern electronic processing.

Another feature of the work described herein is that we have carefully considered, at the initiation of this project, the engineering and operational tradeoffs that will arise in construction of an entire sensor system. For instance, there is little point in basing a technology around a design that employs readout electronics which would consume 10 mW of power for the readout and signal processing of each sensor element signal, if tens or hundreds of thousands of sensor elements are required to obtain a fieldable array-based sensor device. We have also taken into consideration to the factors that will be required in order to transition the operation of these devices out of the laboratory and into the field. One especially critical aspect of this transition is the adaptation issue: in a cluttered field environment of unknown, and generally varying, concentrations of a variety of potentially unknown species, real time adaptation must be employed in order to "zero-out" the clutter so that the signal can be detected as a change relative to the environmental background (i.e., to detect the different signals between when the metal detector is moved from near the "hit" to directly on top of the "hit", for example).

A complete system consists of an input (the odor), along with three major functional parts: sensors for odor detection, preprocessing circuitry for adaptation, filtering, and amplification and measurement of the signal, and classification/identification circuitry, and will produce one output (the odor identification and its location). It is useful to consider a tentative design (Figure 3) to understand the design considerations of each part of the system. We have adopted the tenet that it is desirable to have as many sensors on chip as is

4
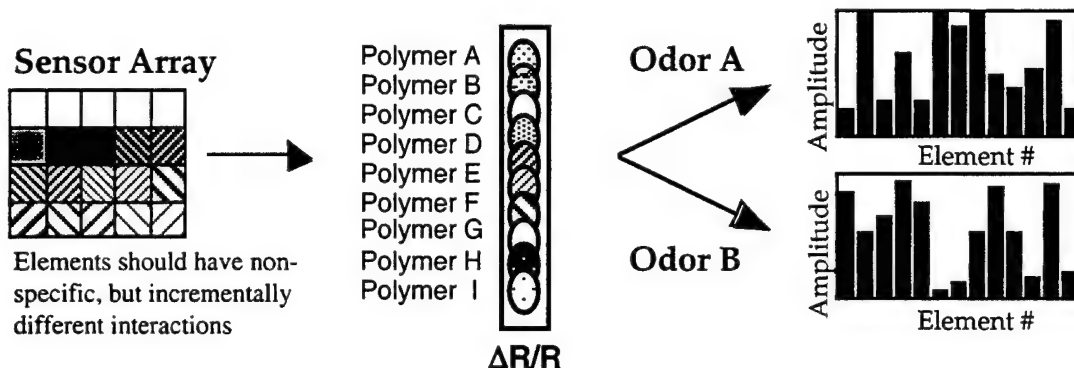
Figure 1. Patterns produced by an array of broadly-responsive vapor detectors. The response of a collection of incrementally different but non-specific sensors, in our case chemically sensitive conducting polymer composite resistors, is used to generate a complex pattern, or fingerprint, characteristic of a given analyte.

a)
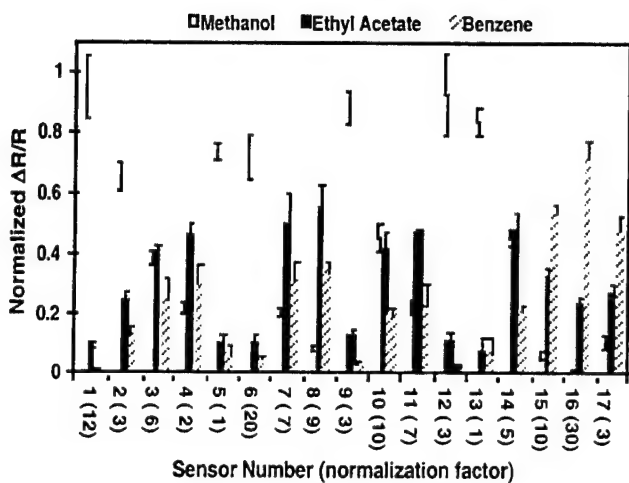
b)
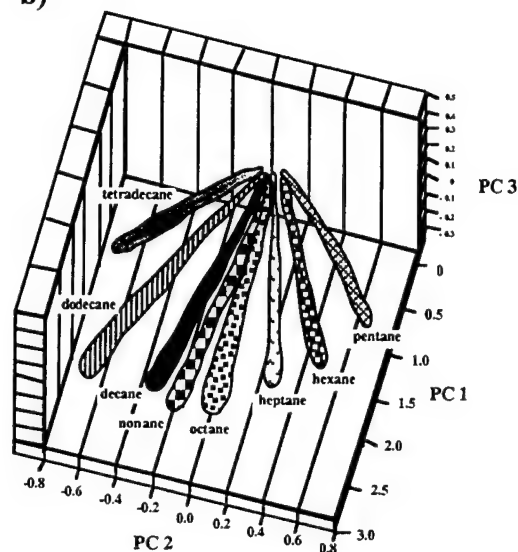
Figure 2. a) Response patterns for three different solvents on a 17 element sensor array. **b)** Data in principal component space from a 20-detector array exposed to n-tetradecane, n-dodecane, n-decane, n-nonane, n-octane, and n-heptane each at $P/P° = 0.005$ to 0.03 in air (with $P°$ being the vapor pressure of the analyte at 300 K), showing that the pattern type identifies the vapor and the magnitude of the pattern signals is linearly proportional to the analyte concentration.

possible (this is justified in detail below), but we must allot space for the associated electronics and processing within a reasonably inexpensive set of process steps (2 micron VLSI technology is assumed for this design). Assuming that sensor films can be deposited into wells that are 200 microns x 200 microns in dimension (Figure 3), a 50 micron spacing between grid cells produces 10,000 sensors on each chip. Finally, the signal outputs must be communicated to the identification/classification circuitry, and chip space must be allotted for these interconnections. Alternative designs to that presented in Figure 3 are also possible, but the goal of working with 1,000-10,000 sensors on chip is thus a reasonable design target for these types of resistance-based sensor arrays.

Work by other research groups has shown that limited collections of conducting polymer sensor elements, each differing slightly through variations in the substituents on the polymer backbone or through variations of the counterion of the polymer, can be used to construct chemiresistor arrays for vapor sensing.[10,11] The conducting polymer composite approach is apparently more versatile and chemically tunable because it is not constrained to variations that can be achieved within pure conducting organic polymeric phases, but instead utilizes conductor/insulator composites, in which the conducting phase serves the chemical-to-electrical signal transduction function with the insulating phase serving the function of achieving controlled differential binding, and therefore differential sensing.[3,4] Thus, in the approach utilized in this project, essentially any conducting element, including carbon blacks, metallic colloids, or organic conducting polymers, can be used as the conductive phase, and essentially any swellable, organic material can be used as the insulating phase. This approach allows one to synthesize readily a very broad, diverse collection of sensor materials without limitations of the stability of conducting organic polymeric materials and without suffering limitations from the types of substituents and/or restrictions on the ranges of swelling variations that can be obtained from backbone modification of pure organic conducting polymers.

There is some discussion in the literature regarding whether it is advantageous to use large numbers of sensors in an array device. This arises because work by Abraham and co-workers has claimed that there are approximately 5 fundamental molecular descriptors of the gas-solid partition coefficients for sorption of vapors into polymers;[12] thus five uncorrelated sensors should be sufficient to uniquely identify any analyte from its pattern on such an array. Although it is possible to describe the gross features of such partitioning with a small number of descriptors, it is interesting to note that there are over 1000 olfactory genes in humans and over 100 million olfactory cells in a canine's nose. Even if the dimensionality of odor space is fairly small, say on the order of 10^1, it is not likely that ideal sensors that produce optimal resolution along the fundamental directions of odor space could be identified. In practice, correlations between the elements of a sensor array will necessitate a much larger number of sensors to successfully distinguish molecules in a complex environment. Also, it is beneficial to measure the same property in many different ways due to noise limitations in a practical system. For example, if sufficient precision could be obtained, it might be possible to identify uniquely any molecule merely from a 38 bit measurement of two parameters, perhaps its dipole moment and its polarizability. But of course it is not practical to make such measurements with this precision; hence at lower precision, useful information on the nature of the analyte is gained by
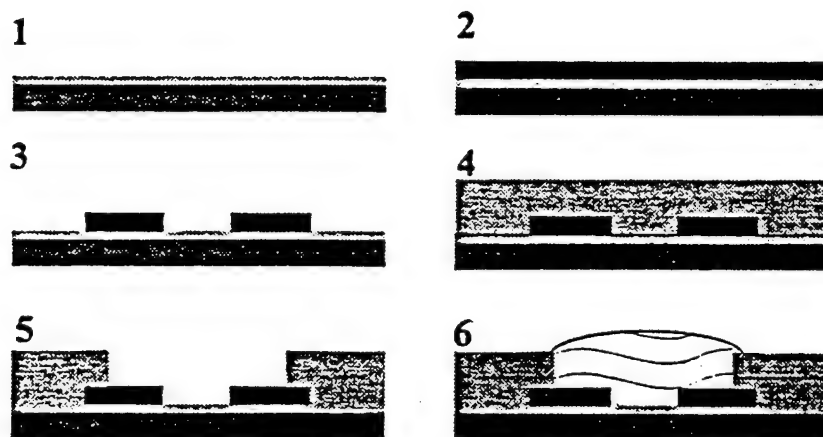
Figure 3. *Simplified process flow to create wells with sensors on Si.* Step 1) A silicon wafer with an insulating oxide. Step 2) Metal is deposited on the oxide. Step 3) The metal is patterned to form pads and wires for connection. Step 4) A thick layer of oxide is grown. Step 5) The oxide is patterned and etched, forming wells for holding the sensor material. Step 6) The sensor material is deposited into the well.

making measurements of the molecular parameters through many independent determinations on different sensor elements. Furthermore, the above arguments on needing a limited number of sensors only hold if one is tasked to distinguish between a series of pure substances that are maintained at one fixed, known concentration. In contrast, if the background is unknown, if mixtures are present, or if the background gases are changing in concentration, many more sensors are needed simply to avoid ambiguity in interpretation of the output signal pattern, and even more are needed if optimal discrimination is to be accomplished between a given target signature and a wide possible range of background clutter and false alarm signatures. Having large numbers of sensors also allows redundancy and provides the ability to veto the output of poorly performing sensors. Because of all of these issues, the number of sensors required to successfully span odor space in a practical device will rapidly multiply from the minimum value defined by the rank of smell space, and we have taken advantage of our ability to integrate large numbers of sensors into an array structure as part of our device design.

2. An Investigation of the Concentration Dependence and Response to Analyte Mixtures of Carbon Black-Insulating Organic Polymer Composite Vapor Detectors

2.1 Introduction

Detector modalities that have been employed in electronic noses[3,4,13-15] include surface acoustic wave (SAW) devices,[16-19] tin oxide detectors,[7,20,21] electrically conductive organic polymers,[3,10,11] coated fiber optic detectors,[9] polymer-coated micromirrors,[22,23] quartz crystal microbalances (QCMs),[24,25] and carbon black-polymer composite chemiresistors.[4] These types of broadly responsive detector arrays can be useful in at least two generic categories of sensing tasks. In one mode of operation, the array is only required to sense changes in an odor relative to a known prior condition. The changes of interest may have many different physical and/or chemical origins, some of which may not be anticipated in advance, but all of which should optimally be probed by the vapor detector array. This mode of operation is useful for applications in quality control and quality assurance of foodstuffs, fragrances, consumer goods, and similar applications.[11,26-28] For such purposes, the detector response need only be reproducible from trial to trial, and no constraints on the form of the detector response are necessarily required to perform the task at hand.

In another operational mode, a detector array could be used to identify a signature of an odor in the field based on a comparison of the array response to the response signature that was recorded and stored for that analyte during a prior training/calibration run.[6,29,30] Such applications might include providing a warning when a particular odor becomes present above a certain concentration level in the vapor phase, tracking and/or localization of an odor in the environment, or determining the concentration of an analyte in a simple, but relatively time-independent, effluent mixture. In these types of applications, it is highly advantageous to utilize detectors that have a linear output signal in response to variations in the concentration of a particular odor, so that the pattern type allows identification of the odor while the pattern height can be straightforwardly related to the odor concentration. It is even more advantageous if the array response to the odor

of concern is the same in the absence and presence of other odors. In this fashion, the initial training requirements from the array response output data are minimized because the pattern produced by the analyte of concern can be associated uniquely with that odor regardless of the changing environmental conditions under which the analysis is performed.

Work in our laboratory has demonstrated that insulating organic polymers interspersed with domains of electrical conductors can provide chemically sensitive detector materials that can be used to produce an "electronic nose" array.[3,4] The conducting polymer composites have been formed using either organic, inorganic, or carbonaceous materials as the conducting phase. Sorption of organic solvent vapors into these types of detectors produces a characteristic, reversible resistance change in the detector element.[4] Because every organic polymer will have a characteristic gas/polymer partition coefficient in response to the presence of a particular odor, a collection of insulating organic polymers provides a diversity in detector materials that produces the diagnostic response pattern of the detector array. Under certain circumstances, analysis of the pattern of signals produced by the detector array then allows information on odor classification and concentration to be extracted through signal processing methods.[31]

In this section, we describe the results of an extensive set of experiments designed to investigate the behavior of arrays of conductive polymer composite detectors when presented with a broadly construed, generic set of test organic vapors at varying analyte concentrations. In addition, we have probed the response when the detectors are exposed to various concentrations of members of homologous series of alkanes or alcohols. Additionally, the detector response properties have been investigated during exposure to various binary vapor mixtures to ascertain whether an array response pattern for a pure odor is transferable, weighted by the mole fraction of its vapor in an analyte mixture, to binary mixtures of analytes. Finally, we describe the results of experiments in which a small but rapidly changing odor concentration has been superimposed upon a relatively slowly-varying baseline odor concentration.

The responses relative to an air background of carbon black/polymer composite vapor detectors have been determined as a function of the concentration of a homologous series of alcohols (n-$C_nH_{2n+1}OH$, $1 \leq n \leq 8$), a homologous series of alkanes (n-C_nH_{2n+2}, $5 \leq n \leq 10$ and $n=12,14$), and a set of diverse solvent vapors. In all cases the steady-state relative differential resistance responses, $\Delta R/R_b$, of the carbon black/polymer composite vapor detectors were well-described by a linear relationship with respect to the analyte partial pressure, at least over the tested concentration range ($P/P^\circ = 0.005$-0.03 where P° is the vapor pressure of the analyte). When two vapors in air were simultaneously presented to the detectors, the $\Delta R/R_b$ response, relative to an air background, was the sum of the $\Delta R/R_b$ values obtained when each analyte was exposed separately to the carbon black/polymer composite detectors under study. Similarly, when an analyte was exposed to the detectors on top of a background level of another analyte, the $\Delta R/R_b$ values of the array of detectors were very close to those obtained when the test analyte was exposed to the detectors only in the presence of background air. The initial training requirements from the array response output data of such detectors are minimized because the $\Delta R/R_b$ response pattern produced by the analyte of concern can be associated uniquely with that odor, under the conditions explored in this work.

2.2   *Experimental*

2.2.1. Materials

The carbon black used in the composites was Black Pearls 2000 (BP2000), a furnace black material that was generously donated by Cabot Co. (Billerica, MA). The polymers used in the composites are (listed as detector #, polymer): 1, poly(4-vinyl phenol); 2, poly(styrene-co-allyl alcohol), 5% hydroxy; 3, poly(α-methylstyrene); 4, poly(vinyl chloride-co-vinyl acetate), 10% vinyl acetate; 5, poly(N-vinylpyrrolidone); 6, poly(vinyl acetate); 7, poly(methyl vinyl ether-co-maleic anhydride); 8, poly(carbonate bisphenol A); 9, poly(styrene); 10, poly(styrene-co-maleic anhydride), 50% styrene; 11, poly(vinyl butyral); 12, poly(sulfone); 13, poly(methyl methacrylate); 14, poly(vinylidene chloride-co-acrylonitrile), 80% vinylidene chloride; 15, poly(caprolactone); 16, poly(ethylene-co-vinyl acetate), 82% ethylene; 17, poly(ethylene oxide); 18, poly(butadiene), 36% cis-1,4, 55% trans-1,4, 9% vinyl-1,2; 19, poly(epichlorohydrin); 20, poly(styrene-co-butadiene), 28% Styrene; 21, addition product of sodium menthoxide to poly(pentafluorostyrene); 22, (+) isopinocampheol derivatized poly(p-chloromethylstyrene); 23, poly(fluorostyrene); 24, poly(styrene-co-isoprene) (Figure 4). All polymers were purchased from Polysciences Inc. or Aldrich Chemical Co. and were used as received, except polymers 20-23, which were synthesized in the Grubbs group at Caltech. The solvents used in this study all were reagent grade and were used as received.

2.2.2. Fabrication of Detectors

Two substrates were used for the detectors. In one configuration, two parallel bands of gold, 50-100 nm thick and separated by either 1 mm or 5 mm, were deposited onto conventional 7.5 cm x 2.5 cm glass slides (Corning Inc.). The slides were then cut into strips to produce 0.7 cm x 2.5 cm pieces of glass, with each strip of glass having one pair of Au leads spaced 1 or 5 mm apart. In the second configuration, a commercial surface mounting breadboard was slightly modified to be used as the substrate. The commercial product ("Surfboards") consisted of parallel leads of metal deposited onto the circuit board material. These leads were soldered to pins that were on 0.10" centers. The commercial product was cut into pairs of leads and was then coated with the composite films.

The detector films were made from a solution of the polymer into which carbon black had been suspended. 160 mg of one of the insulating polymers (Figure 4) was dissolved in 20 mL of tetrahydrofuran, and carbon black (40 mg) was then suspended in this solution, to produce a composition of 80% polymer and 20% carbon black by weight of solids. The solvent was generally tetrahydrofuran, benzene or methylene chloride, depending on solubility of the polymer. The solutions were sonicated for 5 min to suspend the carbon black. Aromatics and chlorinated solvents yielded very good suspensions of the carbon black. A single solution that contained the polymer and the carbon black was used to prepare all the detectors of a given composition that were used in this work. An aliquot of the suspension was spin coated, at 1000 rpm, onto a glass substrate using a Headway (Garland, TX) spin coater, and the resulting film was allowed to dry in air. Multiple coatings of the suspension were applied to each substrate to yield detectors having resistance values of approximately a few hundred kΩ. For the fiberglass substrates, the film was applied by dip coating the substrate two or three times until the desired

1 1
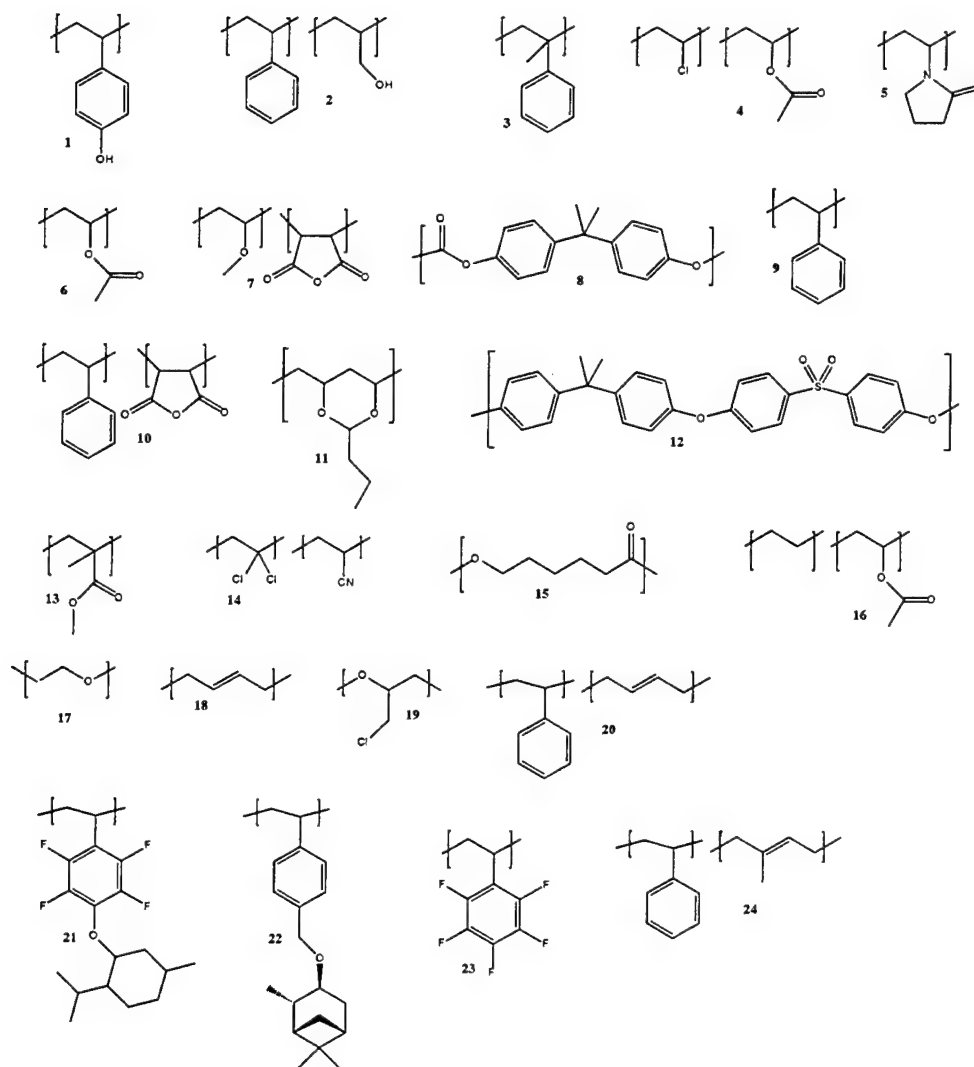
Figure 4: Structures of the polymers used to make composite vapor detectors. Listed as detector, polymer: 1, poly(4-vinyl phenol); 2, poly(styrene-co-allyl alcohol), 5% hydroxy; 3, poly(α-methylstyrene); 4, poly(vinyl chloride-co-vinyl acetate), 10% vinyl acetate; 5, poly(N-vinylpyrrolidone); 6, poly(vinyl acetate); 7, poly(methyl vinyl ether-co-maleic anhydride); 8, poly(bisphenol A carbonate); 9, poly(styrene); 10, poly(styrene-co-maleic anhydride), 50% styrene; 11, poly(vinyl butyral); 12, poly(sulfone); 13, poly(methyl methacrylate); 14, poly(vinylidene chloride-co-acrylonitrile), 80% vinylidene chloride; 15, poly(caprolactone); 16, poly(ethylene-co-vinyl acetate), 82% ethylene; 17, poly(ethylene oxide); 18, poly(butadiene), 36% cis-1,4, 55% trans-1,4, 9% vinyl-1,2, 19, poly(epichlorohydrin); 20, poly(styrene-co-butadiene), 28% Styrene; 21, addition product of sodium menthoxide to poly(pentafluorostyrene); 22, (+) isopinocampheol derivatized poly(p-chloromethylstyrene); 23, poly(fluorostyrene); 24, poly(styrene-co-isoprene)

12

2resistance was achieved. Before use, the detectors were dried in open air and then were placed in air flowing at 20 L/min for 12-24 hours.

2.2.3 Instrumentation and Apparatus

An automated flow system consisting of LabVIEW software, a Pentium computer, and electronically-controlled solenoid valves and mass flow controllers was used to produce and deliver selected concentrations of solvent vapors to the detectors.[32] To obtain the desired analyte concentration, a stream of carrier gas was passed through a bubbler that had been filled with the solvent of choice. Saturation of the carrier gas with the solvent vapor was verified through measurement of the rate of mass loss of the solvent in the bubbler.[33] The vapor-saturated carrier gas was then diluted with pure carrier gas through the use of mass flow controllers (MKS Instruments, Inc). Calibrations of the flow system using a flame ionization detector (Model 300 HFID, California Analytical Instruments, Inc.) verified that the analyte concentrations delivered to the sensors were those expected from the settings of the mass flow controllers.

The carrier gas for all experiments was oil-free air, obtained from the general compressed air lab source, containing 1.10 ± 0.15 ppth (parts per thousand) of water vapor. The air was filtered to remove particulates, but deliberately was not dehumidified nor otherwise purified. Fluctuations in laboratory temperature, 21.5 ± 1.5 °C, could cause an $\approx 10\%$ error in setting and controlling the vapor concentrations between nominally identical exposures over the course of the data collection analyzed in this work. No temperature control of the apparatus or of the carbon black-polymer composite detectors was performed. The flow rate of the vapor stream entering the exposure chamber (≈ 1 liter in total volume) was maintained at 15 L/min.

2.2.4 Measurements

The dc electrical resistance of each detector was monitored in response to the presence of various test vapors and mixtures of vapors. Resistance measurements were performed using a simple two-point configuration across the gold leads that bridged the sensing element. The detectors were multiplexed through a Keithley model 7001 channel switcher to a Keithley model 2002 multimeter that measured the dc resistance of each detector once every 3 - 5 seconds, with the exact time interval depending on the particular experiment.

To initiate an experiment, the detectors were placed into the flow chamber and a background flow of compressed air was introduced until the resistance of the detectors stabilized. Each exposure consisted of a three-step process that began with 60 s of air flow to achieve a smooth baseline resistance. After this period, the detectors were exposed to solvent vapor at a controlled concentration in flowing air. The solvent exposure was then followed by a flow of clean air for a time equal to the total exposure time, to restore the baseline resistance values. For the linearity studies, the 60 s baseline period was followed by 240 s of exposure to the test analyte. To probe the dependence of the detector response on the order of presentation, in some measurements of the mixture studies, the exposure phase consisted of parts. In the sequential mixture measurements, the first analyte (denoted as s_1) was exposed for 120 s, at which time the second solvent, s_2, was introduced and exposed for an additional 120 s. During the exposure of the

13

second analyte, the first analyte was continually flowing (this protocol is denoted as s_1, $s_1 + s_2$). In the measurements when a mixture of two analytes was exposed simultaneously to the sensors (denoted $s_1 + s_2$), the two analytes of the mixture were presented to the detectors for a total of 240 s.

In studies of mixtures, the eight bubblers of the system were divided into two sets of four bubblers each. One mass flow controller was present for "set A" and one for "set B" (Table 1). One-way valves ensured that significant gas back flow did not occur during the experiments. Analytes in the same solvent set could not be exposed simultaneously to the detectors. Therefore, 16 pairs of solvents were available for use in the first set of mixture studies. In the second mixture study only six solvents were used, three in each set, so nine solvent pairs were available. The detectors used for the eight-solvent experiment were formed from polymers 1-18, 21, 23 (Figure 4). The detectors used for the six-solvent experiment, the alcohol linearity study, and the alkane linearity study, were formed using polymers 8, 12, 15-24 (Figure 4). In all experiments, one copy of each type of detector was used.

In both the 8-solvent and 6-solvent mixture experiments, the detectors were exposed to individual solvents (s_1), to pairs of solvents presented simultaneously ($s_1 + s_2$), and to one solvent followed by addition of another solvent (s_1, $s_1 + s_2$). The individual solvents and the pre-selected pairs of s_1, s_2 solvents were exposed to the detectors at analyte concentrations that corresponded to 0.5, 1.0, and 1.5 % of each solvent's vapor pressure, P°. In the 6-solvent experiment, individual solvents were additionally presented at 2.0 and 2.5 % of P°. Solvents forming every compositionally distinct binary mixture were permuted in their order of presentation to the detectors, so that for each solvent pair (one from set A and one from set B) at every distinct analyte concentration, the trials included the exposure protocol s_A, s_A+s_B as well as the exposure protocol s_B, s_B+s_A. Each unique exposure protocol, for each type of mixture and pure analyte presentation, was repeated 5 times. The 8-solvent experiment thus contained 2280 total exposures (8 solvents, 3 concentrations, 5 repeats of each for the individual solvent exposures, 6 x 8 x 5 simultaneous mixture exposures, and 16 x 8 x 2 x 5 sequential mixture exposures). The 6-solvent experiment contained 1365 total exposures (6 x 5 x 5 individual solvent exposures, 3 x 9 x 5 simultaneous mixture exposures, and 9 x 6 x 2 x 5 sequential mixture exposures). Within each experiment, every exposure was assigned a randomly generated index number using the Microsoft Excel random number generator. The exposures were then presented to the detector array in ascending order of the assigned index values.

In the studies designed to quantify the detector response as a function of analyte concentration, two homologous series of vapors, one consisting of straight chain alcohols and the other of straight chain alkanes, were exposed to the detectors. The alcohols used were: methanol, ethanol, 1-propanol, 1-butanol, 1-pentanol, 1-hexanol, 1-heptanol, and 1-octanol. In a separate run, n-pentane, n-hexane, n-heptane, n-octane, n-nonane, n-decane, n-dodecane, and n-tetradecane were used. In another, related set of experiments, the broad test set of solvents used in the studies of mixtures (Table 1) was exposed to the detectors over a wider concentration range ($0.005\ P^\circ \leq P \leq 0.03\ P^\circ$) than was used in the runs to determine the detector's response to mixtures of these particular solvent vapors. Additionally, one run with the straight chain alcohols was performed using vapor concentrations that were in the range $0.01\ P^\circ \leq P \leq 0.06\ P^\circ$.

14

Table 1. Two groups of solvents used in the 8-solvent binary mixture study and the 6-solvent binary mixture study. Binary mixtures were formed between solvents of set A and solvents of set B of each group. Solvents common to one set could not be paired.

Eight-solvent experiment

Set A	Set B
benzene	chloroform
ethyl acetate	ethanol
heptane	hexane
methanol	toluene

Six-solvent experiment

Set A	Set B
benzene	nitrobenzene
2-propanol	chloroform
cyclohexanone	heptane

In each of these experiments, each unique presentation of an analyte was repeated 10 times, with the entire presentation order (within a run) randomized with respect to solvents, concentrations of solvents, and repeated exposures to a solvent.

2.2.5 Data Processing

Sample responses for a single exposure and for a sequential mixture exposure are shown in Figure 5. Although the resistance of each detector was sampled once every 3 - 5 seconds during each exposure, only the maximum relative differential resistance change, $\Delta R_{js,max}/R_{jb,air}$, where $\Delta R_{js,max}$, produced by exposure to an individual solvent, is the maximum resistance change of the jth detector during exposure to solvent s, and $R_{jb,air}$ is the baseline resistance of the jth detector exposed to the initial 60 s period of exposure to background air, was used in analysis of the data. In the mixture studies when solvents were exposed sequentially to the detectors, three separate $\Delta R/R$ values, $\Delta R_{j,s1,max}/R_{jb,air}$, $\Delta R_{j,s2,max}/R_{jb,s1}$, and $\Delta R_{j,s1,s1+s2}/R_{jb,air}$ were calculated from the data from each exposure protocol s_1, s_1+s_2 (Figure 5).

For these solvents and detectors, the exposure time was sufficiently long that the maximum response value, $\Delta R_{js,max}/R_{jb}$, was a very good approximation to the change in the steady-state resistance value of the detectors in response to the specified analyte concentration relative to the baseline resistance of the detector in an air background flow alone. Examples of the temporal dependence of individual carbon black-insulating polymer composite detectors are shown in Figure 5. For some exposures in the 8-solvent system, the value $R_{jb,s1}$ had not completely reached steady state. Therefore, to calculate $\Delta R_{js2,max}/R_{jb,s1}$ in those cases, the slope of the resistance values 30 s prior to the start of the exposure was calculated and subtracted from the R_{js2} values. If this correction were not made, then the detector's response to s_2 would have been overestimated.

2.3   Results

2.3.1. Linearity of Detector Response for Pure Odors

Figure 6a displays the maximum relative differential resistance data, $\Delta R_{js,max}/R_{jb,air}$, for a 12-element conducting organic polymer composite detector array towards a series of test analytes when each analyte was maintained at a partial pressure, P, in air equal to 3% of its vapor pressure, P°, at 22°C. Each analyte can be seen to produce a distinct $\Delta R_{js,max}/R_{jb,air}$ response pattern on the array of conducting polymer composite detectors. Principal component analysis was used in order to aid visualization of the differences between $\Delta R_{js,max}/R_{jb,air}$ patterns produced by the various analytes.[34] Figure 6b presents the $\Delta R_{js,max}/R_{jb,air}$ data in principal component space, with the axes representing the first and second principal components of the data set. All analytes were well-separated from each other based on the differences between their characteristic $\Delta R_{js,max}/R_{jb,air}$ response patterns on the array of detectors.

16
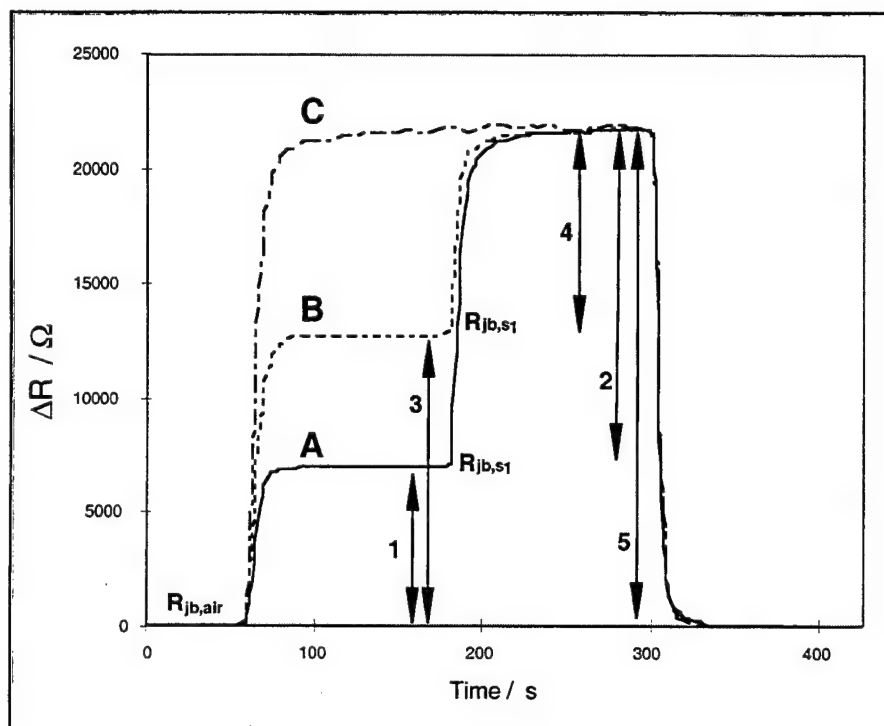
Figure 5. Representative differential resistance responses for three types of vapor presentations to a poly(ethylene-co-vinyl acetate)-carbon black composite vapor detector. **A)** Exposure to benzene at $P/P° = 0.02$ ($\Delta R_{js1,max}$ indicated by arrow 1) followed by exposure to benzene at $P/P° = 0.02$ and chloroform at $P/P° = 0.02$ ($\Delta R_{js2,max}$ indicated by arrow 2). The combined response, $\Delta R_{js1,max} + \Delta R_{js2,max}$, is indicated by arrow 5. **B)** Exposure to chloroform at $P/P° = 0.02$ ($\Delta R_{js1,max}$ indicated by arrow 3) followed by exposure to chloroform at $P/P° = 0.02$ and benzene at $P/P° = 0.02$ ($\Delta R_{js2,max}$ indicated by arrow 4). The combined response, $\Delta R_{js1,max} + \Delta R_{js2,max}$, is also indicated by arrow 5. Arrow 1 ≈ Arrow 4; Arrow 3 ≈ Arrow 2. **C)** Benzene at $P/P° = 0.02$ and chloroform at $P/P° = 0.02$ both presented simultaneously to the detector (response, $\Delta R_{js1+s2,max}$ is again indicated by arrow 5).

17
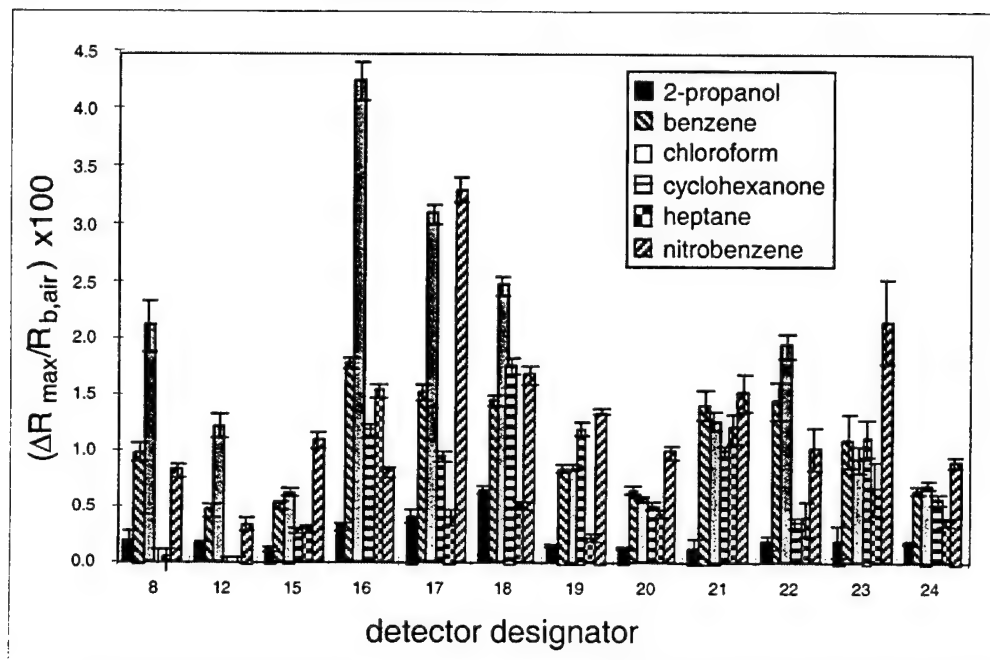
Figure 6. Relative differential resistance responses of 12 carbon black-polymer composite detectors exposed to various analytes **a)** A histogram of the maximum relative differential resistance response of 12 carbon black-polymer composite detectors exposed to n-heptane, cyclohexanone, benzene, chloroform, nitrobenzene, and 2-propanol each presented at $P/P° = 0.03$ in air. Each analyte was presented 10 times to the array, with the order of presentation randomized over all repetitions of all test solvents.
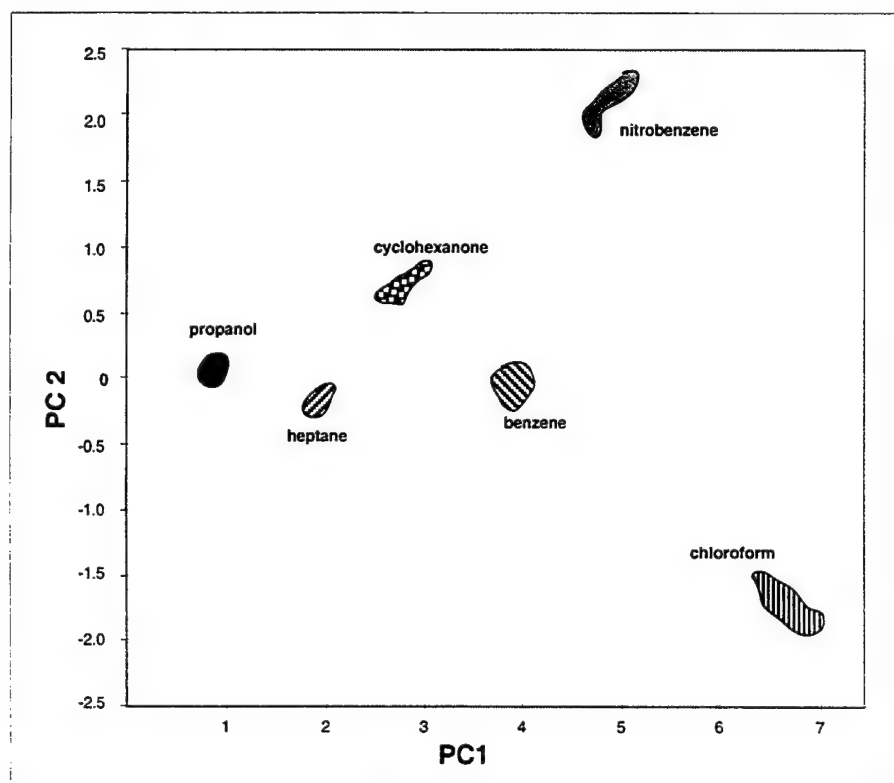
Figure 6. b) Results from the exposures described in (**a**) as represented by the first two dimensions of principal component-space, which contain 96% of the total variance in the data. The ellipsoids contain 95% of the data for each analyte in principal component space.
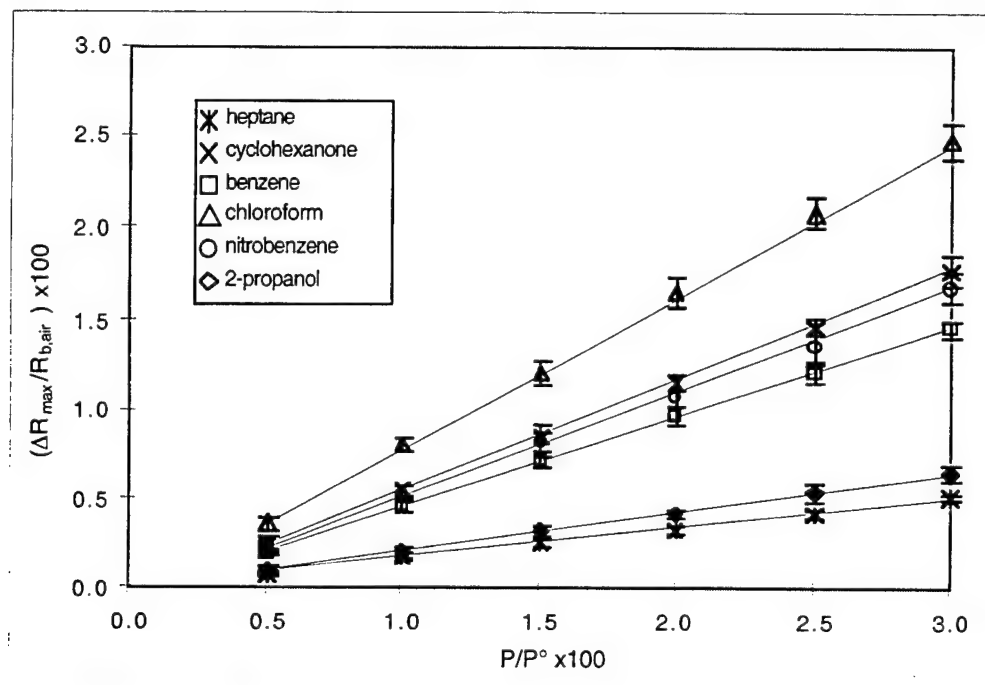
Figure 7. Relative differential resistance responses of composite detector films consisting of carbon black and poly(butadiene), when exposed to n-heptane, cyclohexanone, benzene, chloroform, nitrobenzene, and 2-propanol. Average maximum relative differential resistance responses, $\Delta R_{js,max}/R_{jb,air}$, each at $P/P° = 0.005$ to 0.03 in air in six even steps. Each analyte was presented 10 times to the array, with the order of presentation randomized over all repetitions of all test solvents. The error bars represent 1σ values computed from 10 exposures at each $P/P°$.

The concentration of each analyte was then varied over six even steps in the range $0.005\ P° \leq P \leq 0.03\ P°$. Figure 7 depicts the responses of a representative detector to all of the test solvent vapors. The data were well-fit by a linear dependence of $\Delta R_{js,max}/R_{jb,air}$ on $P/P°$ over the $P/P°$ ranges probed in this experiment. A summary of the correlation coefficients calculated for these lines is presented in Table 2, while statistics for all of the sensor/analyte combinations are provided in the supporting material that accompanies this work. For some sensor-analyte combinations the correlation coefficients were low because the sensor exhibited only a very small response to the analyte. For example, poly(sulfone) had a small response to non-polar solvents and so the correlations coefficients for these presentations are low. Similarly, essentially no response was exhibited by poly(sulfone) to dodecane. The intercepts of such plots were statistically indistinguishable from zero for all sensor/analyte combinations investigated

Figure 8 presents the concentration-dependent $\Delta R_{js,max}/R_{jb,air}$ response data for the entire detector array in principal component space. For each test vapor, the analytes produced a unique signal response pattern, with the pattern direction in principal component space diagnostic of the analyte and the pattern height proportional to the analyte concentration in the vapor phase. This behavior is further illustrated by normalization of the detector response patterns with respect to analyte concentration according to eq 1.

$$ S_{js} = \left(\frac{\Delta R_{js,max}}{R_{jb,air}} \right) \left(\frac{P°}{P} \right) \tag{1} $$

where S_{js} is the normalized signal for 12 detector films exposed to benzene, chloroform, and nitrobenzene each presented at $P/P° = 0.005 - 0.03$ in six even steps. As can be seen from Figure 9, the characteristic S_{js} pattern of each test vapor was maintained, within experimental error, as the analyte concentration was varied.

Additional experiments were performed using a homologous series of alkanes, and then using a homologous series of alcohols, as test analytes. Figures 10 and 11 display the $\Delta R_{js,max}/R_{jb,air}$ values for selected detectors. The statistical information on these runs is summarized in Table 2. Again the data were well-fit by a linear dependence of $\Delta R_{js,max}/R_{jb,air}$ on $P/P°$ over the $P/P°$ range probed in these experiments.

Figure 12a shows that all of the test alcohols could all be distinguished from one another visually in principal component space when the responses of all detectors in the array are considered. Additionally, like the analytes in the broad test set, the normalized patterns of $\Delta R_{js,max}/R_{jb,air}$ were essentially invariant as the analyte concentration was varied. Identical behavior was observed for the alkanes, as seen in Figure 12b. Thus, the $\Delta R_{js,max}/R_{jb,air}$ pattern type is diagnostic of the analyte and the pattern height indicates the concentration of each of these analytes, at least under the conditions of these test runs.

Table 2. Correlation coefficients, intercepts, slopes, intercept errors, and errors in the slopes for three sets of analytes exposed at P/P° = 0.005-0.03.

	Poly(butadiene)				**Poly(epichlorohydrin)**		
	R^2	intercept	slope		R^2	intercept	slope
1-propanol	0.9998	-0.0136	0.2200	ethanol	0.9956	0.0024	0.0367
benzene	1.0000	-0.0429	0.5017	1-propanol	0.9990	-0.0048	0.0542
chloroform	0.9998	-0.0563	0.8509	1-butanol	0.9997	-0.0031	0.0629
cyclohexanone	1.0000	-0.0668	0.6128	1-pentanol	0.9992	-0.0060	0.0670
n-heptane	0.9993	-0.0003	0.1682	1-hexanol	0.9998	-0.0036	0.0703
nitrobenzene	0.9995	-0.0397	0.5656	1-heptanol	0.9991	-0.0033	0.0691
n-hexane	0.9994	-0.0344	0.1788				
n-heptane	0.9999	-0.0175	0.1659				
n-octane	0.9994	-0.0223	0.1688				
n-nonane	0.9995	-0.0294	0.1713				
n-decane	0.9988	-0.0162	0.1599				
n-dodecane	0.9997	-0.0136	0.1478				
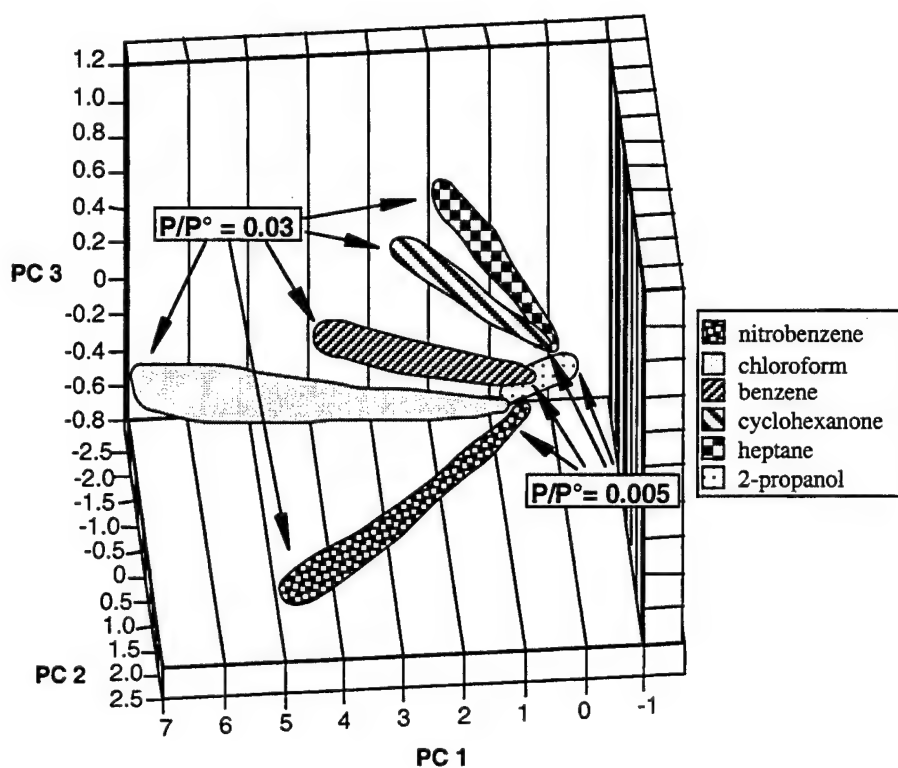
Figure 8. Data in principal component space from a 12-detector array exposed to n-heptane, cyclohexanone, benzene, chloroform, nitrobenzene, and 2-propanol. Each at P/P° = 0.005 to 0.03 in air in six even steps. The first three principal components depicted contained 98% of the total variance in the data. The ellipsoids contain 95% of the data for each analyte. Each analyte was presented 10 times to the array, with the order of presentation randomized over all repetitions of all test solvents.
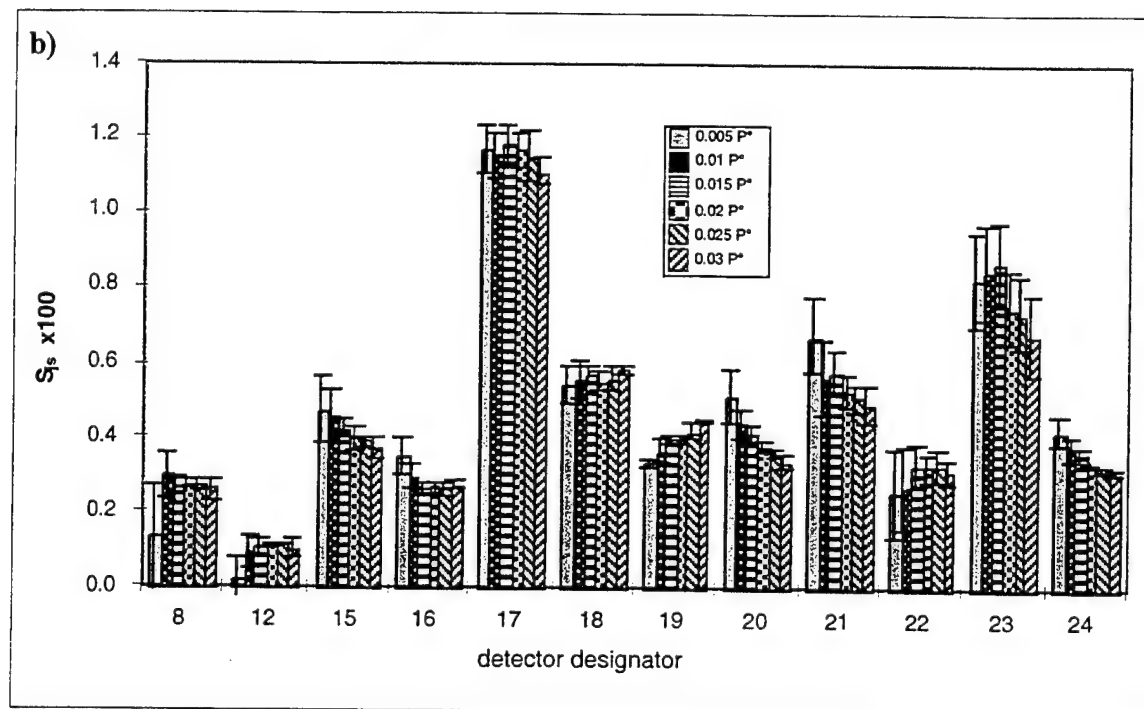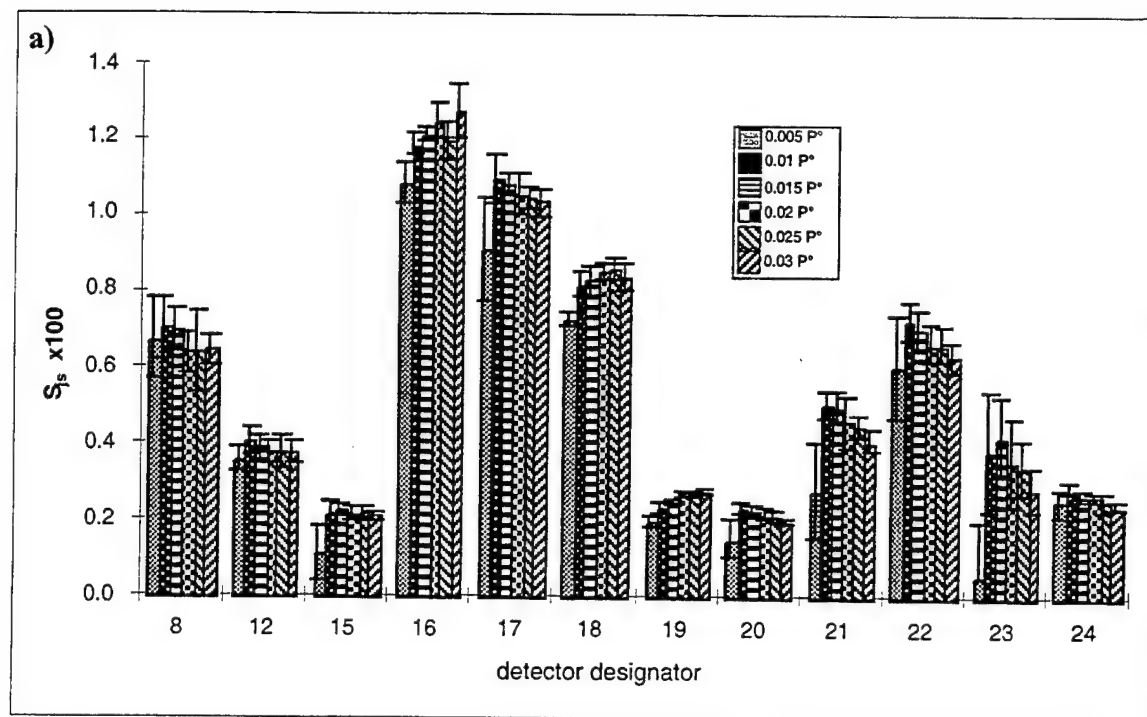
Figure 9. Histogram of the average normalized response of a 12-element array of carbon black-polymer detector films exposed to three analytes; **a)** Chloroform, **b)** Nitrobenzene, each presented 10 times at $P/P° = 0.005 - 0.03$ in air in six even steps. The data were normalized according to equation (1) in the text.
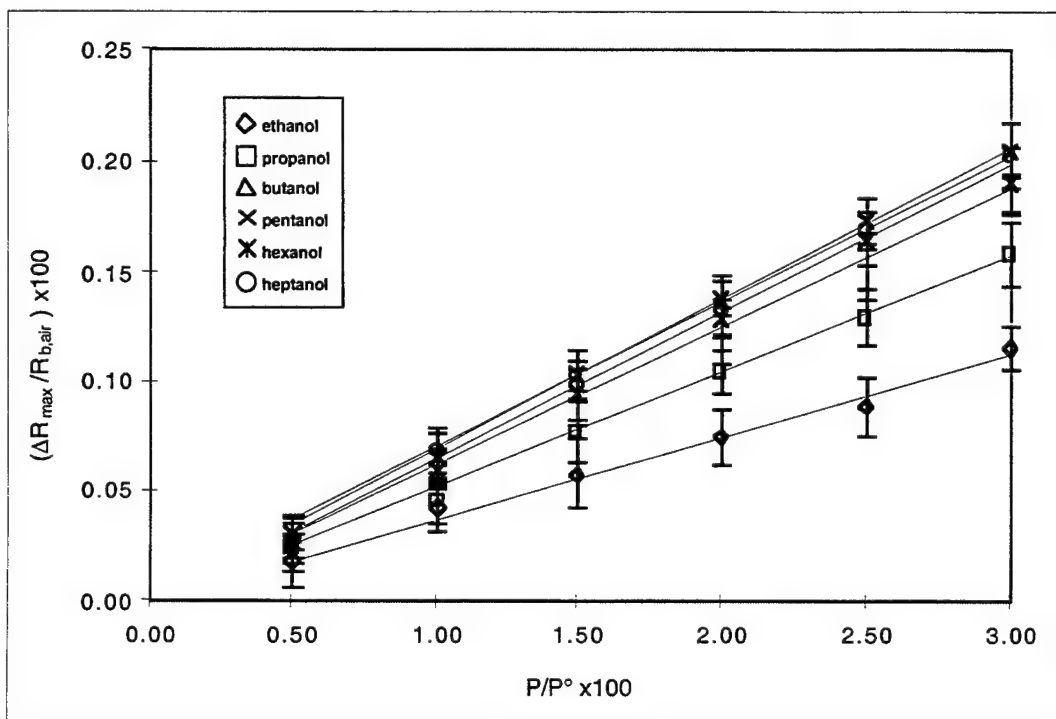
Figure 10. Maximum relative differential resistance responses, $\Delta R_{js,max}/R_{jb,air}$, of composite detector films consisting of carbon black and poly(epichlorohydrin), when exposed to ethanol, 1-propanol, 1-butanol, 1-pentanol, 1-hexanol, and 1- heptanol. Each at $P/P° = 0.005$ to 0.03 in six even steps in air. Each analyte was presented 10 times to the array, with the order of presentation randomized over all repetitions of all test solvents. The error bars represent 1σ values computed from 10 exposures at each $P/P°$.
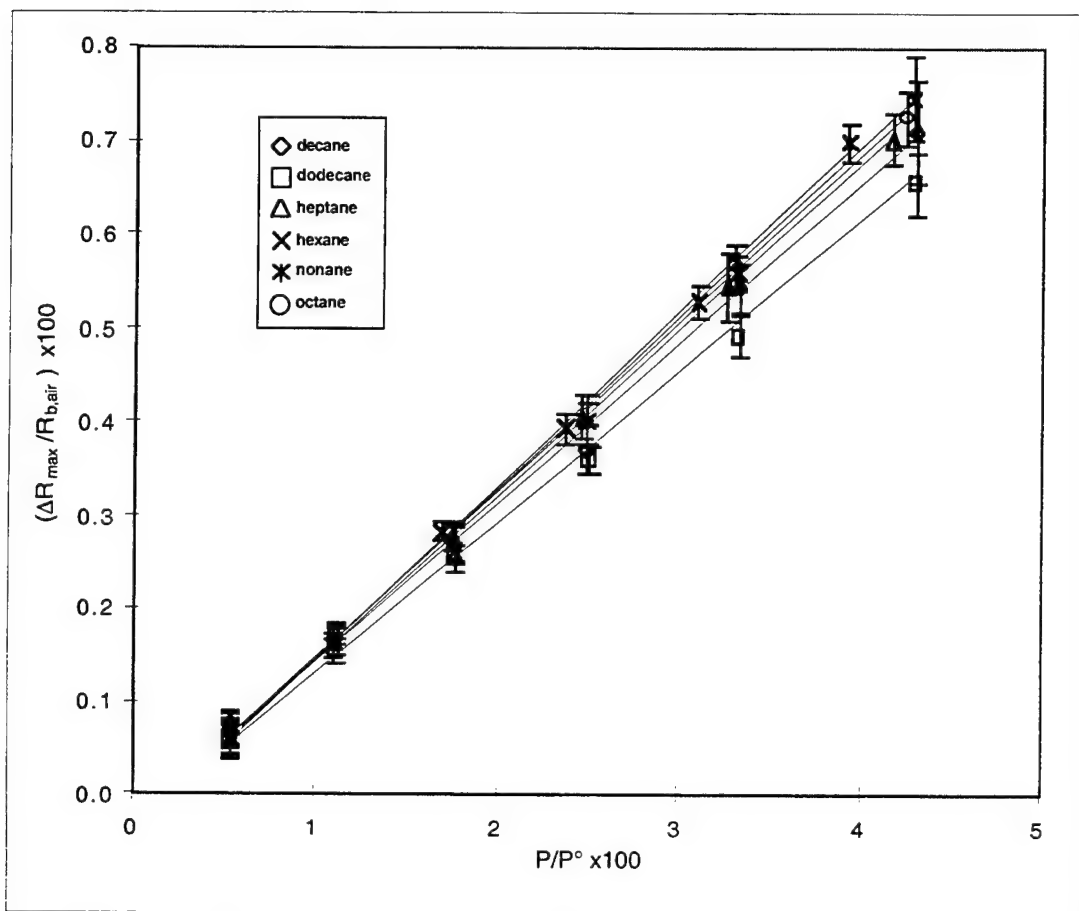
Figure 11. Maximum relative differential resistance responses, $\Delta R_{js,max}/R_{jb,air}$, of composite detector films consisting of carbon black and poly(butadiene), when exposed to n-dodecane, n-decane, n-nonane, n-octane, n-heptane, and n-hexane. Each at $P/P° = 0.005$ to 0.03 in six even steps in air. Each analyte was presented 10 times to the array, with the order of presentation randomized over all repetitions of all test solvents. The error bars represent 1σ values computed from 10 exposures at each $P/P°$.
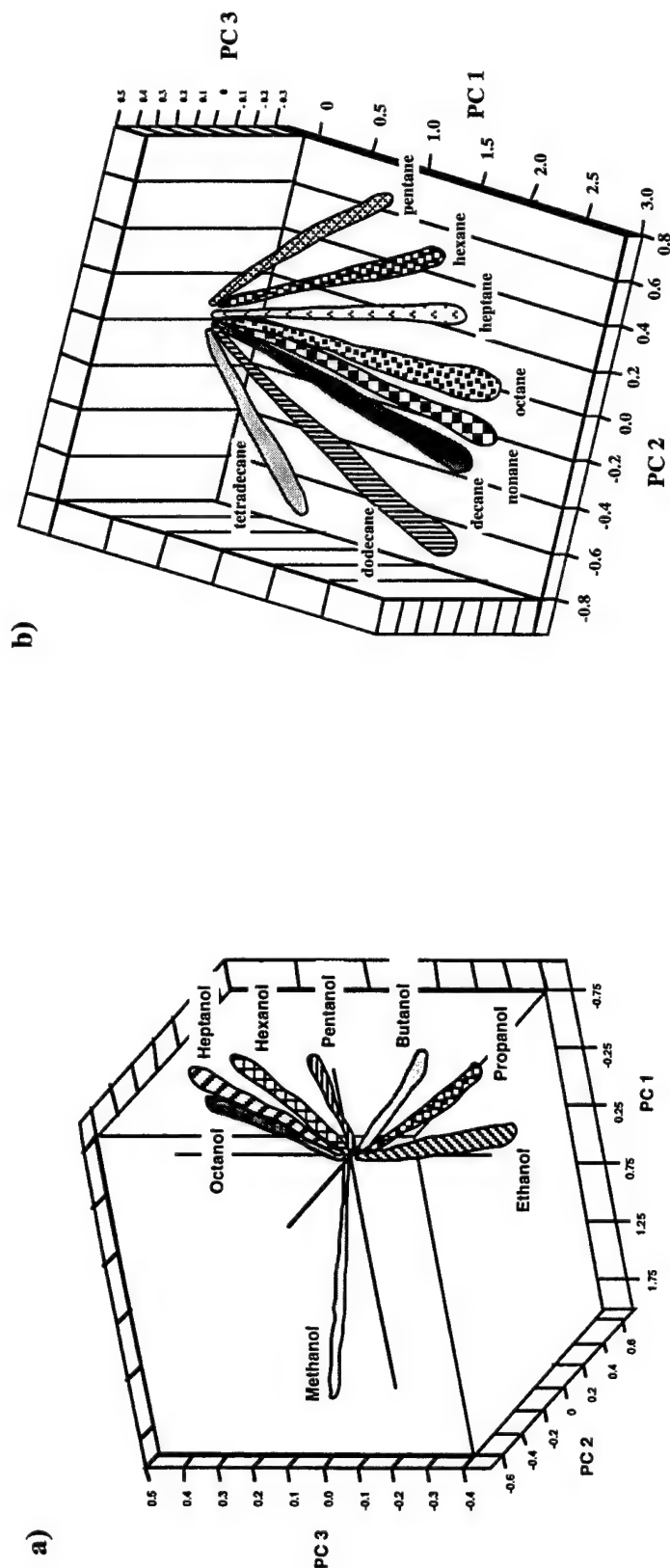
Figure 12. b) Data in principal component space from a 20-detector array exposed 5 times each to n-tetradecane, n-dodecane, n-decane, n-nonane, n-octane, and n-heptane each at $P/P^o = 0.005$ to 0.03 in air in 27 even steps. The first three principal components contain 99% of the total variance in the data. The ellipsoids contain 99% of the data for each analyte. All presentations in each set were randomized over all repetitions of all test solvents.

Figure 12. a) Data in principal component space from a 20-detector array exposed 10 times each to methanol, ethanol, 1-propanol, 1-butanol, 1-pentanol, 1-hexanol, 1-heptanol, and 1-octanol each at $P/P^o = 0.005$ to 0.03 in air in 27 even steps. The first three principal components contain 99% of the total variance in the data. The ellipsoids contain 99% of the data for each analyte.

27

2.3.2. Detector Response to Analytes in the Presence of Background Odors

The response of the detectors to various test vapors was also investigated when the detectors were first exposed to, and then maintained in the presence of, a fixed concentration of another solvent vapor. Figure 13 exhibits the $\Delta R_{js,max}/R_{jb,air}$ values displayed by poly(ethylene-co-vinyl acetate) and poly(caprolactone) detectors in response to varying concentrations of heptane in the range $0.005\ P° \leq P \leq 0.025\ P°$, relative to an air background gas flow. The responses for heptane vapor at $0.005\ P° \leq P \leq 0.015\ P°$ in air were then recorded when the detector was exposed to the analyte gas stream in the presence of a constant background gas that consisted of air with either 2-propanol, benzene, or cyclohexanone at $P/P° = 0.005$, 0.010, and 0.015 for each background gas. As displayed in Figure 13, $\Delta R_{jheptane,max}/R_{jb,s_1}$ and $\Delta R_{jheptane,max}/R_{jb,air}$ were essentially constant for s_1 = benzene, cyclohexanone, 2-propanol at the three values of $P/P°$. Figure 14 shows the same result in principal component space for the responses of the entire array of detectors, illustrating that this behavior is characteristic of the response pattern in the detector array as well as of the individual detectors displayed in Figure 13.

2.3.3. Detector Response to Binary Analyte Mixtures

Figure 15 shows the $\Delta R_{s2,max}/R_{jb,s1}$ and $\Delta R_{s1,s1+s2,max}/R_{jb,air}$ values of a carbon black-poly(ethylene oxide) detector to mixtures of benzene and heptane. For this detector for both the $\Delta R_{s2,max}/R_{jb,s1}$ and $\Delta R_{s1,s1+s2,max}/R_{jb,air}$ values, s_1 and s_2 were each presented to the detectors at $P/P° = 0.005$, 0.010, and 0.015. The linear dependence of $\Delta R_{js,max}/R_{jb}$ on $P/P°$ exhibited by an individual detector was maintained when the analyte was a constituent of a binary solvent mixture. The lines that have been drawn in Figure 15 to connect the data points also correspond to the change in response that would be expected based on the $\Delta R_{js,max}/R_{jb,air}$ behavior of the detector when presented with corresponding changes in the concentration of the individual solvent vapor in an air background. Additionally, the total $\Delta R_{js1+s2,max}/R_{jb,air}$ response to two solvents relative to a background air baseline was independent of whether the two solvents were exposed simultaneously or sequentially to the detector. Furthermore, in the case of sequential solvent vapor exposures, the maximum relative differential response values for a given solvent were independent of the order in which the solvents were presented to the detector. Figure 16 shows similar data, in principal component space, that was produced by an entire array of carbon black-polymer composite detectors during individual analyte exposure, and simultaneous and sequential exposures of binary mixtures of benzene and nitrobenzene. Similar behavior was observed for all nine binary mixtures explored in this work.

28
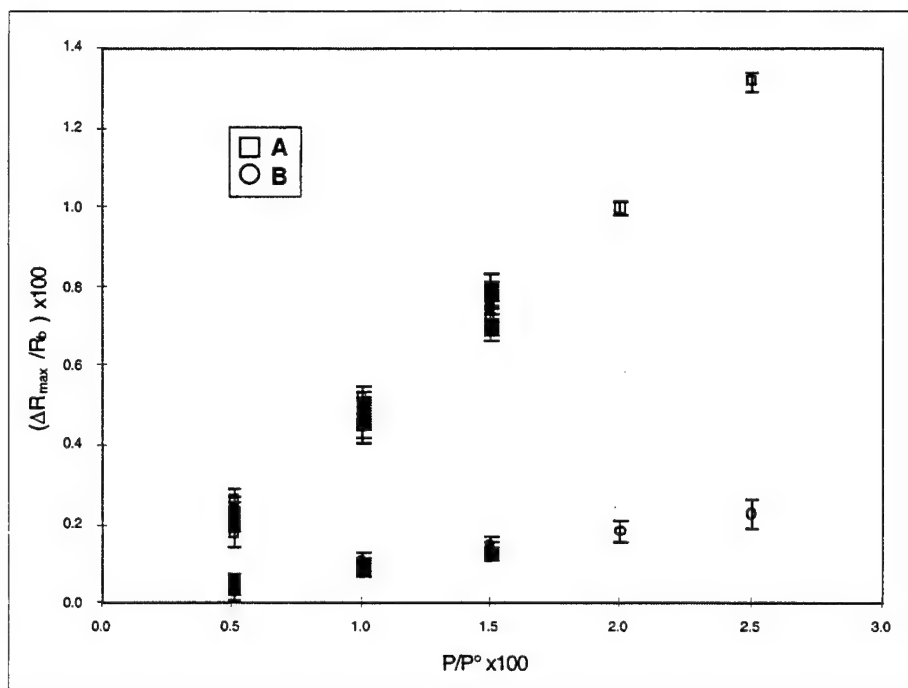
Figure 13. Maximum relative differential resistance responses, $\Delta R_{js,max}/R_{jb,air}$, of composite detector films consisting of carbon black and poly(ethylene-co-vinyl acetate), poly(caprolactone), when exposed to n-heptane at $P/P° = 0/005 - 0/025$ in air in five even steps (represented by the open symbols). Additional exposures (solid symbols) to n-heptane were performed at $P/P° = 0.005, 0.01,$ and 0.015 while the detector film was exposed to either benzene, cyclohexanone, or 2-propanol at $P/P° = 0.005, 0.01,$ or 0.015.

29
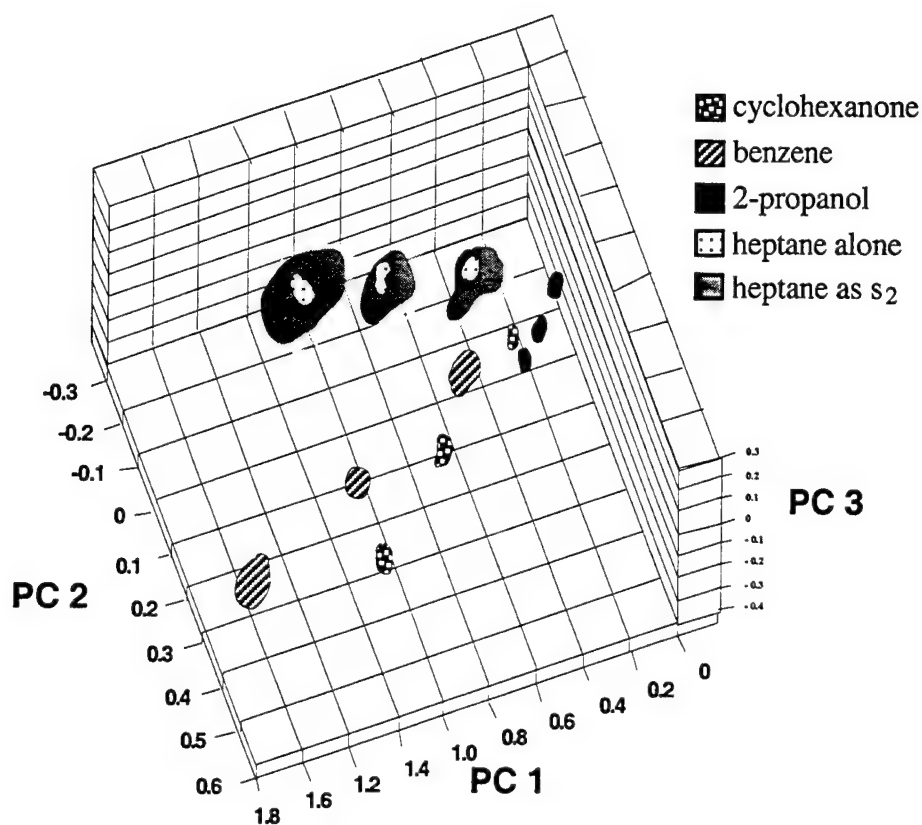
Figure 14. Data in principal component space from a 12-detector array exposed to n-heptane, benzene, cyclohexanone, or 2-propanol at $P/P^\circ = 0.005$, 0.01, and 0.015, and to exposures of n-heptane at $P/P^\circ = 0.005$, 0.01, and 0.015 while the detector film was exposed to either benzene, cyclohexanone, or 2-propanol each at $P/P^\circ = 0.005$, 0.01, or 0.015. The first three principal components contain 98% of the total variance in the data. The ellipsoids contain 95% of the data for each analyte. Each analyte was presented 5 times to the array, with the order of presentation randomized over all repetitions of all exposure types.

3 0
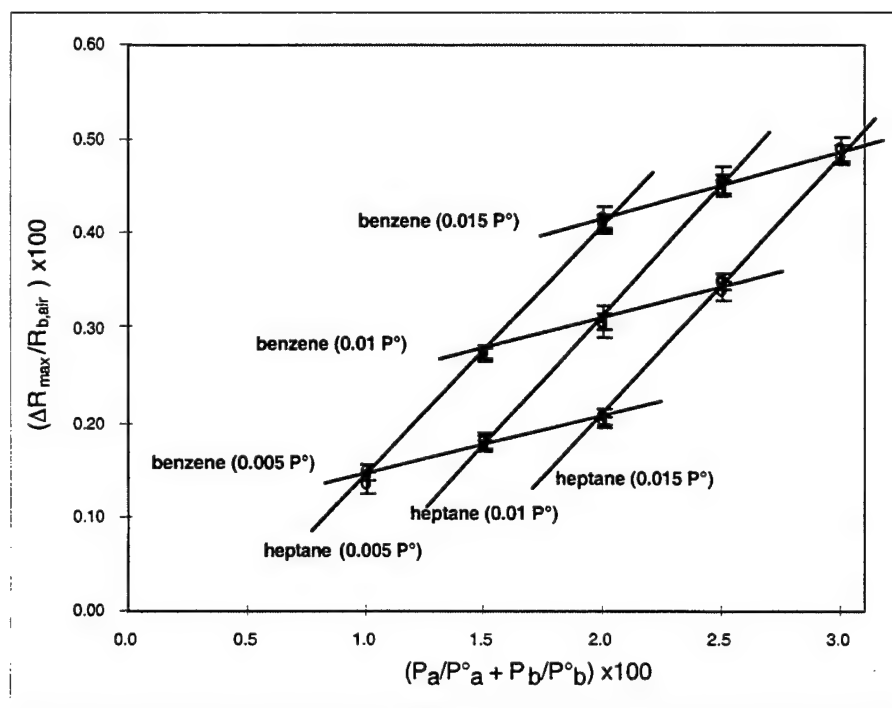
Figure 15. Maximum relative differential resistance responses of a poly(ethylene-co-vinyl acetate)-carbon black composite detector film when exposed to simultaneous and sequential binary mixtures of benzene at $P/P° = 0.005$, 0.01, or 0.015, and n-heptane at $P/P° = 0.005$, 0.01, or 0.015. Each of the 9 binary mixture combinations was presented 5 times to the array, with the order of presentation randomized over all repetitions. The error bars represent 1σ values computed from 5 exposures at each $P/P°$.
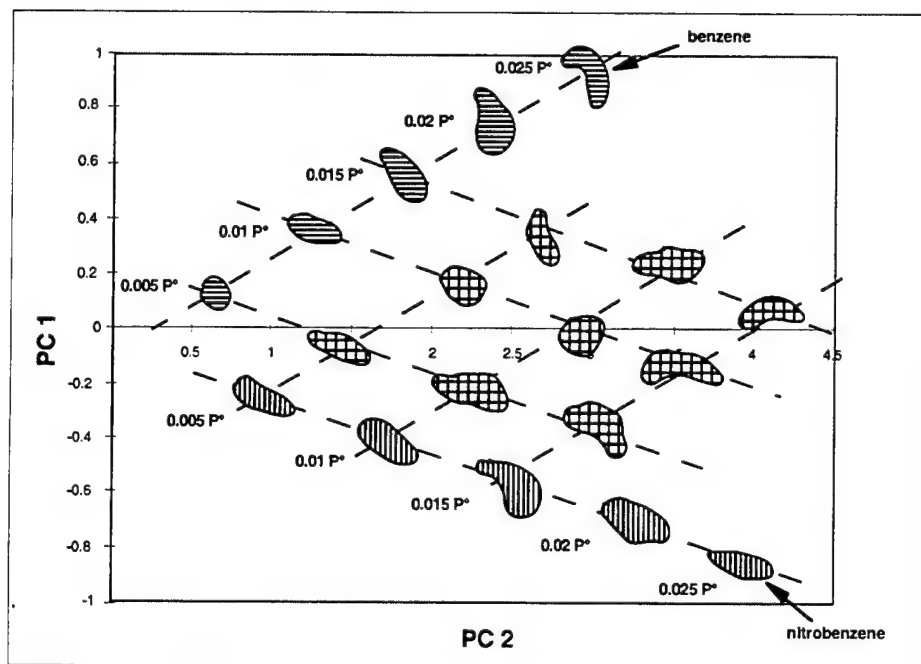
Figure 16. Data in principal component space from a 12-detector array exposed to benzene at $P/P° = 0.005$-0.025 in air in five even steps, nitrobenzene at $P/P° = 0.005$-0.025 in air in five even steps, and binary mixtures of benzene at $P/P° = 0.005$, 0.01, or 0.015, and nitrobenzene at $P/P° = 0.005$, 0.01, or 0.015. The first three principal components contain 99.6% of the total variance in the data. The ellipsoids contain 95% of the data for each analyte. Each analyte was presented 5 times to the array, with the order of presentation randomized over all repetitions of all exposure types. The error bars represent 1σ values computed from 5 exposures at each $P/P°$.

2.4. Discussion

2.4.1. Linearity of Detector Response vs. Analyte Concentration

The linearity in $\Delta R_{js,max}/R_{jb}$ response of the conducting organic polymer composite detectors vs. the concentration of a pure analyte is readily understood based on the signal transduction mechanism of these types of vapor detectors. Sorption of the vapor into the detector leads to swelling of the polymer, which then produces an increase in the electrical resistance through the network of conducting regions in the composite film. Although the absolute $\Delta R_{js,max}$ of the composite is sensitive to the fractional loading of the conductive filler in the insulating polymer of the conductive material,[35-37] the relative swelling of the film in response to the presence of an analyte vapor should remain constant provided that the filler material does not significantly affect the properties of the insulating portion of the composite. Under such conditions, the ratiometric quantity $\Delta R_{js,max}/R_{jb}$ is expected to be the key parameter that characterizes the response of conducting polymer composite vapor sensors to various analytes of interest. The present work quantitatively confirms these expectations.

Based on the expectations discussed above, for small fractional film swellings, the observed $\Delta R_{js,max}/R_{jb}$ response should be a linear function of the concentration of the vapor that partitions into the film. This appears to be the case for the solvents studied during the course of this work. This type of behavior has been observed for poly(pyrrole) conducting polymer vapor sensors,[38] and for vapor sensors that monitor the capacitance change of dielectric polymer films in response to the presence of vapor analytes, where again the response is a linear function of the analyte concentration.[39-41] Polymer films that are exposed to analytes that either bind very strongly to the polymer, or that induce significant structural distortions in the chains of the polymeric material, could certainly produce a saturation of the detector response at concentrations well below the saturated vapor pressure of the analyte; however, such behavior was not observed for any of the solvents or detectors explored in this work.

For mixtures, as long as the concentration of analyte molecules is dilute in the polymer film, the linear swelling relationship as a function of the analyte concentration in the vapor phase is expected to be a good microscopic description of the signal transduction properties of the detectors when exposed to combinations of these same gaseous analytes. Thus, the swelling response of a polymer to binary analyte mixtures is expected to be a weighted linear combination of the response to the individual analytes in the vapor phase. Previous work in our laboratory has shown that the fraction of the partial pressure of the odor, as opposed to the concentration of the odor, is the key variable in determining the response of the carbon black organic polymer composite vapor detectors.[42] Thus, to first order, the response of a polymer composite detector array to a mixture of solvents should be readily obtained by calculating the fractional composition of the constituents in the mixture relative to their individual vapor pressures under the experimental test conditions of concern. This additive behavior is, in fact, in excellent accord with experimental observations for the response of the conducting polymer composite arrays to the binary mixtures studied during the course of this work.

33

2.4.2. Implications for Algorithm Development/Pattern Recognition Requirements

All architectures that rely on array-based sensing require some type of training set and signal processing algorithm in order to classify and/or identify an analyte upon presentation to the detector array. In this respect, the performance and range of applicability of such detector arrays is intimately coupled to the data reduction algorithms and computational capabilities that are required to achieve the sensing task of concern.

The minimum possible training set, and the minimum requirements on computational capabilities to analyze a mixture or to classify and/or identify a particular analyte, are clearly achieved when the detector response is a linear function of the analyte concentration and when the differential detector response to the analyte of concern is independent of whether or not other analytes are present in the environment. Both of these conditions were met for the carbon black organic polymer composite chemiresistor response characteristics over the ranges of concentrations and for the ranges of analyte/background concentrations that were explored during the course of this study. This behavior contrasts with the properties reported for tin oxide chemiresistors[43] or for dye-impregnated organic polymer coatings on fiber optics,[15,43] whose responses are nonlinear with analyte concentration and/or with variations in environmental background. Such nonlinearities imply that significantly more computational resources and algorithm development will be required to achieve similar system performance in varying background environments or when an analyte concentration is to be quantified either alone or in a mixture of vapors. The exact tradeoffs imposed by more complex data reduction and more involved computational requirements, relative to the opportunity to exploit possibly increased information content of a richly varying signal response pattern, will be array and task specific, and will require a detailed analysis for the specific task of interest.

For odors that are more complex compositionally than simple binary or ternary mixtures of analytes, it could be envisioned that a single array-based detector response fingerprint would not be sufficient to produce a unique vector decomposition of the mixture into the signatures of each of the components of a training set of vapors. Thus, one response pattern might not be sufficient to provide a unique solution to the chemical composition of the odor mixture of concern. For example, if most of the variance amongst the data is contained in 3-5 principal components and if the cannonical variance tracks the total variance in the data, then mixtures of only 3-5 components can be decomposed uniquely from the use of the equilibrium response data alone. It is likely that, even for complex odors, useful information will be obtained, however, if some temporal or spatio-temporal variation in the composition of the odor is present. Under such conditions, changes in detector response can be identified with individual portions of the analyte based on their differential response patterns relative to the integrated baseline response of the odor on the detector array. The detector response characteristic that is least demanding on the signal processing and computational resources under such circumstances is when the pattern for an analyte remains linearly proportional to the analyte concentration regardless of the composition, or concentration, of the other components of the background ambient. This behavior was observed experimentally for the conducting polymer composite detectors for the various solvents and background ambient vapors evaluated in this work.

34

2.5. Conclusions

Under the conditions of this study, carbon black-organic polymer composite vapor detectors displayed a linear steady-state relative differential resistance signal in response to changes in the concentration of analyte vapor in the gas phase. This behavior was observed relative to either an air background or relative to a background that contained an organic solvent vapor in air. Moreover, the steady-state relative differential resistance response patterns produced by an array of carbon black-polymer composite detectors upon exposure to a test series of binary mixtures of analytes were the arithmetic sums of the maximum relative differential resistance responses that were obtained upon independent exposure of the array to each individual component of the mixture. This behavior implies that, under our test conditions, a relatively simple algorithm and training set, based on identifying a solvent vapor through its pattern type and quantifying the vapor concentration through the pattern height, would be sufficient to identify and quantify the test vapors and test vapor mixtures studied in this work.

3. The Relationship Between Resonant Frequency Changes on a Coated Quartz Crystal Microbalance, Thickness Changes, and Resistance Responses of Polymer-Carbon Black Composite Chemiresistors

3.1 Introduction

The resistance response of carbon black composites[3,4,31] can, in general, be understood by percolation theory, which relates the resistance response of a composite of an insulating polymer filled with regions of an electrical conductor to the change in volume fraction of the conducting (filler) phase of the composite.[35-37,44] The goal of the this portion of the work was to elucidate the factors that control the resistance change of such films in response to a change in the concentration of a vapor that is exposed to the detector. Unlike polymer-coated quartz crystal microbalances, where the frequency change of the detector is primarily determined by the change in mass of analyte sorbed into the polymer film for relatively small frequency shifts and/or small changes in the viscoelastic properties of the film[45,46] or polymer-coated surface acoustic wave devices, where changes in sorbed mass and modulus of the polymer film contribute to the detected signal,[13] the hypothesis that was challenged in this portion of the work is that the volume change, and thus the fractional swelling, of the polymer film upon exposure to a test vapor is the key variable that determines the change in dc electrical resistance of the carbon black-polymer composite detectors.

To test this hypothesis, we have performed measurements to determine the resonant frequency change of a film-coated quartz crystal microbalance (QCM) , the thickness change, and the resistance change of various composite and non-composite polymer films exposed to a variety of test organic vapors. The resonant frequency change and the dc electrical resistance changes of a set of carbon black-organic polymer composite films were determined on a QCM. QCM measurements and thickness measurements using fixed wavelength ellipsometry methods were then performed on clear (non-carbon black filled) films formed from the same polymers. Relationships between the two sets of measurements were facilitated because at a given analyte concentration in the vapor phase, the measured QCM resonant frequency changes were very similar for polymers that did, and did not, contain the carbon black filler material.

3.2 Experimental

QCM crystals (10 MHz, blank dia = 13.7 mm)) with a custom electrode pattern were obtained from International Crystal Manufacturing (ICM) in Oklahoma City, OK. The standard oscillation electrodes were configured at 90° angles to make room for two other tabs that would serve as electrodes for resistance measurements of the carbon black-polymer composite films (Figure 17). The crystals were polished to a surface roughness of less than 5 microns, which produced a mirror-like finish on the gold electrodes. To facilitate reflection of the ellipsometer's laser beam when the crystals were used with transparent films during the thickness measurements, one oscillator electrode was larger than the other (larger electrode dia. = 7.8 mm, smaller electrode dia. = 5.1 mm). The resistance tabs were not used during the thickness vs. QCM frequency measurements on films that were not filled with carbon black. Similarly, the ellipsometer was not used during the resistance vs. QCM frequency measurements, in which optically opaque, carbon-black filled, composite films were used.

36
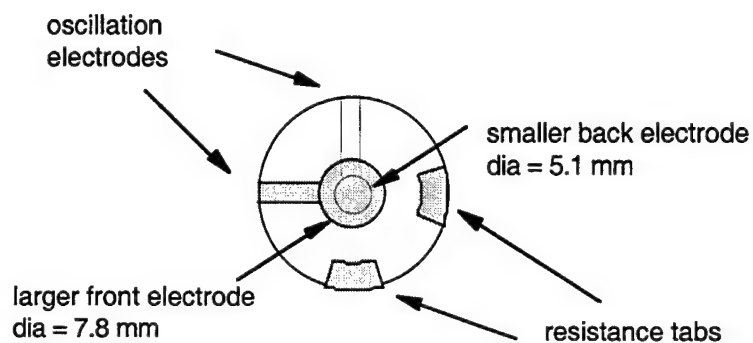
Figure 17. Custom 10 MHz quartz crystal microbalance with oscillation electrodes and tabs for reading the resistance of the composite film. Shaded areas indicate regions coated with Au. The larger electrode was used to facilitate ellipsometry measurements. The smaller back electrode is shown with solid lines.

The vapor stream was produced by passing general laboratory compressed air through analyte solvents contained in custom bubblers. The solvents used were HPLC quality (Aldrich Chemical Co.) and were used as received. Saturation of the vapor with solvent was confirmed by mass loss experiments.[33] The solvent-saturated air was then diluted to the desired concentration with lab compressed air. The air flows through the bubbler and in the background gas were regulated by needle valves, and the flows in both streams were monitored with Gilmont rotamers (VWR Scientific). The concentration of analyte in the vapor stream was independently verified using a calibrated flame ionization detector (California Analytical, Santa Ana, CA).

Two polymers were used in this work, poly(caprolactone) (PCL) and poly(ethylene oxide) (PEO). Films of these polymers that contained carbon black were used for the resistance measurements, while transparent, pure polymer films were used for the thickness measurements. All films were cast from standard solutions that consisted of 160 mg of polymer dissolved in 20 ml of benzene to which 40 mg of carbon black was added to the solutions used to make composite films (resulting in a solution that was 20% by weight of carbon black). All solutions were sonicated for at least 5 min immediately prior to casting the films. The polymer films were spun-cast on a Headway spin coater (Headway Research, Garland, TX) at 2000 rpm and the average film thickness was obtained by profilometry (Dektak 3030, Sloan Technology Corp., Santa Barbara, CA).

The QCM crystals were weighed before and after film application using a Cahn microbalance (resolution 0.001 mg; Cahn C-35, Orion Research, Beverly, MA) to obtain the mass of the films that were deposited over the active electrode (5.1 mm diameter area) of the QCM. The PCL clear film was 40 μg cm^{-2} and 375 nm thick, while the PCL-carbon black composite film was 185 μg cm^{-2} with a baseline resistance of $\approx$ 12 kΩ. The PEO clear film was 120 μg cm^{-2} and 1090 nm thick, while the PEO-carbon black composite film was 19 μg cm^{-2} with a baseline resistance of $\approx$ 16 kΩ. Using the clear polymer film areas and the mass and thickness values above, densities for the clear films of PEO and PCL were calculated and agreed with literature values for these polymers.

Resistance readings were measured using a Keithley 2002 digital multimeter (Cleveland, OH), and the resonant frequency of the QCM was obtained using a HP 5384A frequency counter (Palo Alto, CA). Ellipsometry measurements were taken on a Gaertner L116C ellipsometer (Gaertner Scientific, Chicago, IL). Optical constants were obtained for each surface before the films were applied. The index of refraction of each polymer film was taken from the literature. The absorption coefficient for the film was obtained using the two-angle technique[47,48] which also provided an independent measurement of the index of refraction and thickness of the film. The film thicknesses obtained by ellipsometry agreed to within 10% with the values obtained by profilometry.

To initiate an experiment, a baseline value was recorded for the QCM resonant frequency, resistance, and/or thickness of the film. The film was then exposed to analyte vapor until steady state values were reached as determined by constant output readings from the instruments. The data were recorded manually for convenience. Each thickness measurement was taken 3 - 5 times

3 8

after steady state had been reached for a given vapor, and the average result was recorded for both the baseline and steady-state, solvent-exposed values of concern.

3.3 Results

Figure 18a shows the relative thickness change, $\Delta h_{max}/h_b$, where Δh_{max} is the thickness change of the film during exposure to the analyte vapor and h_b is the baseline thickness of the film in air prior to analyte exposure, of poly(caprolactone) films as a function of the fraction of the analyte's vapor pressure, $P/P°$. The series of test vapors used in these experiments are representative of a broad test set of analytes that has been used previously to investigate the discrimination ability of arrays of conducting polymer composite vapor detectors.[3,4,31] The data of Figure 18a are well-fit to a linear dependence of $\Delta h_{max}/h_b$ vs. $P/P°$ (Table 3). Figure 19a shows similar data for poly(ethylene oxide) films.

Figures 18b and 19b depict the steady-state relative differential resistance responses, $\Delta R_{max}/R_b$, where ΔR_{max} is the resistance change of the film during exposure to the analyte vapor and R_b is the baseline resistance of the film in air prior to analyte exposure, of carbon-black filled poly(caprolactone) and poly(ethylene oxide) films, respectively, as a function of the analyte concentration, for the same set of test analytes. Over the concentration ranges probed in the experiment, the data are well-fit by straight lines passing though the origin (Table 3).

Figures 20a and 20b depict the mass-normalized maximum resonant frequency change, Δf^*_{max}, of the poly(caprolactone) films on a QCM crystal during exposure to the analyte vapor. The observed resonant frequency change was normalized by the mass of the films (as determined by the Cahn microbalance measurements) in the active QCM area to remove any variability due to the use of different film thicknesses and/or film masses between experiments on a given type of polymer. Figures 21a and 21b depict the same data for poly(ethylene oxide) films. Data are depicted for films of polymer that were, and were not, respectively, filled with carbon black. Again the data are well-fit by straight lines over the analyte concentration range of experimental interest (Table 3). For all the solvents, the Δf^*_{max} value of the pure polymer films was the same as the Δf^*_{max} value of the analogous carbon black filled composite, to within the error in the measurements. For example, Figure 22 depicts the Δf^*_{max} value as a function of $P/P°$ for $CHCl_3$ for poly(caprolactone) and poly(ethylene oxide) carbon black composites and for pure polymer films without carbon black added.

3.4 Discussion

Figure 23a depicts a plot of the dc relative differential resistance change of the poly(caprolactone) film, from electrical measurements, as a function of the fractional swelling of the polymer, as determined by optical ellipsometry measurements. The same analysis for a second poly(caprolactone) film is shown in Figure 23b to illustrate the variance in the data. For both polymer systems, the slopes and intercepts of the $\Delta R_{max}/R_b$ vs. $P/P°$ data for the composite films were used to predict what value of $\Delta R_{max}/R_b$ would be expected for the $P/P°$

Table 3. Correlation coefficients, slopes, intercepts, intercept error, and slope error for the eight solvents and two polymer systems used in this work. Mass-normalized maximum resonant frequency change, Δf^*_{max} vs. the fraction of the analyte's vapor pressure (Δf^*_{max} vs. P/P°), differential relative resistance increase vs. the fraction of the analyte's vapor pressure ($\Delta R_{max}/R_b$ vs P/P°), differential relative thickness increase vs. the fraction of the analyte's vapor pressure ($\Delta h_{max}/h_b$ vs P/P°), differential relative resistance increase vs. mass-normalized maximum resonant frequency change ($\Delta R_{max}/R_b$ vs Δf^*_{max}), and differential relative thickness increase vs. mass-normalized maximum resonant frequency change, ($\Delta h_{max}/h_b$ vs Δf^*_{max}) are tabulated.

PCL composite film	Δf^* max vs. P/P°					$\Delta R_{max}/R_b$ vs P/P°					$\Delta R_{max}/R_b$ vs Δf^* max				
	R^2	intcpt	slp	intcpt err	slp error	R^2	intcpt	slp	intcpt err	slp error	R^2	intcpt	slp	intcpt err	slp error
hexane	0.9997	0.00	3.64	0.006	0.034	0.9989	0.00	17.99	0.066	0.344	0.9991	0.01	11.61	0.059	0.197
isopropanol	0.9934	0.02	3.44	0.028	0.161	0.9933	0.04	15.93	0.130	0.754	0.9999	-0.05	10.88	0.018	0.070
benzene	0.9976	0.38	15.18	0.078	0.429	0.9968	0.40	76.98	0.456	2.520	0.9987	-1.52	11.89	0.330	0.252
dichloromethane	0.9998	-0.06	20.91	0.046	0.159	0.9993	-0.60	71.15	0.317	1.099	0.9987	-0.38	7.98	0.420	0.165
chloroform	0.9998	0.19	46.08	0.078	0.384	0.9988	0.21	145.40	0.604	2.962	0.9984	-0.38	7.40	0.694	0.170
hexafluorobenzene	0.9937	0.54	13.65	0.113	0.628	0.9969	0.78	35.03	0.203	1.124	0.9987	-0.58	5.99	0.158	0.127
dibromomethane	0.9974	-0.04	55.04	0.280	1.620	0.9960	-1.31	105.29	0.668	3.861	0.9991	-1.23	4.49	0.319	0.079
bromoform	0.9989	0.41	76.41	0.245	1.481	0.9982	-1.16	137.74	0.558	3.375	0.9983	-1.88	4.22	0.558	0.101

Table 3 (continued)

PCL clear film	Δf^* max vs. P/P°					$\Delta hmax/hb$ vs P/P°					$\Delta hmax/hb$ vs Δf^* max				
	R^2	intcpt	slp	intcpt err	slp error	R^2	intcpt	slp	intcpt err	slp error	R^2	intcpt	slp	intcpt err	slp error
hexane	0.9981	0.01	1.84	0.012	0.031	0.9909	0.02	0.55	0.008	0.021	0.9926	0.01	0.70	0.007	0.024
isopropanol	0.9971	-0.02	3.67	0.040	0.081	0.9932	-0.03	1.10	0.019	0.037	0.9987	-0.02	0.70	0.008	0.010
benzene	0.9956	0.18	10.40	0.039	0.273	0.9928	0.05	3.02	0.015	0.101	0.9967	0.00	0.68	0.011	0.015
dichloromethane	0.9992	-0.13	17.70	0.041	0.192	0.9963	-0.03	3.65	0.018	0.084	0.9950	0.00	0.48	0.020	0.013
chloroform	0.9984	0.00	42.96	0.121	0.685	0.9967	-0.03	8.43	0.033	0.189	0.9984	-0.03	0.46	0.023	0.007
hexafluorobenzene	0.9973	0.15	9.20	0.097	0.175	0.9984	-0.02	1.43	0.012	0.021	0.9985	-0.04	0.36	0.011	0.005
dibromomethane	0.9980	0.56	44.16	0.154	0.667	0.9989	-0.01	5.88	0.015	0.064	0.9993	-0.08	0.31	0.012	0.003
bromoform	0.9977	-0.05	66.71	0.187	1.256	0.9977	-0.05	7.94	0.022	0.151	0.9981	-0.04	0.28	0.020	0.005

PEO composite film	Δf^* max vs. P/P°					$\Delta Rmax/Rb$ vs P/P°					$\Delta Rmax/Rb$ vs Δf^* max				
	R^2	intcpt	slp	intcpt err	slp error	R^2	intcpt	slp	intcpt err	slp error	R^2	intcpt	slp	intcpt err	slp error
hexane	0.9985	0.01	0.97	0.003	0.014	0.9990	-0.02	9.89	0.025	0.117	0.9970	-0.06	23.83	0.044	0.479
isopropanol	0.9972	0.01	2.19	0.009	0.054	0.9992	0.11	22.57	0.048	0.305	0.9979	-0.02	24.13	0.079	0.527
benzene	0.9996	0.02	7.92	0.013	0.072	0.9963	0.13	69.49	0.358	2.006	0.9967	-0.07	20.59	0.342	0.561
dichloromethane	0.9993	0.13	16.60	0.073	0.255	0.9991	0.50	91.89	0.464	1.615	0.9986	-0.20	12.97	0.591	0.284
chloroform	0.9985	0.22	39.47	0.182	0.879	0.9975	1.34	210.58	1.260	6.096	0.9991	0.16	12.52	0.758	0.213
hexafluorobenzene	0.9979	0.11	6.91	0.034	0.185	0.9997	0.25	24.76	0.047	0.259	0.9968	-0.12	8.37	0.157	0.272
dibromomethane	0.9985	0.38	45.18	0.179	1.028	0.9975	0.47	143.09	0.726	4.176	0.9985	-0.73	7.43	0.586	0.168
bromoform	0.9989	0.23	55.20	0.179	1.069	0.9992	0.40	155.11	0.420	2.510	0.9998	-0.24	6.59	0.235	0.058

Table 3 (continued)

PEO clear film	Δf* max vs. P/P°					Δhmax/hb vs P/P°					Δhmax/hb vs Δf* max				
	R^2	intcpt	slp	intcpt err	slp error	R^2	intcpt	slp	intcpt err	slp error	R^2	intcpt	slp	intcpt err	slp error
hexane	0.9975	0.00	0.60	0.006	0.014	0.9922	0.00	0.26	0.004	0.011	0.9945	0.00	1.01	0.004	0.036
isopropanol	0.9986	0.01	2.12	0.012	0.040	0.9980	0.02	0.92	0.006	0.020	0.9989	0.01	1.01	0.004	0.017
benzene	0.9966	0.05	5.72	0.021	0.167	0.9929	0.03	2.41	0.013	0.102	0.9963	0.01	0.99	0.010	0.030
dichloromethane	0.9916	0.05	14.55	0.094	0.600	0.9892	0.04	3.88	0.028	0.182	0.9970	0.02	0.63	0.015	0.015
chloroform	0.9975	0.04	38.52	0.052	0.789	0.9957	0.02	9.94	0.018	0.267	0.9983	0.01	0.61	0.011	0.010
hexafluorobenzene	0.9986	-0.01	2.05	0.016	0.031	0.9981	0.00	0.39	0.003	0.007	0.9989	0.01	0.44	0.003	0.006
dibromomethane	0.9978	0.13	40.44	0.062	0.742	0.9974	0.03	7.48	0.013	0.150	0.9985	0.00	0.43	0.010	0.006
bromoform	0.9905	0.06	51.26	0.139	1.972	0.9905	0.01	8.61	0.023	0.331	0.9986	0.00	0.39	0.009	0.006
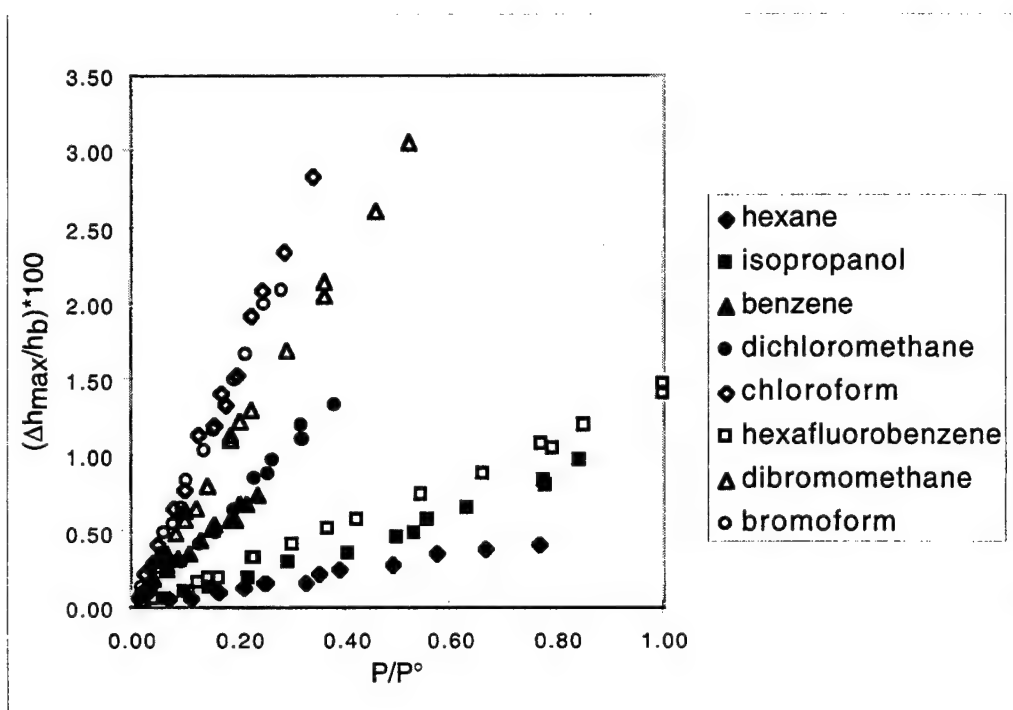
Figure 18. a) Differential thickness increase for a pure PCL film vs. fraction of analyte vapor pressure exposed to the film.
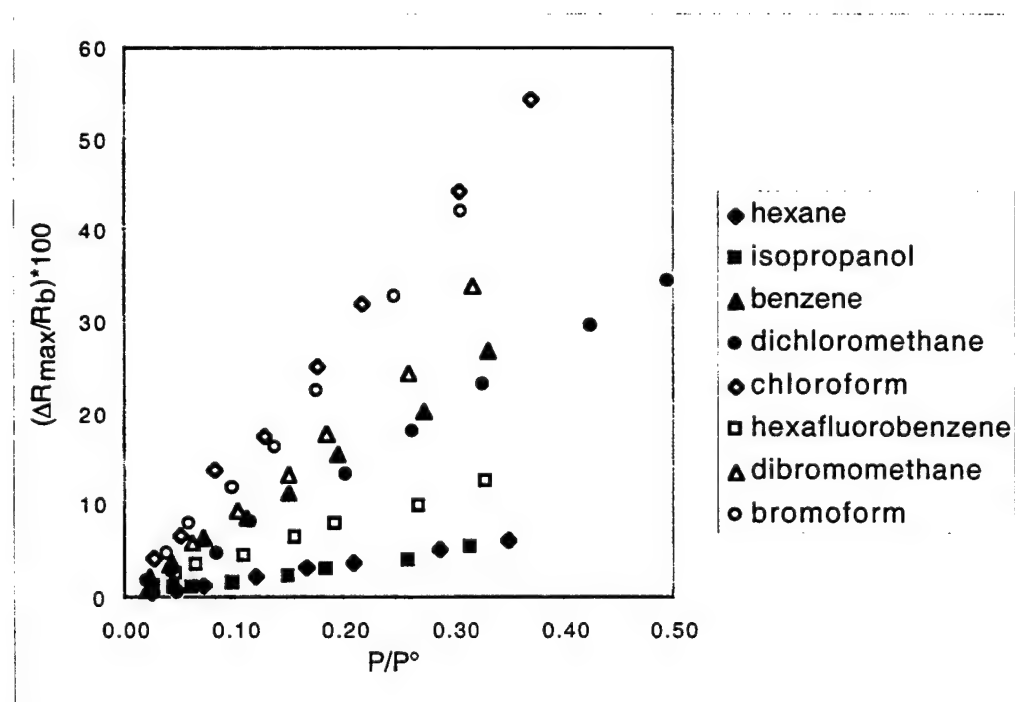
Figure 18. b) Differential relative resistance increase in a PCL-carbon black composite vs. fraction of analyte vapor pressure exposed to the film.

43
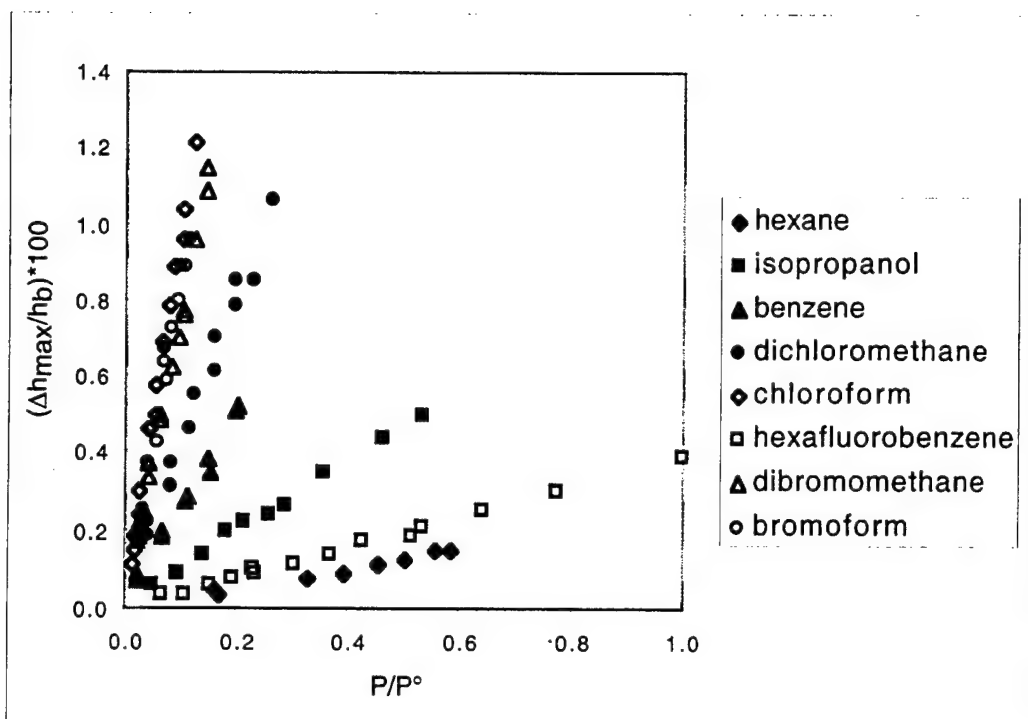
Figure 19. a) Differential thickness increase for a pure PEO film vs. fraction of analyte vapor pressure exposed to the film.
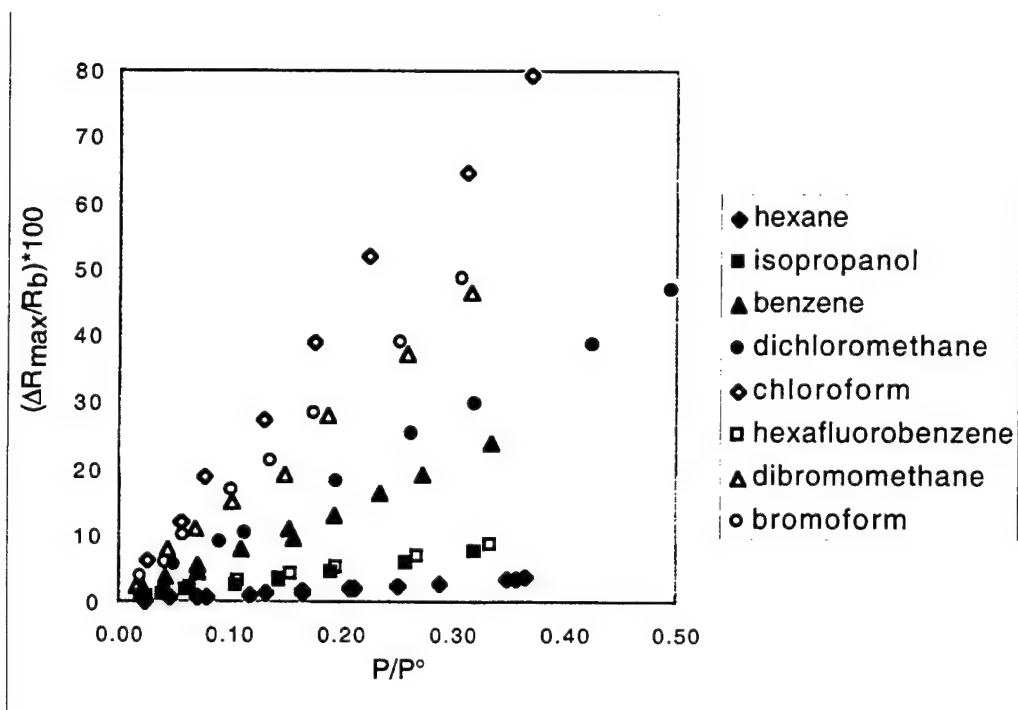
Figure 19. b) Differential relative resistance increase in a PEO-carbon black composite vs. fraction of analyte vapor pressure exposed to the film.

44
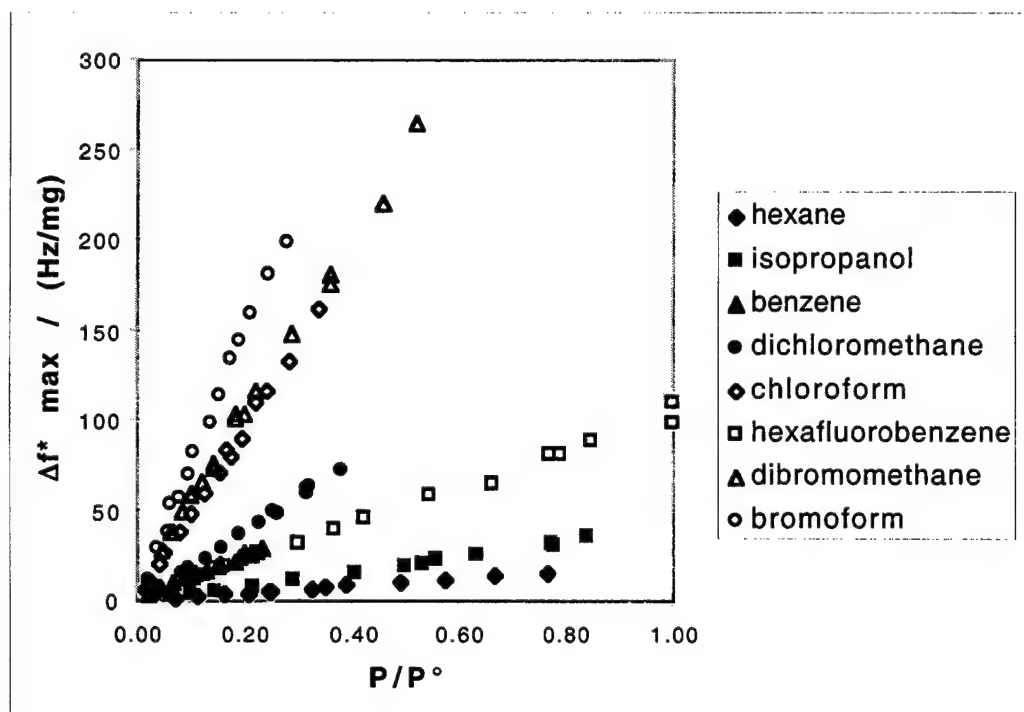
Figure 20. a) Mass-normalized maximum resonant frequency change, $Df^*_{max,}$ vs. fraction of analyte vapor pressure exposed to the film for a PCL film without carbon black.
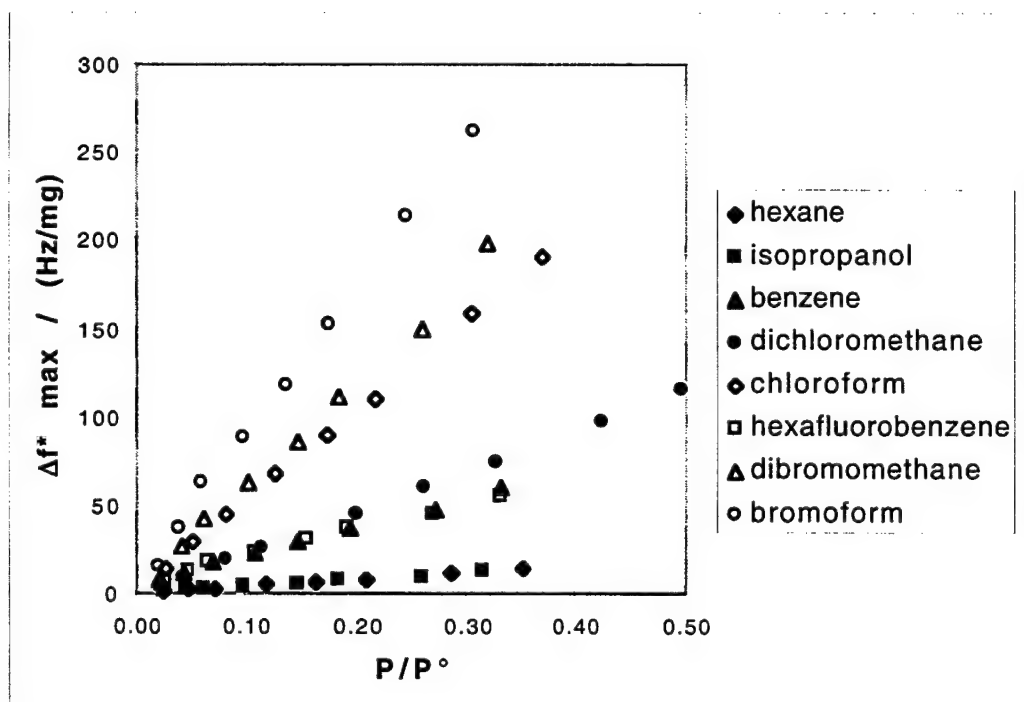
Figure 20. b) Mass-normalized maximum resonant frequency change, $Df^*_{max,}$ vs. fraction of analyte vapor pressure exposed to the film for a PCL carbon black composite.
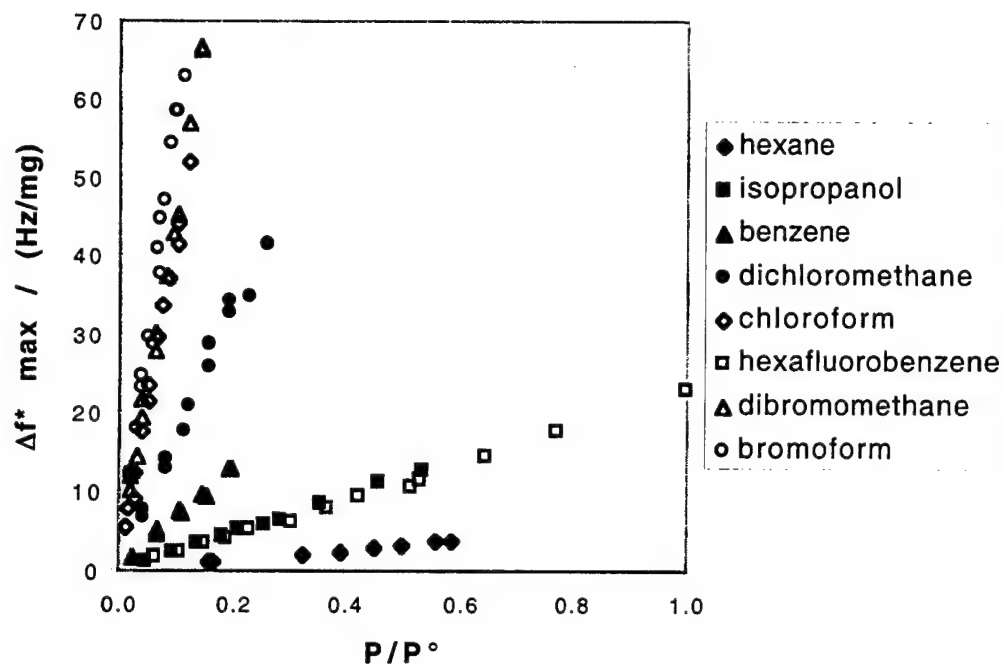
Figure 21. a) Mass-normalized maximum resonant frequency change, $Df^*_{max,}$ vs. fraction of analyte vapor pressure exposed to the film for a PEO film without carbon black.
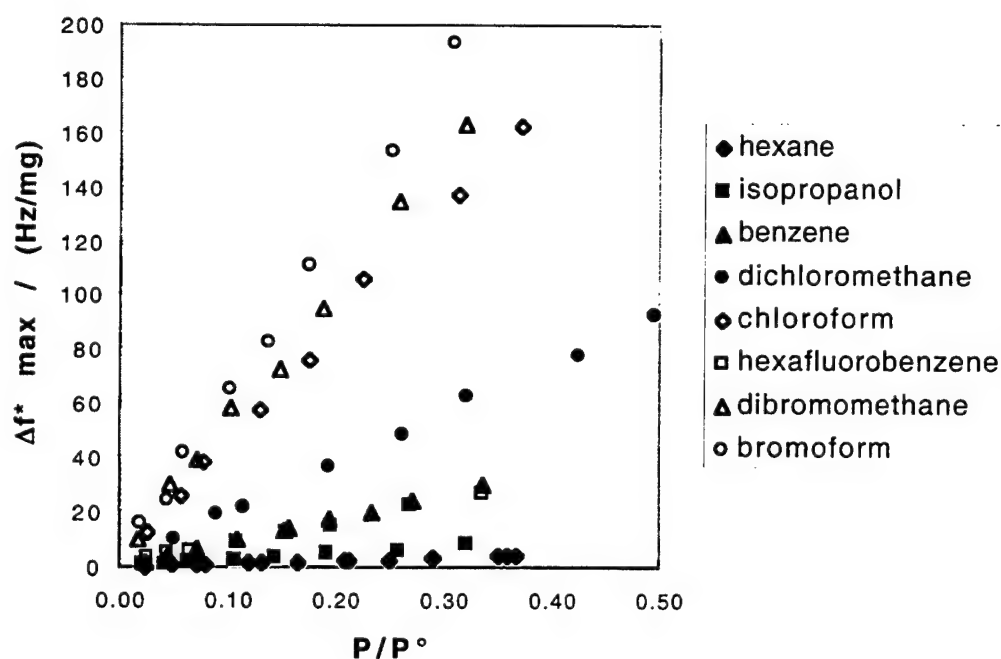
Figure 21. b) Mass-normalized maximum resonant frequency change, $Df^*_{max,}$ vs. fraction of analyte vapor pressure exposed to the film for a PEO carbon black composite.
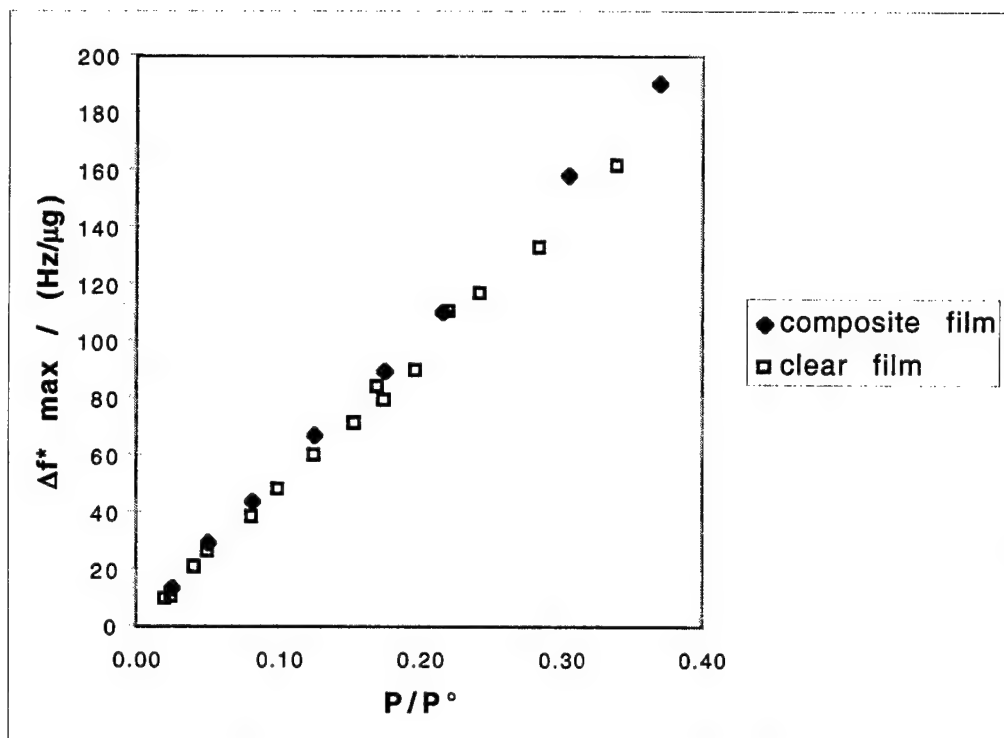
Figure 22. **a)** Mass-normalized maximum resonant frequency change, $Df^*_{max,}$ vs. fraction of analyte vapor pressure exposed to the film for PCL-carbon black composite and PCL films without carbon black.
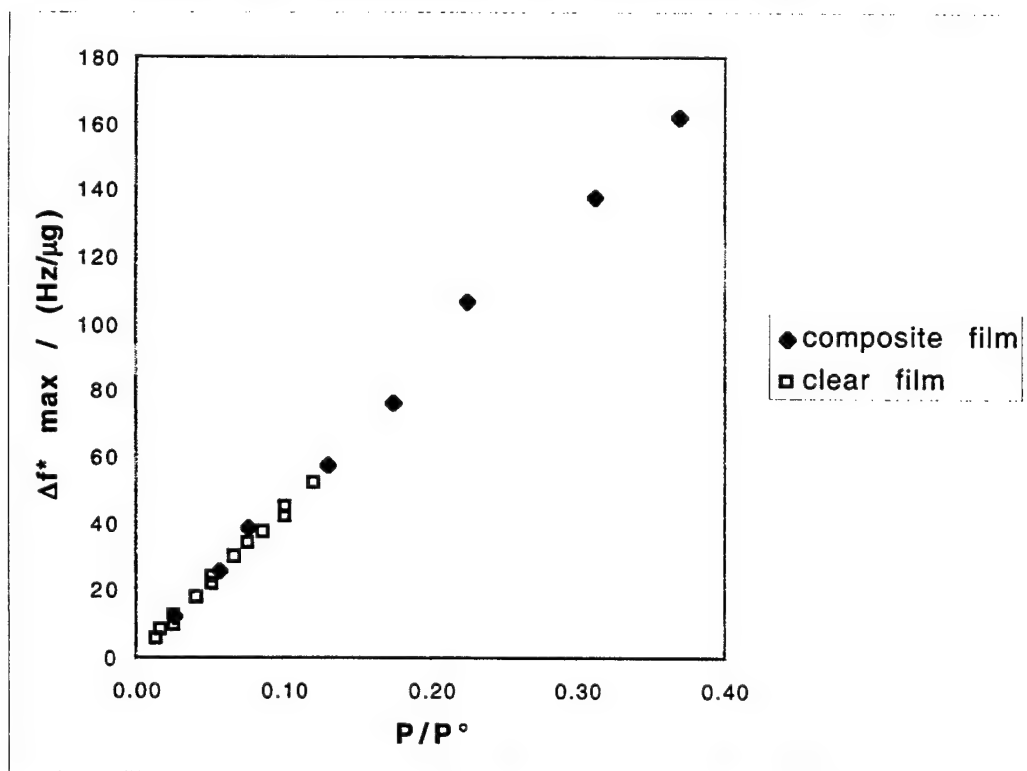
Figure 22. **b)** Mass-normalized maximum resonant frequency change, $Df^*_{max,}$ vs. fraction of analyte vapor pressure exposed to the film for PEO-carbon black composites and PEO films without carbon black.

a)
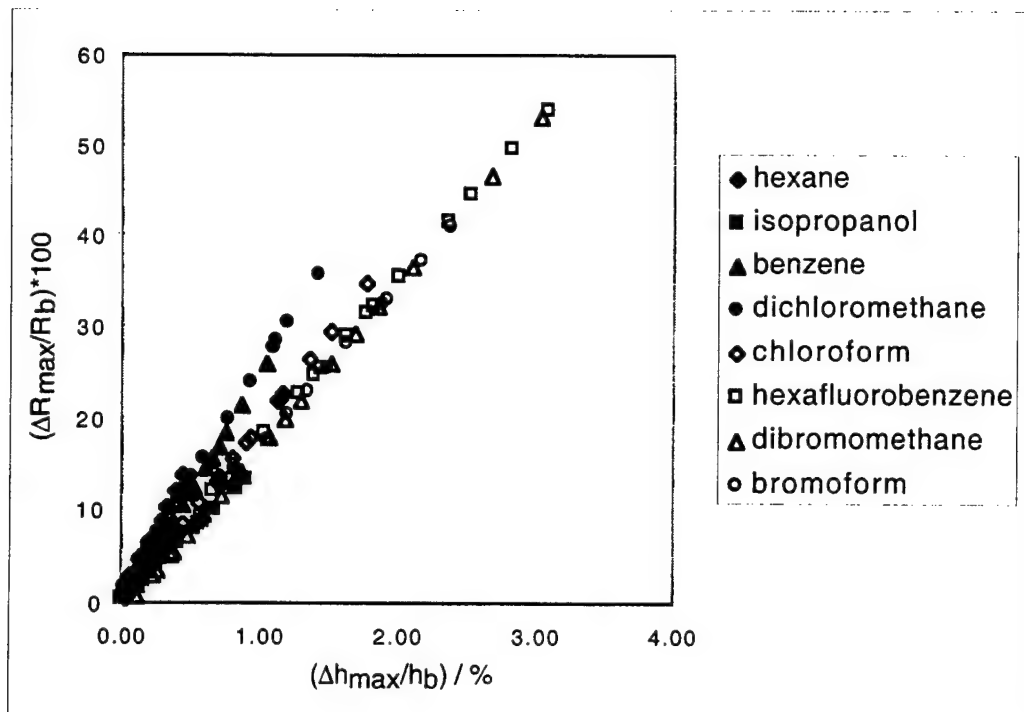
b)
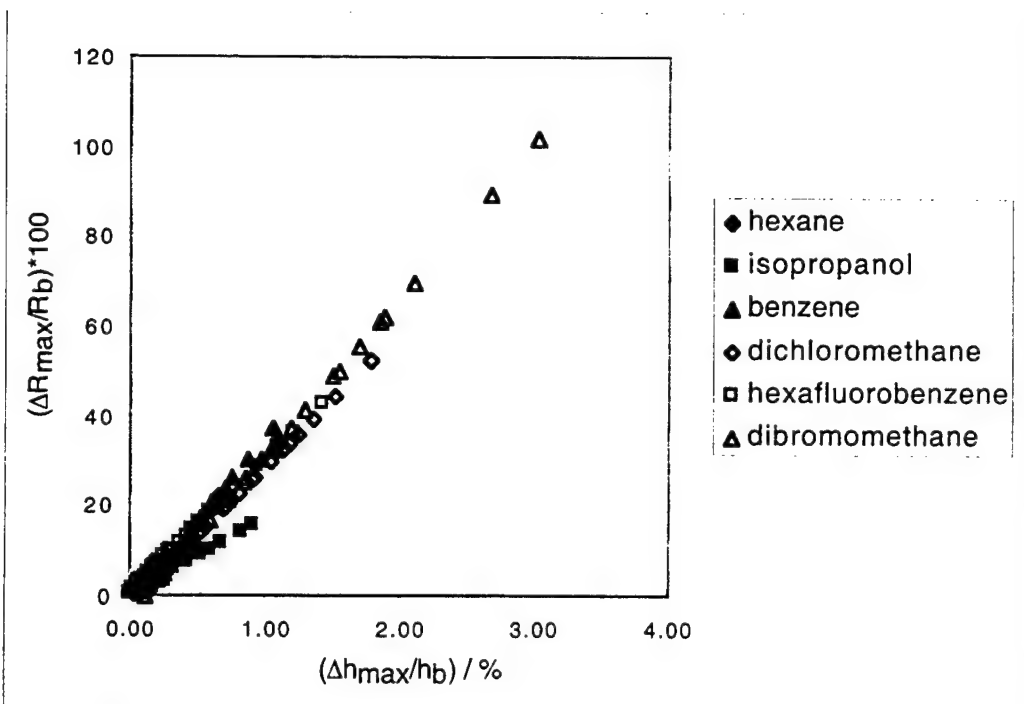
Figure 23. Relative resistance increase for a PCL-carbon black composite film verses relative thickness increase for a PCL clear film when both films were exposed to various analytes at various fractional vapor pressures, correlated by the analyte fractional vapor pressure for two separate (**a** & **b**) PCL films.

48

values used in measurement by the non-filled polymer films. Likewise, the slopes and intercepts of the $\Delta h_{max}/h_b$ vs. P/P° data for the non-filled polymer films were used to predict what value of $\Delta h_{max}/h_b$ would be expected for the P/P° values used in measurement by the composite films. The predicted values of $\Delta R_{max}/R_b$ were then plotted vs. the predicted $\Delta h_{max}/h_b$ values at the corresponding P/P° value of the analyte. As displayed in Figure 23, the data are linear and roughly fall on the same line for all of the test vapors investigated in this work. In each film some solvents do not lie on the common line, but this is presumed to be due to experimental error in the delivery of the vapor. (The relationship between the resistance change and the volume swelling depends on the carbon black loading and other parameters involved in making the films. Under controlled conditions when several films are made in a single batch process from a single carbon black/polymer suspension, the variability in response between films to a given analyte concentration is typically less than 10% . The higher variability between the two films of Fig. 23 results from the fact that they were made on two separate occasions with no attempt to control fully the deposition process or the suspension properties for consistency between batches.) A robust interpretation of the relatively small deviations of the behavior of the various analytes on a given polymer film vs the common line would require implementation of methods that could determine the resistance and thickness changes simultaneously on one detector, and such methods were not available in this study. The data of Figure 23 clearly indicate that regardless of the analyte used, a given fractional thickness change of the polymer produces a given steady-state relative differential resistance response of the corresponding carbon-filled composite, at least for the polymer-analyte combinations explored in this work. Thus, the hypothesis of concern -- that volumetric film swelling is the key variable determining $\Delta R_{max}/R_b$ in the composite carbon black-insulating polymer detectors -- seems to be confirmed from the data obtained in this work, at least for the analytes and polymers investigated to date. Also, these data indicate that the relationship between relative thickness change and steady-state relative differential resistance change is linear, at least over the range of analyte concentrations investigated in this work.

One complicating factor is that the thickness measurements obtained in this work were performed on pure polymeric materials, while the $\Delta R_{max}/R_b$ measurements were performed on carbon black-filled polymer composites. The assumption made above in interpreting the data of Figure 23 is that the volumetric swelling of the polymer is similar whether or not the material is filled with carbon black. Given the linear relationship deduced between $\Delta h_{max}/h_b$ and $\Delta R_{max}/R_b$, and the low intuitive likelihood that, over a range of analytes and concentrations, two separate functional dependencies of swelling on analyte concentration would precisely counteract each other to yield the data of Figure 23, this assumption seems quite reasonable. Given the linear dependence of $\Delta R_{max}/R_b$ on P/P° that has been observed for other test analytes,[49] it seems reasonable to assume that the relationship between relative volumetric swelling and relative differential resistance measurements is extendible, at least to first order, for those composite-analyte combinations as well.

An independent check on the validity of the relationship between swelling in the carbon-black filled composites and the pure polymer films is available through the QCM resonant frequency measurements. The relationship between $\Delta R_{max}/R_b$ vs. Δf^*_{max} and $\Delta h_{max}/h_b$ vs. Δf^*_{max} is

linear as seen in Figure 24 for PCL and Figure 25 for PEO (See also Table 3). The slopes and intercepts of the $\Delta R_{max}/R_b$ vs. Δf^*_{max} data for the composite films were used to predict what value of $\Delta R_{max}/R_b$ would be expected for the Δf^*_{max} values measured for the non-filled polymer films at the various analyte concentrations used in the measurements. Likewise, the slopes and intercepts of the $\Delta h_{max}/h_b$ vs. Δf^*_{max} data for the non-filled polymer films were used to predict what value of $\Delta h_{max}/h_b$ would be expected for the Δf^*_{max} values measured for the composite films at the various analyte concentrations used in the measurements. The predicted value of $\Delta R_{max}/R_b$ was then plotted vs. the predicted $\Delta h_{max}/h_b$ values at the corresponding $P/P°$ value of the analyte. As displayed in Figure 26, the data for each solvent are linear and roughly fall on the same line for all of the test vapors investigated in this work. This strongly implies the presence of a correlation between volume change and resistance change in these composite films. This is a stronger indicator than the correlation through $P/P°$ because the Δf^*_{max} for each presentation for each film was taken simultaneously with the $\Delta R_{max}/R_b$ and $\Delta h_{max}/h_b$ measurements. The correlation calculated through $P/P°$ presented above was less precise due to variance in the flow system, whereas any changes in the concentration of the exposed analyte would be reflected in the Δf^*_{max} as well.

In our work, the frequency shift of the polymer-coated QCM crystals arising from sorption of the analyte vapor was <2% of the resonant frequency of the polymer-coated crystal. Under such conditions prior work has concluded that mechanical losses are minimal and that the frequency shifts are predominantly due to changes in mass uptake.[8a] Although under such conditions the frequency shifts observed in the QCM data can be related, through the proportionality between Δf_{max} and Δm_{max} implied by the Sauerbrey equation[8a,b], to the fractional mass uptake of these films, the validity of this relationship is not necessary to support any of the key conclusions of our study. Regardless of the physical phenomena that produce a shift in the resonant frequency of the polymer-coated QCM crystals upon vapor sorption, it is clear that the key variable that correlates with the $\Delta R_{max}/R_b$ response of various analytes for a given type of polymer is not Δf_{max}, Δf^*_{max}, or $\Delta m_{max}/m_b$ (with Δm_{max} deduced from Δf_{max} through the Sauerbrey equation), but instead that the experimentally-observed correlation is between $\Delta R_{max}/R_b$ and $\Delta h_{max}/h_b$.

Further support for the swelling-induced resistance change hypothesis can be obtained by investigating the relationship between $\Delta R_{max}/R_b$ and $\Delta h_{max}/h_b$ as a function of analyte density. As seen in Figures 27 and 28, the slopes of the $\Delta h_{max}/h_b$ vs. Δf^*_{max} lines and the $\Delta R_{max}/R_b$ vs. Δf^*_{max} lines depend linearly on the density (as measured in the pure liquid phase) of the sorbing species. These data are in agreement with recently reported results that were obtained in parallel with our study, in which the relative differential resistance response of carbon black filled poly(ethylene oxide) composites was shown to correlate with the density of the gaseous analyte (as measured in its pure liquid phase).[50]

50
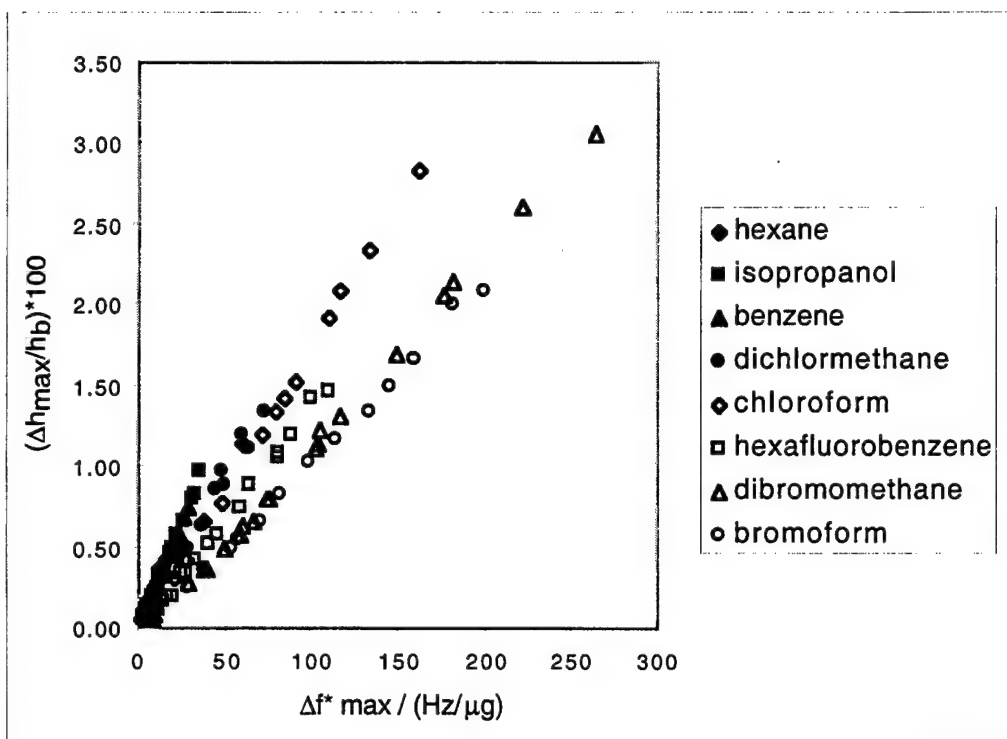
Figure 24. a) Differential relative thickness increase vs. mass-normalized maximum resonant frequency change, $\Delta f^*_{max,}$ for a PCL film when exposed to various analyte fractional vapor pressures.
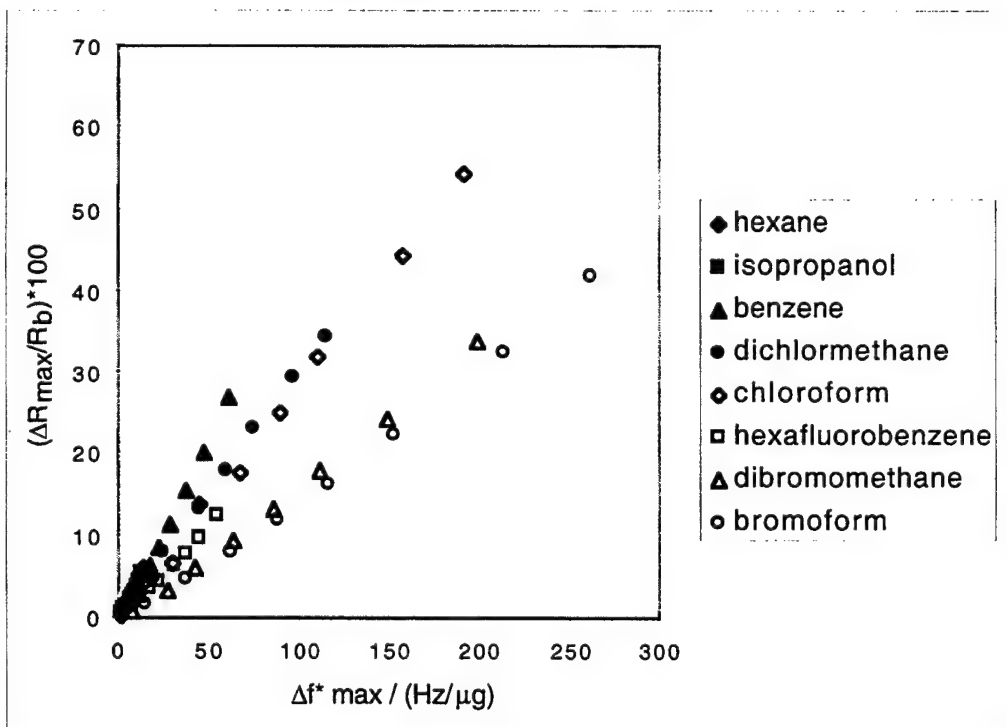
Figure 24. b) Differential relative resistance increase vs. Δf^*_{max} for a PCL film when exposed to various analyte fractional vapor pressures.
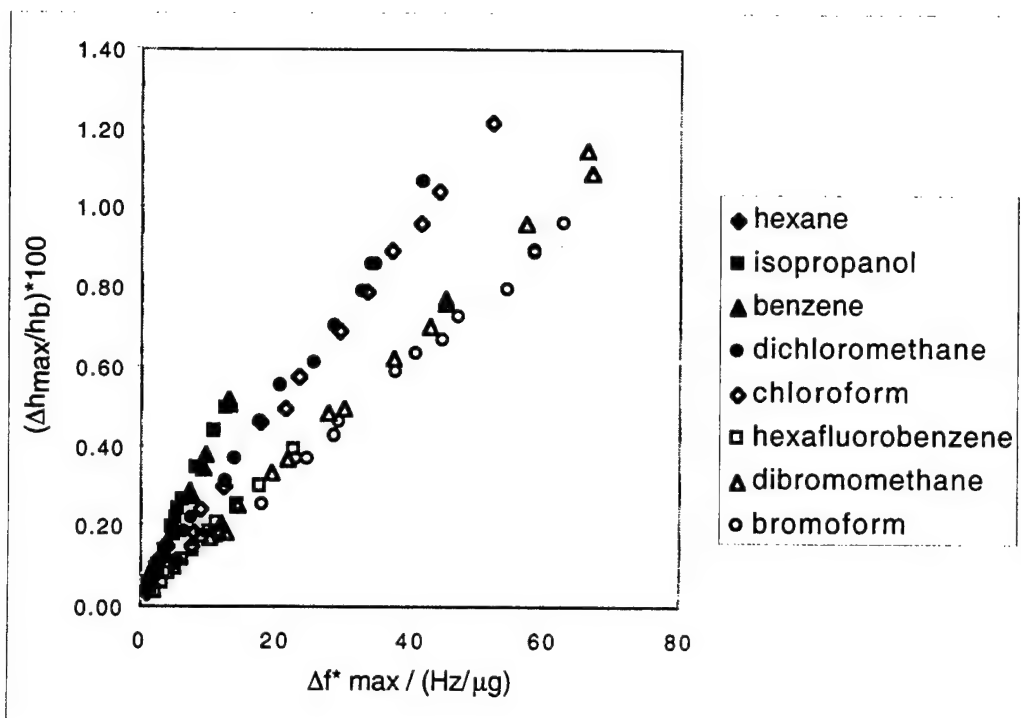
Figure 25. a) Differential relative thickness increase vs. mass-normalized maximum resonant frequency change, $Df^*_{max,}$ for a PEO film when exposed to various analyte fractional vapor pressures.
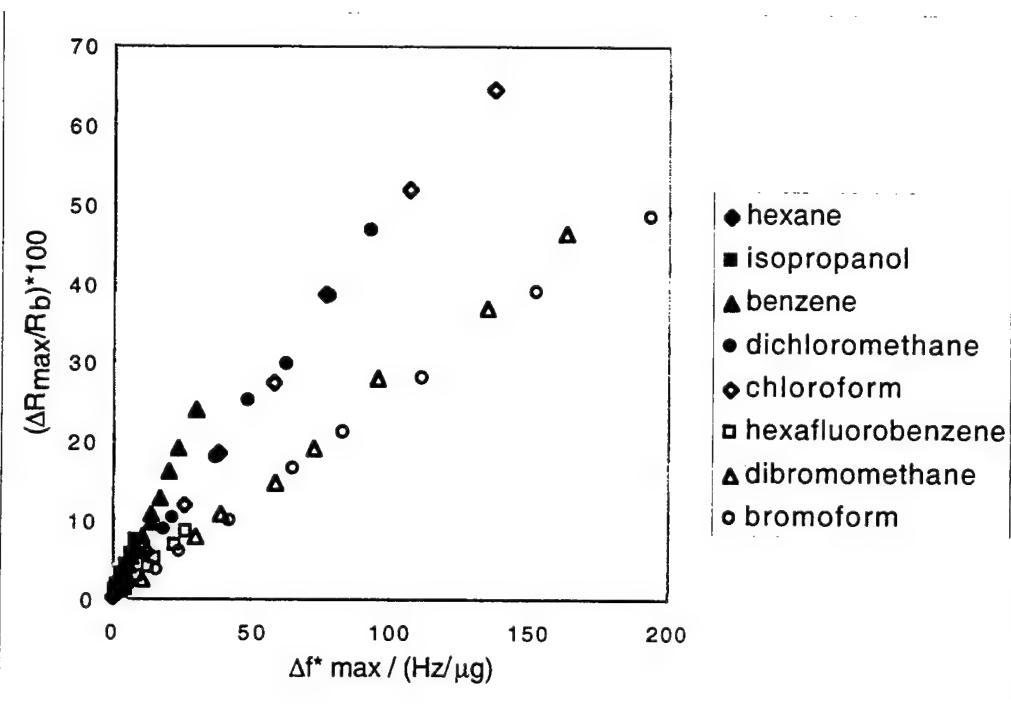
Figure 25. b) Differential relative resistance increase vs. Df^*_{max} for a PEO film when exposed to various analyte fractional vapor pressures.

52
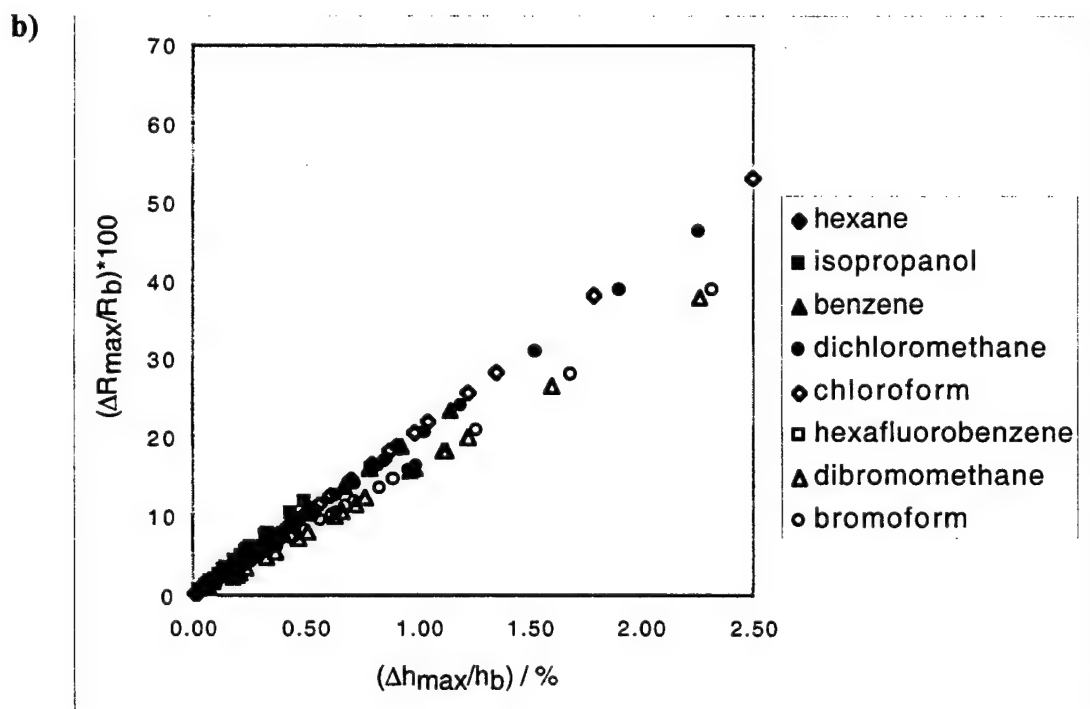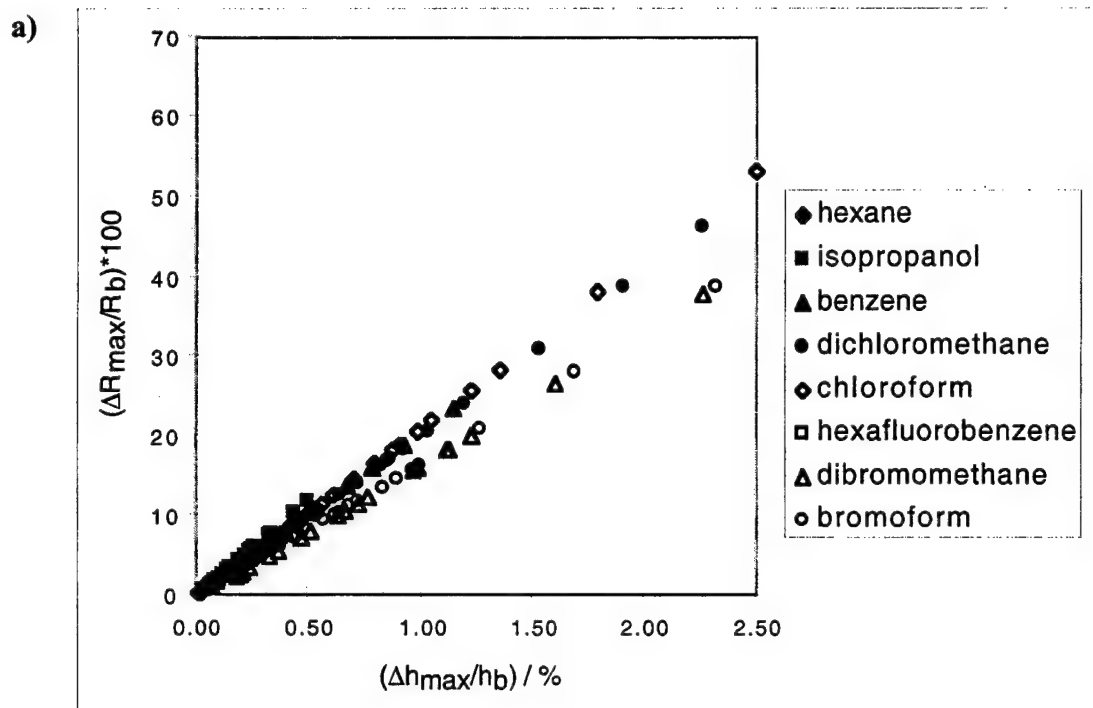
Figure 26. Relative resistance increase for a polymer-carbon black composite film vs. relative thickness increase for a polymer clear film when both films were exposed to various analytes at various fractional vapor pressures, correlated by the mass-normalized maximum QCM resonant frequency change in each film recorded during those analyte exposures for **(a)** PCL and for **(b)** PEO films.

53
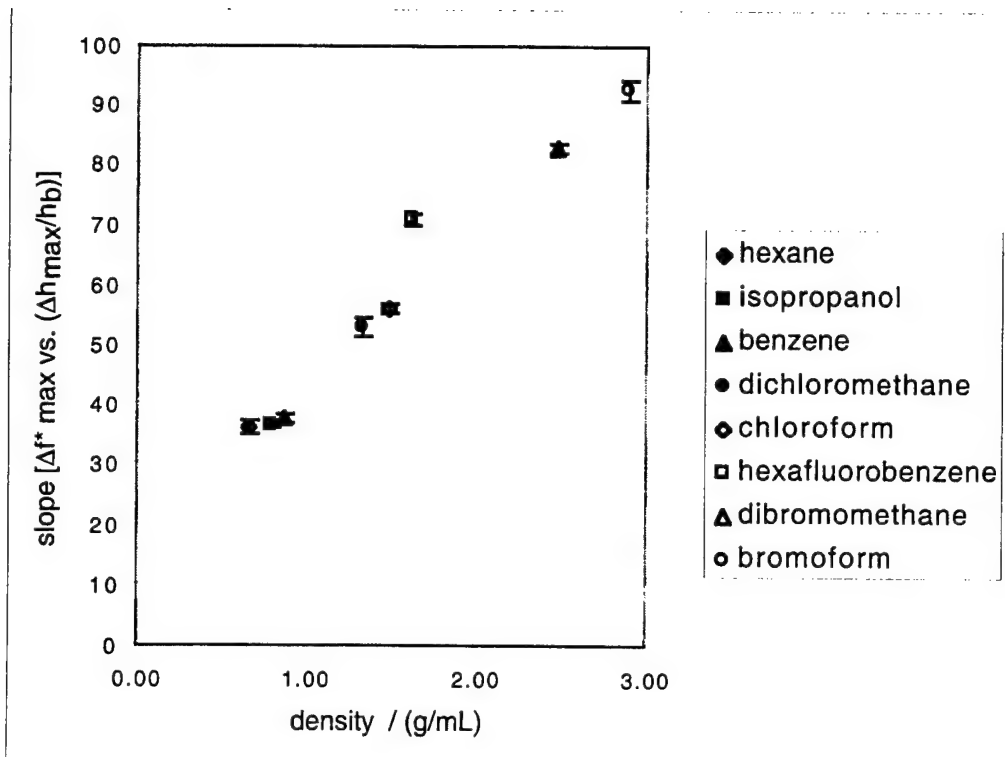
Figure 27. a) Value of the slope of the line corresponding to $[Df^*_{max}/(Dh_{max}/h_b)]$ for a clear PCL film for various analyte presentations at various analyte fractional vapor pressures vs. the analyte liquid-phase density for the exposed analyte.
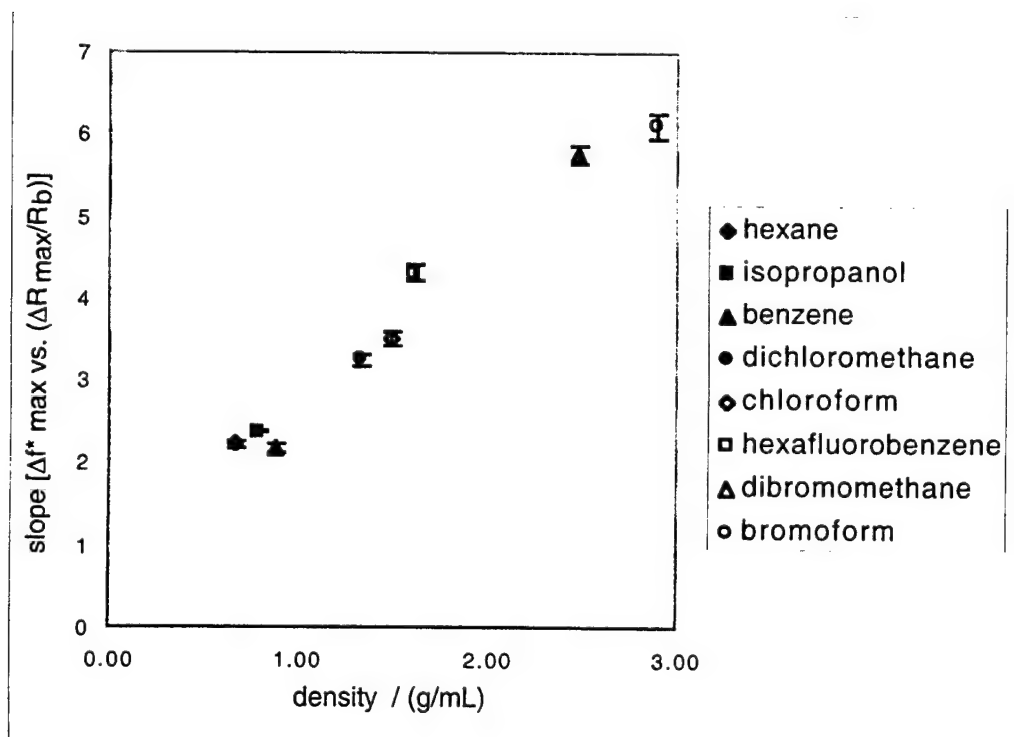
Figure 27. b) Value of the slope of the line corresponding to $[Df^*_{max}/(DR_{max}/R_b)]$ for a PCL-carbon black composite film for various analyte presentations at various analyte fractional vapor pressures vs. the analyte liquid-phase density for the exposed analyte.

54
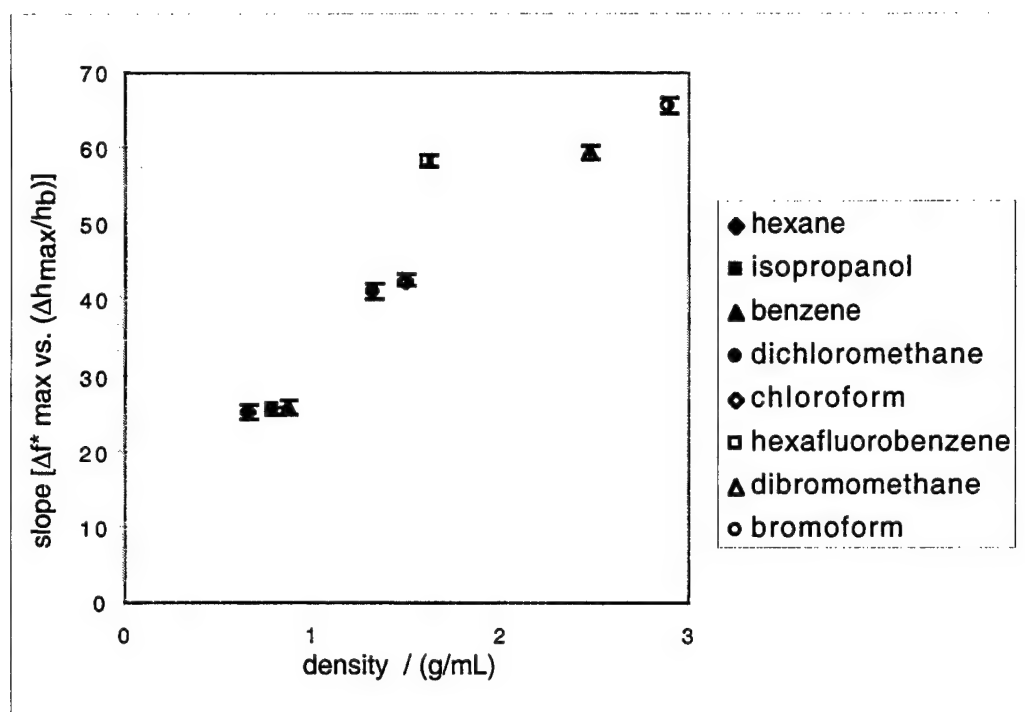
Figure 28. a) Value of the slope of the line corresponding to $[Df^*_{max}/(Dh_{max}/h_b)]$ for a clear PEO film for various analyte presentations at various analyte fractional vapor pressures vs. the analyte liquid-phase density for the exposed analyte.
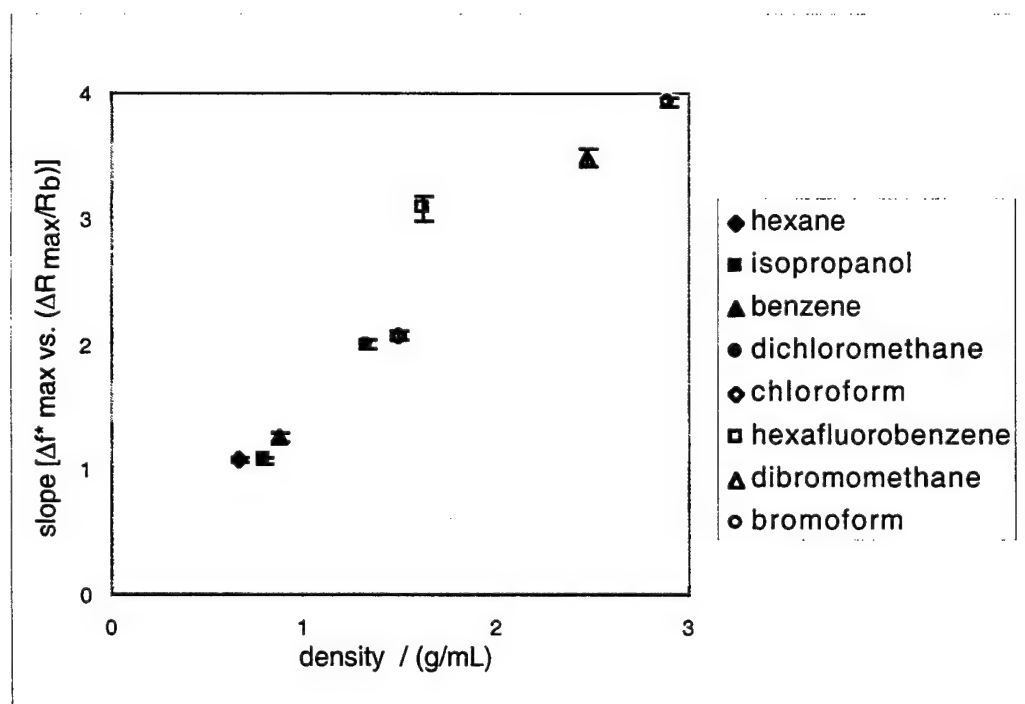
Figure 28. b) Value of the slope of the line corresponding to $[Df^*_{max}/(DR_{max}/R_b)]$ for a PEO-carbon black composite film for various analyte presentations at various analyte fractional vapor pressures vs. the analyte liquid-phase density for the exposed analyte.

These data support the hypothesis that the resistance response is primarily induced by a change in volume of the film, as reflected in the thickness change. A straight line of any slope for $[\Delta f^*_{max}/(\Delta R_{max}/R_b)]$ vs. density that goes through the origin would imply a precise correlation between the density and the detector response. The $[\Delta f^*_{max}/(\Delta R_{max}/R_b)]$ ratio for hexafluorobenzene is larger in all cases most likely because the molecules do not chemisorb into the polymer matrix in proportion to the amount that physisorbs because molecular interactions between the perfluorinated analyte and the polymer chains are not likely to be sufficiently favorable energetically to disrupt the polymer inter-chain interactions. This would cause an increase in QCM resonant frequency response for hexafluorobenzene (due to adsorption) without a concomitant increase in resistance or thickness response (which requires absorbtion), leading to larger $[\Delta f^*_{max}/(\Delta R_{max}/R_b)]$ and $[\Delta f^*_{max}/(\Delta h_{max}/h_b)]$ ratios for that solvent.

Generally, the slope of the line for the thickness response vs. the density is about an order of magnitude larger than the slope of the line for the related resistance response measurements. In both the thickness and resistance measurements the Δf^*_{max} response is similar, therefore the difference in slopes is due to differences in relative response between the thickness and resistance measurements. In all cases, the relative differential resistance response is greater than the relative thickness change for a given Δf^*_{max} change. This finding is consistent with percolation theory, which relates the fractional volume change of a conductor in a composite with a fractional resistivity change of that composite for a given initial conductor volume fraction. We are unable to make direct comparisons with percolation theory because we do not have a complete understanding of the morphology of the carbon black in the composites; however, these data are consistent with reasonable values for the variables in the percolation theory equation for high conductivity carbon black.[51-53]

An implication of these findings is that low density analytes will cause a larger resistance response in our detectors for a given Δf^*_{max} value. We have shown in a previous section that the amount of analyte that sorbs into these detector films is a function of the fraction of vapor pressure of the analyte.[42] This P/P° dependence accounts for most of the response by a detector to an analyte, but the differences in response by a detector to a set of analytes are due to differences in chemical affinity between the polymer film and the analytes as well as the molecular properties of the analytes such as their molecular volume. Therefore, a lower density analyte will be easier to detect at lower levels of sorption (mass uptake) than high density analytes.

In conclusion, we have shown that the composite detectors respond based on the volume change of the composite film as evidenced by a linear dependence on the analyte densities by the slopes of the lines for the thickness and resistance responses vs. film-coated QCM resonant frequency change and by a linear relationship between percent resistance change and percent thickness change when these two are correlated by the film-coated QCM resonant frequency changes. Additionally, we have developed a single element densitometer that can be used to characterize a molecular characteristic of many different types analytes presented to these types of detectors.

4. Exploitation of Spatiotemporal Information and Geometric Optimization of Signal/Noise Performance Using Arrays of Carbon Black-Polymer Composite Vapor Detectors

4.1 Introduction

In most studies to date, the detectors in an electronic nose array are placed in nominally spatially-equivalent positions relative to the analyte flow path.[3,4,9,10,11,19,25,43,54-59] In such a configuration, any spatiotemporal differences between detectors are minimized, and the array response pattern is determined by the differing physicochemical responses of the various detectors towards the analyte of interest. The variations in analyte diffusivities and gas/solid analyte sorption amongst various detectors thus determines the resolving power of the detector array and determines the other performance parameters of such vapor detection systems.

In this portion of the work, we have deliberately placed detectors in spatially-nonequivalent positions relative to the flow path of the sampled analyte. We demonstrate below that the spatiotemporal response properties of such an array can be used advantageously to obtain information on the identity of analyte vapors and also to produce information on the composition of analyte mixtures.

Additionally, in most studies of detector arrays to date, the form factor of the individual detectors is constrained by factors related to the mode of signal transduction. For example, most film-coated QCM devices must have specific dimensions to successfully sustain a bulk specified dimensions so that a resonant bulk acoustic wave can be maintained in the quartz crystal transducer element.[60,61] Similarly, the geometry of SAW devices is constrained by the need to sustain a Rayleigh wave of the appropriate resonant frequency at the surface of the transducer crystal.[60] Each detector in a QCM or SAW vapor detector array typically has an identical area and form factor; consequently, the array response is based solely on the different polymer/analyte sorption properties of the differing detector films. Although in principle, these types of devices could be constructed to cover a range of form factors, In contrast, relatively little attention has been focused on variation of the form factors of the detector to optimize the signal/noise ratio (S/N) for a particular analyte. Spray-coating deposition techniques using masked substrates permits the fabrication of chemiresistor-type vapor detectors in virtually any geometry where the film can bridge two electrically conducting contact leads.[62] This freedom to explore various form factors allows convenient exploration of the geometrical aspects of sorption-based vapor detector design.

We demonstrate in this section of the work that different form factors of a given detector film can provide very different detection performance for different types of analyte vapors. An analytical expression has been derived to predict the optimum sensor volume of a detector film as a function of the sample volume and the analyte/polymer partition coefficient. Under certain conditions, detectors of very small areas are expected to have the best S/N performance, whereas for other conditions, relatively large detector areas are optimal. These predictions have been verified through measurements of the response properties of conducting polymer composite chemiresistor vapor detectors. We also demonstrate that, based on these principles, the use of an array of detectors that are nominally identical chemically, but which have different form factors relative to the analyte flow path, can provide useful information on the composition and identity

of an analyte vapor. Finally, we report S/N data that allow comparisons between the detection limits of several polymer/analyte combinations using two different modes of signal transduction: frequency shifts in SAW devices and dc electrical resistance changes in composites of carbon black composites and insulating organic polymers.

4.2   *Theoretical Considerations*

4.2.1   Dependence of the Noise Power on the Area of a Carbon Black-Polymer Composite Vapor Detector

At open circuit, resistors exhibit voltage fluctuations whose power spectrum is constant at different frequencies as the frequency is varied. These fluctuations are known as Johnson noise. The root mean squared (rms) noise voltage density of the Johnson noise, v_{JN}, is related to the resistance, R, of a resistive detector as follows:

$$Noise = (4RkT)^{1/2}, v_{JN} = (4kTRB)^{1/2} \tag{2}$$

where k is Boltzmann's constant, T is the temperature in degrees K, and B is the bandwidth.[18] This Johnson noise is the fundamental lower limit on the noise of any device of resistance R, and its magnitude is independent of the volume or of other fabrication-dependent properties of the resistor. However, when current flows through most types of resistive materials, a voltage fluctuation is observed with a power spectral density that displays an inverse dependence on frequency. This additional noise, which is typically of the form $1/f^\gamma$ where $\gamma = 1 \pm 0.1$, is designated 1/f noise.[63-65]

Even for a series of resistors that are fabricated by an identical process, the magnitude of the 1/f noise depends on the volume, V, of the resistor. Consequently, when the correlation length of the resistive particle network is small compared to the physical length scale of interest the 1/f noise of a resistance-based detector is expected to be proportional to $V^{-1/2}$.[66] For a given film thickness, this implies that the total noise of a resistive detector scales as $A^{-1/2}$, where A is the total area of the detector film between the electrical contact leads. This dependence requires that the magnitude of the 1/f noise, in the frequency window of the measurement, is much greater than the magnitude of the Johnson noise, so that the total noise is dominated by the 1/f contribution. For 1/f noise, acquisition of data on several equivalent detectors of individual area A_i connected in series is therefore equivalent to making a single reading on one larger detector whose area is $n_d * A_i$, where n_d is the number of detectors of area A_i.

As a consequence of Ohm's law, the power spectral density, $S_n(V_b)$, of the 1/f resistance noise scales with the square of the voltage, V_b, applied to the resistor, thus, the quantity of fundamental interest in characterizing the noise of a resistive detector element is:

$$S_n = S_n(V_b)/V_b^2 \tag{3}$$

where S_n is the relative noise power spectral density and V_b is the biasing voltage.[67,68] In contrast to the Johnson noise, the level of the 1/f noise in carbon black polymer composite resistors varies with many factors, including the structure of the carbon black, its volume fraction in the composite, the type of insulator, the resistivity of the composite, and the methods of preparation.[67,69]

4.2.2 Dependence of Signal/Noise on the Area of a Carbon Black Composite Chemiresistor

Given the above expectations for the scaling of the noise power of a chemically-sensitive resistor with the area of the detector (at constant film thickness), we now consider how the signal induced by sorption of the analyte will scale with detector area. Consider an analyte at an initial density ρ_a^i in a gaseous sample having a total volume of V_a. Sorption of the analyte into a polymer of volume V_p will produce a mass of sorbed analyte equal to $\rho_a^f K V_p$, where K is the gas/polymer partition coefficient of the specific analyte/polymer combination and ρ_a^f is the final density. The total analyte mass, m_a, is therefore:

$$m_a = \rho_a^i V_a = \rho_a^f V_a + \rho_a^f K V_p \tag{4}$$

Solving for ρ_a^i one obtains:

$$\rho_a^i = \rho_a^f (V_a + K V_p) / V_a \tag{5}$$

$$\text{i.e.,} \quad \rho_a^f = \rho_a^i \{1/[1 + K (V_p/V_a)]\} \tag{6}$$

For chemically-sensitive resistors (or any other sorption-based device whose signal is linearly proportional to the mass of analyte sorbed into the detector film), the signal, S, is:

Signal $= S \propto$ (mass of analyte in polymer)/(mass of polymer) =

$$\rho_a^f K V_p/\rho_{poly} V_p \tag{7}$$

$$\text{so} \quad = S \propto \rho_a^i/\rho_{poly} \{K/[1 + K (V_p/V_a)]\} \tag{8}$$

where ρ_{poly} is the density of the polymer composite. In the limit where the 1/f noise dominates the total noise of a chemically-sensitive resistor, this measurement noise, N, scales as $V^{-1/2}$ (vide supra). Hence one can write:

$$\text{Noise} \approx N \propto V_p^{-1/2} \propto 1/[K (V_p/V_a)]^{1/2} \tag{9},$$

because V_n and K are constants and do not affect the validity of the proportionality relationship between N and $V_p^{-1/2}$. Using eqs 8 and 10, the signal/noise ratio (S/N) is therefore:

$$S/N = C \propto \varepsilon^{1/2}/(1 + \varepsilon) \tag{10}$$

where $\varepsilon = K V_p/V_a$.

Under such conditions, the S/N therefore attains a maximum value when $\varepsilon = 1$, i.e., when $K\,V_p/V_a = 1$. The maximum S/N value is obtained when:

$$\rho_a^{\ f} = 1/2\ \rho_a^{\ i} \qquad\qquad\qquad (11)$$

In practice, the film thickness of the detector is typically as small as possible to minimize the time needed for sorbtion/desorbtion of analyte. Hence, at constant, minimized film thickness, eq 11 implies that there is an optimum detector film area for a given sampled analyte volume and initial analyte concentration. Smaller detector areas than this value fail to exhibit optimally low noise, while larger detector areas result in the sorbtion of analyte into too large of a polymer volume and therefore produce a reduced magnitude of signal. Another consequence of the analysis presented above is that the different response properties of a set of detectors having a common polymer sorbent layer, but having different form factors, can provide information on the value of K, if V_a is known and/or is held constant during the experiment. Below we evaluate the validity of these predictions experimentally for sorption-based detectors fabricated using carbon black-filled chemiresistors as exemplary systems.

4.3   *Experimental*

4.3.1   Materials

Ethylene-co-vinyl acetate 25% acetate (PEVA)Poly (ethylene-co-vinyl acetate) with 25% acetate (PEVA), and poly(caprolactone) (PCL) were purchased from Scientific Polymer Products. The solvents n-hexane, n-nonane, n-decane, n-dodecane, and n-hexadecane were purchased from Aldrich Chemical Corp, while toluene and methanol were purchased from EM Science. All solvents were used as received.

4.3.2. Fabrication of Substrates and Detector Films

Two types of substrates were used for the spectral noise and detector response experiments. For experiments measuring noise spectra, glass substrates were used. For measurements of the noise properties of the detector films, glass microscope slides were coated with a 50 nm thick layer of Au on top of a 15-30 nm thick layer of Cr, in a pattern that produced rectangular gaps between two parallel contacts. The ratio of the rectangular edge length to the gap length was 8:1, and this aspect ratio was held constant as the area of the gap was varied. After film deposition, this procedure resulted in detector films of similar resistance values that had systematically varying film volumes.

Two additional types of substrates were used for investigation of the spatiotemporal and geometric aspects of the chemiresistive vapor detectors. In the first set of experiments (Scheme I), a series of parallel Cr/Au contacts was formed on both sides of a 75 mm x 25 mm glass slide. These contact electrodes were 1.8 mm long and were separated by a gap of 0.4 mm. Each pair of electrodes, which defined the contacts for an individual detector film, was spaced 5 mm apart, permitting formation of 15 individual detectors on each side of the glass slide. The area surrounding the electrodes was coated with a thin layer of Teflon. A second set of experiments (Scheme II) used 20 mm by 23 mm substrates that were fabricated by a commercial vendor (Power Circuits, Santa Ana, CA) using standard printed circuit board technology. These

60

substrates had three each of two electrode types. On the separate types, each detector film was repeated three times on a given substrate. Three small detectors were formed on the 840 μm thick edge of the substrate, with parallel contacts for these detectors placed on each face of the circuit board. The 20 mm by 23 mm face of the circuit board supported three larger detectors, each having dimensions of 2.0 mm x 15 mm.

The carbon black-polymer composite suspensions used to form the detector films were prepared by dissolving 160 mg of polymer in the toluene, followed by addition of 40 mg of carbon black (Cabot Black Pearls 2000).[4] The mixtures were sonicated for 10 min and were then sprayed in several lateral passes using an airbrush (Iowata HP-BC) held at a distance of 10 to 14 cm from the substrate. For the set of spatiotemporal experiments that used detectors arranged as depicted in Scheme I, carbon black-PEVA composites were sprayed onto one side of the glass microscope slide and carbon black-PCL composites were sprayed onto the other side of the glass slide. After spraying, the carbon black-polymer film covered the entire surface of the substrate. The resulting detectors had resistance values that ranged from 75 to 120 kΩ on the PCL-sprayed side and from 180 to 240 kΩ on the PEVA-sprayed side. This substrate was placed into a small Teflon-lined sample chamber which, in conjunction with the walls of the chamber, formed a channel 400 μm high and 3.5 mm wide down the length of each row of 15 sensors.

For the set of experiments that used detectors arranged as depicted in Scheme II, six geometrically-optimized detectors of each polymer type (PEVA and PCL) were prepared, three on the edge of the circuit board and three on the face. After application of the composite film, these sensors were assembled into a stack that also contained 760 μm thick Al plates and 105 μm thick Teflon spacers. This assembly created a small channel, of dimensions 0.105 by 12 by 23 mm, that permitted vapor to flow over each set of face detectors. Only two such substrates were coated with detector films, but the stack used in this experiment contained eight total channels, with the remaining channels formed between Al plates and uncoated substrates.

4.3.3 Spectral Noise Measurements

Carbon black composite films containing either PEVA or PCL, and having areas of 0.080, 0.30, 1.2, 1.3, 5.0, 33.0, and 132 mm^2, with resistance values ranging from 70 to 160 kΩ, were prepared as described above. The film thicknesses were then measured with a profilometer (Sloan Dektak model 3030), and a standard method was used to determine the noise of these films.[21,24] Briefly, the films were placed into a metal box and were biased with a stack of batteries (18 volts) which was connected in series to a 1 MΩ resistance. The 1 MΩ low-noise resistance was (10 100kΩ wire-wound resistors (Newark Electronics) that were soldered together in series). The bias voltage across the resistor was ac coupled to a SR560 wide-band low noise voltage preamplifier (Stanford Research Systems), and the output of the preamplifier was sent to an SR785 dynamic signal analyzer (Stanford Research Systems). Using an average of 100 measurements, a power spectral density from 1 Hz to 800 Hz was collected for each film. These spectra were divided by the square of the bias voltage applied to the chemiresistor, V_b^2, to yield the relative power spectral density S_n for each detector film.[21]

A control experiment was performed to evaluate whether film-substrate contacts dominated the observed noise properties of the detectors. Two composite films of approximately the same thickness, film area, and resistance were fabricated, with one film deposited in five 0.38 mm gaps between ten parallel 5.0 mm wide Cr/Au electrical contact pads, and the other film deposited across only one 2.0 mm gap between two parallel 5.0 mm wide Cr/Au contact pads. The additional film/substrate contacts produced no change in the relative noise power of the resistive films, suggesting that the measured noise resulted primarily from the properties of the bulk detector film as opposed to the properties of the film electrode contacts. The properties of commercial, low noise, wire-wound resistors that had resistances similar to those of the carbon black composite films were also measured. The much lower noise values observed for these wire-wound resistors, which are known to exhibit little or no 1/f noise, confirmed that the Johnson noise of the resistors plus any additional amplifier noise of the experimental setup was much lower than the 1/f noise observed for the carbon black composite films. No correction for the amplifier noise was therefore performed in analysis of the noise data of the carbon black composite detector films.

4.3.4 Vapor Flow Apparatus

An automated flow system was used to deliver pulses of a diluted stream of solvent vapor to the detectors.[59] The carrier gas was oil-free air obtained from the house compressed air source (1.10 $\pm$ 0.15 parts per thousand (ppth) of water vapor) controlled with a 28 L min^{-1} or 625 ml min^{-1} mass flow controller (UNIT). To obtain the desired concentration of analyte in the gas phase, a stream of carrier gas- controlled by a 625 or 60 ml min^{-1} mass flow controller -was passed though one of five bubblers containing the desired solvent. Saturation of the gas flow through the bubbler of interest was confirmed with a flame ionization detector (Model 300 HFID, California Analytical Instruments, Inc.). The saturated gas stream was then mixed with background air to produce the desired analyte concentration while maintaining the total air flow at the desired value for the linear flow chamber experiments (Scheme I) and at a constant value of 2 L min^{-1} for the geometrically-optimized detector experiments (Scheme II).

For detectors in the linear flow chamber, the air flow was connected directly to the channel adjacent to the row of detectors. To produce the low flow rates required by this experiment, the analyte-containing vapor was generated at higher flow rates, and a constant 200 ml min^{-1} was subtracted with a flow-regulated pump, permitting the difference to flow into the detector chamber. For detectors arranged as in Scheme II, this flow was directed at the front end of the sampling device through use of a Teflon tube that was slightly larger in diameter than the opening of the stack device. The stack device was fitted into an Al chamber with an open front and a tube connector on the back (away from the leading edge sensors). This tube connector was piped to a vacuum pump through a combination airflow meter and regulator (Cole Parmer). Vapor flow through the channels in the stack assembly was maintained at a rate of 100 ml min^{-1}, i.e., 12.5 ml min^{-1} per channel.

All exposed parts of the flow system were constructed from Teflon, stainless steel, or aluminum. The temperature during data collection was approximately 21 °C, and the temperature was passively controlled by immersing the solvent bubblers into large tanks of water. For the linear

62

row of detectors, vapor presentations were 300 s in duration, separated in time by 60 min. The analyte was delivered at a constant activity of $P/P^o = 0.10$, where P is the partial pressure and P^o is the vapor pressure of the analyte. For experiments with geometrically-optimized detectors (Scheme II), the vapor presentations were 90 s in duration, separated in time by 20 min, and were randomized with respect to the identity of the solvent. These experiments were carried out at $P/P^o = 0.05$ except where otherwise specified. A personal computer running programs developed with LabVIEW 5.0 controlled both the flow system and the data acquisition apparatus.

4.3.5 DC Resistance Measurements

DC resistance data were collected using a Keithley 2002 multimeter and a Keithley 7001 multiplexer. Shielded, twisted pair cables were used, and each resistance value was integrated over 10 power line cycles to reject 60 Hz pickup. Data were processed using a program written in Microsoft Excel Basic. The relative differential resistance change, $\Delta R_{final}/R_b$, was calculated for each detector, where R_b is the baseline resistance averaged for 20 s prior to vapor presentation, and ΔR_{final} is the differential resistance change relative to R_b. The value of ΔR_{final} was evaluated as the mean value of the differential resistance change between either 60 to 80 s or 240 to 260 s after the start of the vapor presentation. The rms noise, N_{rms}, of a detector was measured as the standard deviation of the data points obtained from the multimeter in a period immediately prior to vapor presentation, divided by the average resistance value of the multimeter data points produced over that same measurement period. The period of measurement of this baseline noise was equal to the time elapsed between determination of the baseline resistance and the determination of the differential resistance change upon analyte exposure. In determining the S/N, the values of $\Delta R_{final}/R_b$ were not averaged over any time window, but were instead determined using single data points immediately before starting the vapor presentation and after 60 seconds of vapor exposure. This was done to ensure that the signals were measured in the same bandwidth as the noise. The multimeter was used to determine both the signal and noise values for this calculation because it was desirable to measure the signal and noise of the detectors using the same instrumental apparatus (i.e., the N in S/N is N_{rms}). For the multimeter measurement of the noise of the films of different sizes described above, the same analysis was used, except the noise was calculated over an interval of only 20 s, and 5 of these values were averaged to generate N_{rms}. Unlike the values for S_n, which is a measure of the noise power, these noise values, N_{rms}, were first squared to yield N^2_{rms} prior to plotting them against film volume.

4.4 Results

4.4.1 Noise Spectral Density Measurements for Carbon Black Composite Vapor Detectors

Figure 29 displays the noise power spectral density, $S_n(V_b)$ between 1 Hz and 800 Hz for a set of carbon black composite thin film detectors as a function of the area covered by the composite between the electrical contact pads. The electrode contact dimensions in these experiments were scaled such that the resistance (≈ 100 kΩ) was approximately constant as the film area was varied. Any variation in the noise thus arose from the film area and not from a variation in response of from the preamplifier to different absolute input resistance values. An additional advantage of maintaining a constant aspect ratio for the different volume films is to reduce the variation in the noise that has been observed in some thick-film resistors of different aspect

ratios.[70] Figure 29 also displays the power spectral density for a commercial, low noise, wire-wound resistor.

The power spectral density of the carbon black polymer thin film composites was well-fit to a function of the form $S_n(V_b) \propto 1/f^{\gamma}$ with an exponent of $\gamma=1.1$. Some deviation from the $1/f$ behavior was observed at very low frequencies (< 5 Hz), but this deviation may have resulted from the mechanical contacts used to make connections to the Au/Cr/glass substrates. This noise power spectral density of the wire-wound resistor was much lower than the $1/f$ noise of any of the detector films at the frequencies investigated in this study.

Figure 30 depicts the $S_n * f$ product for carbon black composite detectors fabricated from PEVA and PCL as a function of the volume of the detector film. For these comparisons, the data were taken as the value of S_n at 10 Hz to avoid the lower frequency contact noise. These values are directly comparable because they were taken at the same frequency, but the $S_n * f$ product was displayed because it is essentially independent of frequency for the $1/f$ region above about 5 Hz in frequency. Also shown are the square of the noise values, N^2_{rms}, derived from analysis of the standard deviation of the baseline resistance values verses time as determined on these same films using the multimeter. The detector films used in these experiment were all approximately the same thickness, but the film volume data were calculated using the actual thickness values determined from profilometry on each film.

The N^2_{rms} and $S_n * f$ values decreased approximately linearly with the film volume, with a plot of $S_n * f$ versus V for PEVA-containing carbon black composites having a slope of -0.95 ($R^2 = 0.989$) and a plot of N^2_{rms} versus V having a slope of -0.91 ($R^2 = 0.964$). For the PCL-containing carbon black composite films, the slope of $S_n * f$ versus V was -0.60 ($R^2 = 0.933$) whereas the slope of N^2_{rms} versus V was -0.58 ($R^2 = 0.833$). It is difficult to perform a quantitative comparison between the $S_n * f$ and N^2_{rms} values, due to the impedance mismatch between the input amplifier of the multimeter and the resistive load of the detector, the variable bandwidth of the multimeter during various resistance readings, and other well-known electronic circuit considerations.[71] However, the inverse dependence of the N^2_{rms} value on the volume of the detector film is clearly seen in both sets of measurements. Deviations from a strictly linear dependence of the relative oise power on V with a slope of -1 have been observed previously for polymer film resistors, and have been explained by factors arising from the film-electrode contacts, inhomogeneities in film composition, and/or variability in film thickness over the measured detector area.[68-70] The deviations that we observed may also have resulted from properties related to the relatively thin nature of the films used in this study.
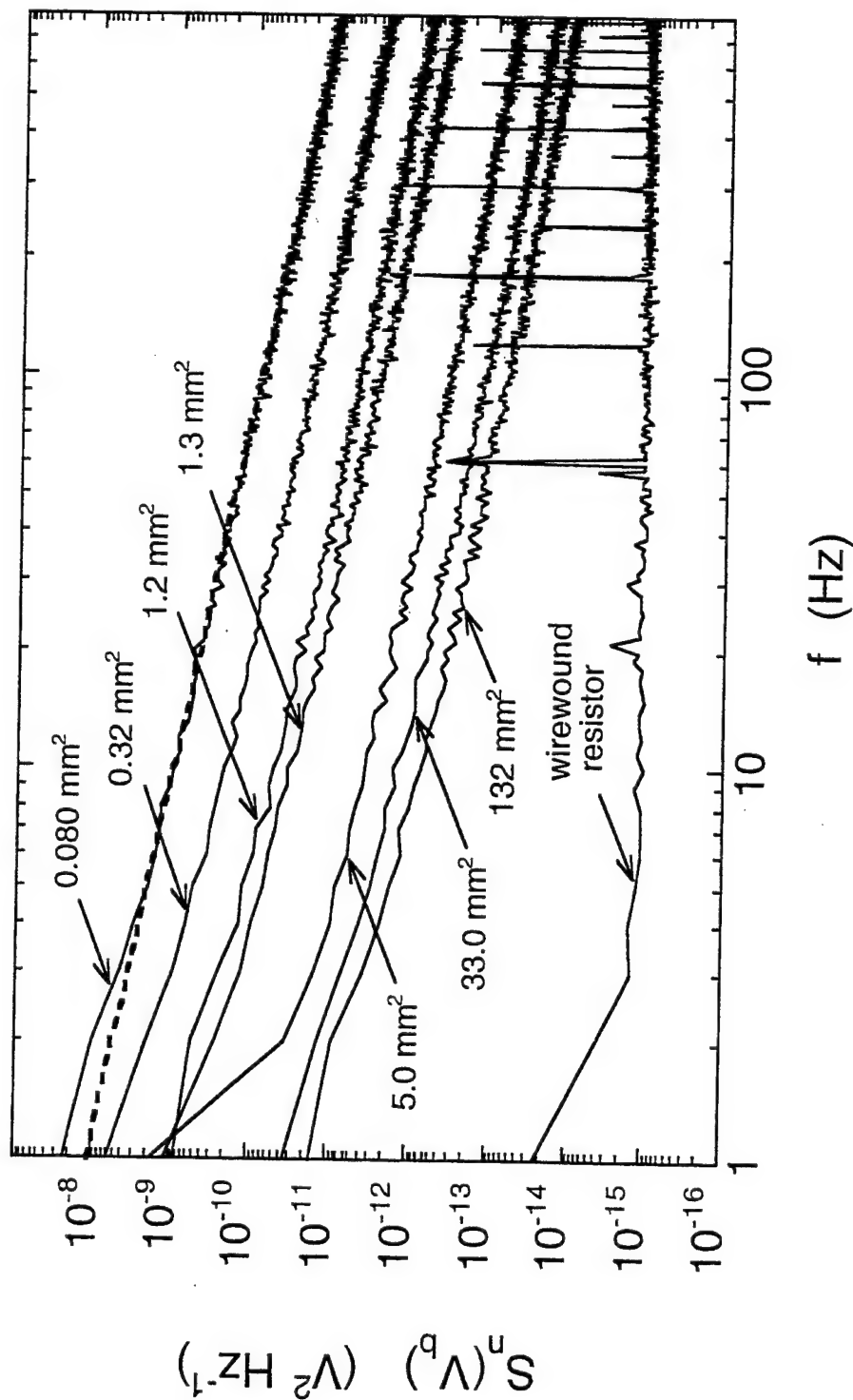
Figure 29. Power spectral density of the noise, $S_n(V_b)$, vs frequency, f, for seven PEVA-carbon black composite detector films of varying area. The dimensions of the rectangularly-shaped regions bridged by polymeric composite between the electrical contact pads were (in mm): 0.10 x 0.80, 0.20 x 0.16, 0.38 x 3.05, 0.40 x 3.20, 0.79 x 6.3, 2.03 x 16.3, 4.06 x 32.5. The PEVA-carbon black composite films were ≈ 230 nm in thickness as determined by profilometry. The dashed line indicates a fit of one such plot to a function of the form $S_n(V_b)=1x10^{-8}/f^{1.054}$. Also shown are data for a wire-wound, low noise, 70 kΩ resistor.

6 5

a)

Volume (mm³)

b)

Volume (mm³)
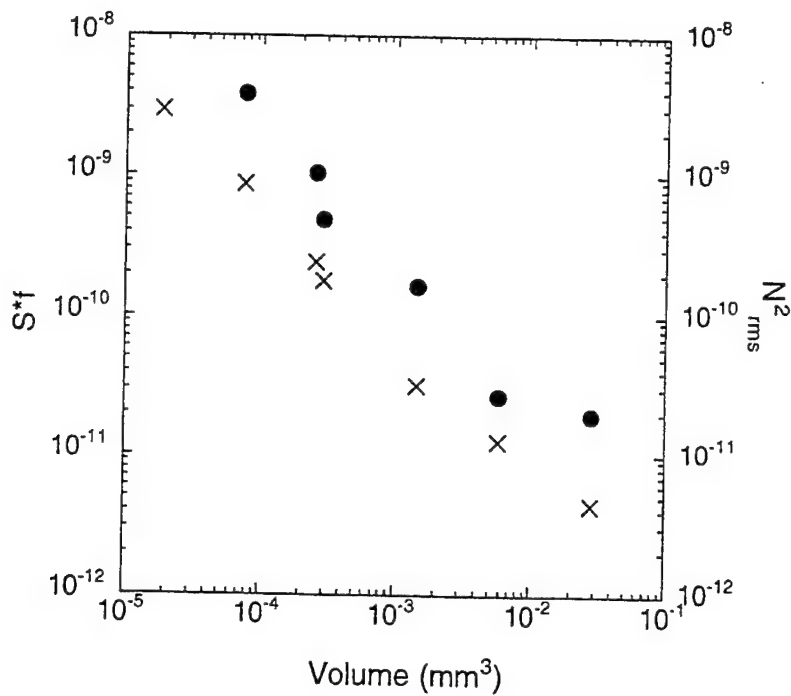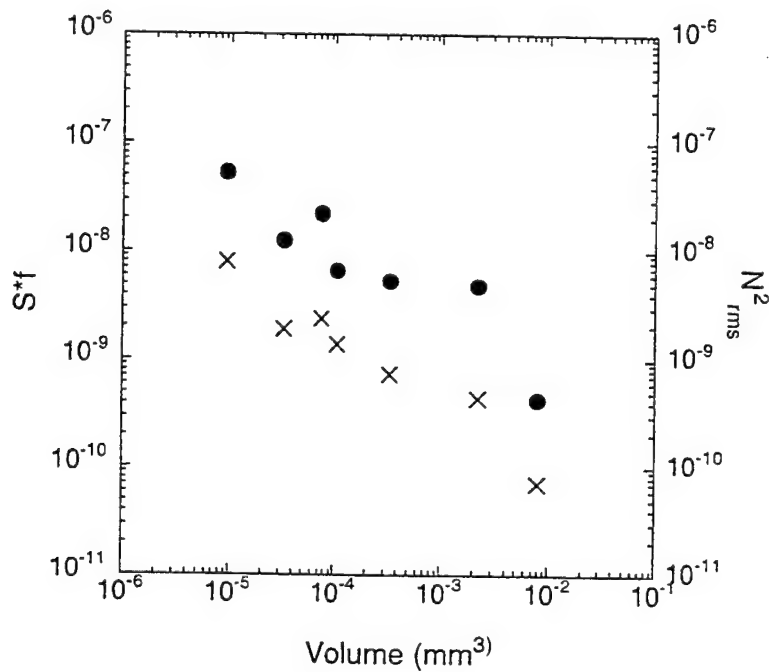
Figure 30. Values of $S_n * f$ (crosses) at 10 Hz and N^2_{rms} (filled circles) vs volume for carbon black composite detectors fabricated from **a)** PEVA and **b)** PCL. The PEVA-carbon black composite films were ≈ 230 nm in thickness and the PCL-carbon black composites were ≈ 80 nm in thickness as determined by profilometry.

4.4.2 Spatiotemporal Response Data from Linear Arrays of Carbon Black Composite Chemiresistive Vapor Detectors

The responses of an array of carbon black polymer composite vapor detectors were investigated as a function of position relative to the location of analyte flow injected into the detection chamber. The detectors were placed in a linear geometry, parallel to the analyte flow path, and were spaced at 5 mm intervals downstream from the flow injection position (Scheme I). Data were obtained for a series of test analytes at various velocities of the carrier gas through the chamber.

Figure 31 displays data at a low carrier gas flow rate during presentation of three analytes of differing vapor pressure (hexane, decane, and dodecane) to a series of PEVA-carbon black composites. Figure 32 displays similar data for two analytes, one having a high vapor pressure (hexane) and the other having a low vapor pressure (dodecane), as a function of analyte flow velocity, on PEVA-carbon black and PCL-carbon black composite detector films.

For high vapor pressure analytes (i.e., analytes with moderate gas/polymer partition coefficients), all of the detectors exhibited essentially the same $\Delta R/R_b$ response values at all tested flow rates, regardless of their position in the array relative to the point of analyte injection. This is expected because the analyte sorption process determines the steady-state value of $\Delta R/R_b$,[42] and all of the detectors experienced essentially identical concentrations of analyte and rapidly produced equilibrium response values after the analyte was introduced into the system.

Low vapor pressure analytes (i.e. analytes with high gas/polymer partition coefficients), however, produced different behavior. At high flow rates, all detectors produced essentially identical $\Delta R/R_b$ signals, but low flow rates resulted in significantly higher $\Delta R/R_b$ values on the detectors nearest to the location of analyte injection into the chamber. Clearly the low vapor pressure analyte is depleted by sorption onto the first detectors that it encounters, leaving less analyte remaining to produce a signal onto subsequent detectors. This relative effect is still clear in the row of PCL sensors even though there is some variation in the responsiveness from detector to detector. For analytes of intermediate vapor pressure, all detectors produced essentially identical responses at high flow rates, whereas at low flow rates different responses were observed for detectors located in different positions relative to the position of analyte injection into the chamber. Figure 31 shows this effect quite clearly for hexane, decane, and dodecane.
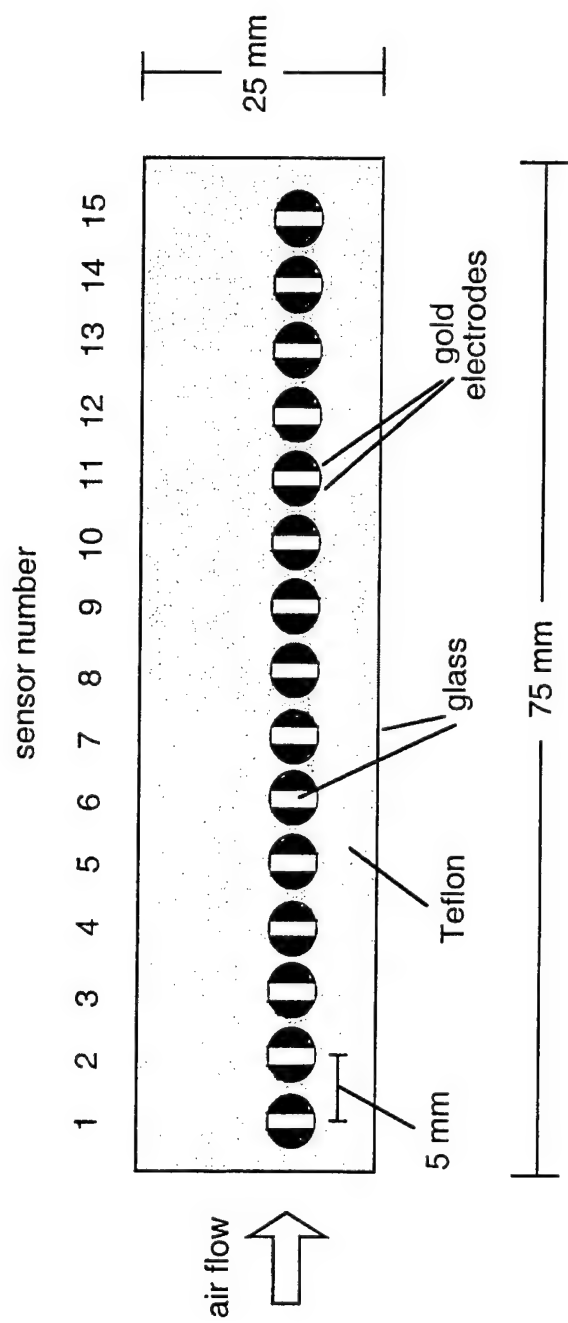
Scheme I. Layout of the substrate used to fabricate a linear array of detectors.
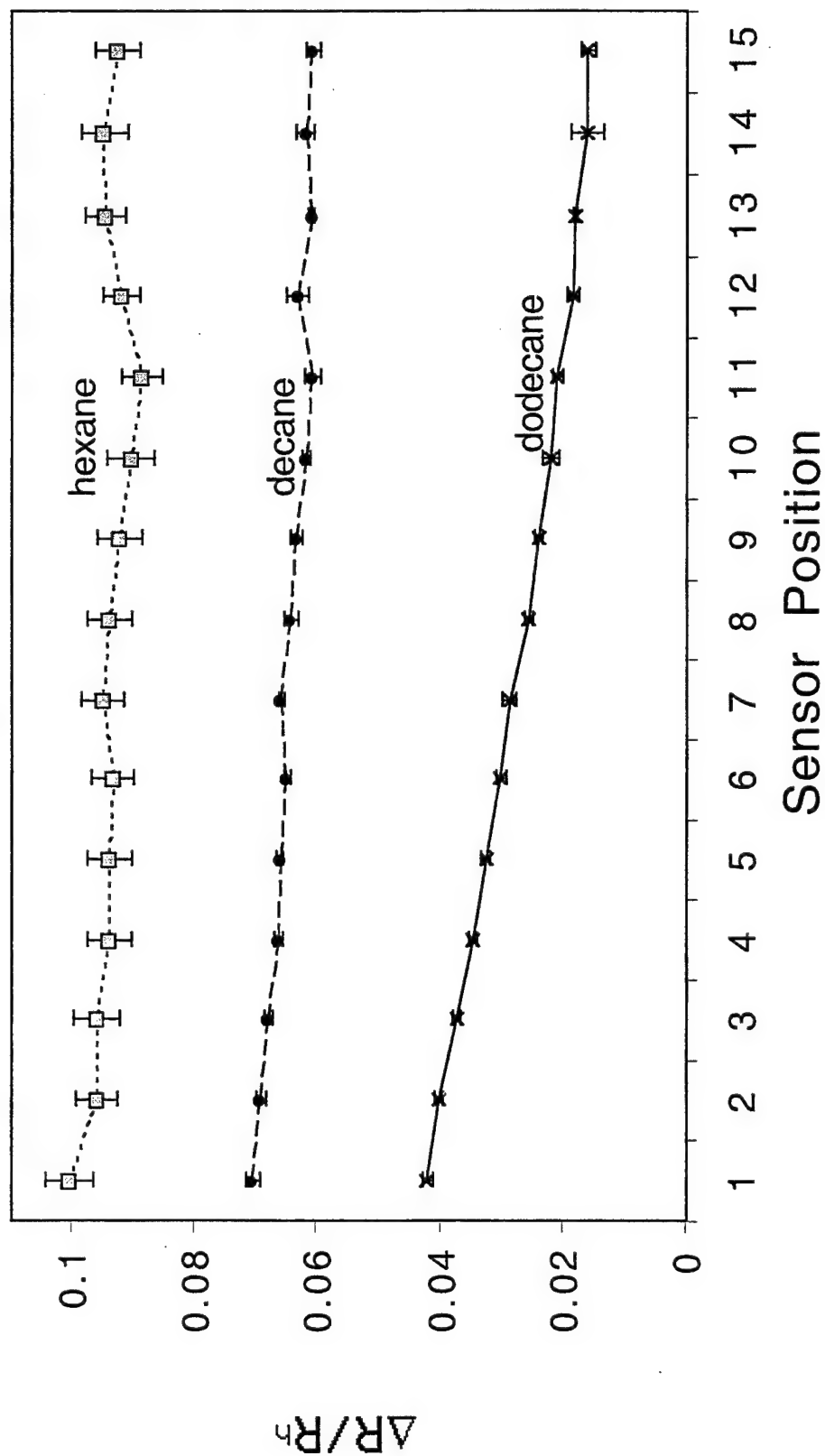
Figure 31. Relative differential resistance responses after 240 seconds, $\Delta R/R_b$, of carbon black-PEVA composite vapor detectors to an analyte having a high vapor pressure (hexane), an intermediate vapor pressure (decane), and a low vapor pressure (dodecane) at a constant activity of $P/P^o = 0.10$ and a flow rate of 2.5 ml min^{-1}. Data are averages of 5 $\Delta R/R_b$ responses, and the error bars indicate one standard deviation values around the mean. The detectors were arranged in a linear geometry as depicted in Scheme I, and the analyte flowed from the leftmost detector (corresponding to the detector with the lowest numbered position) towards the rightmost detector.
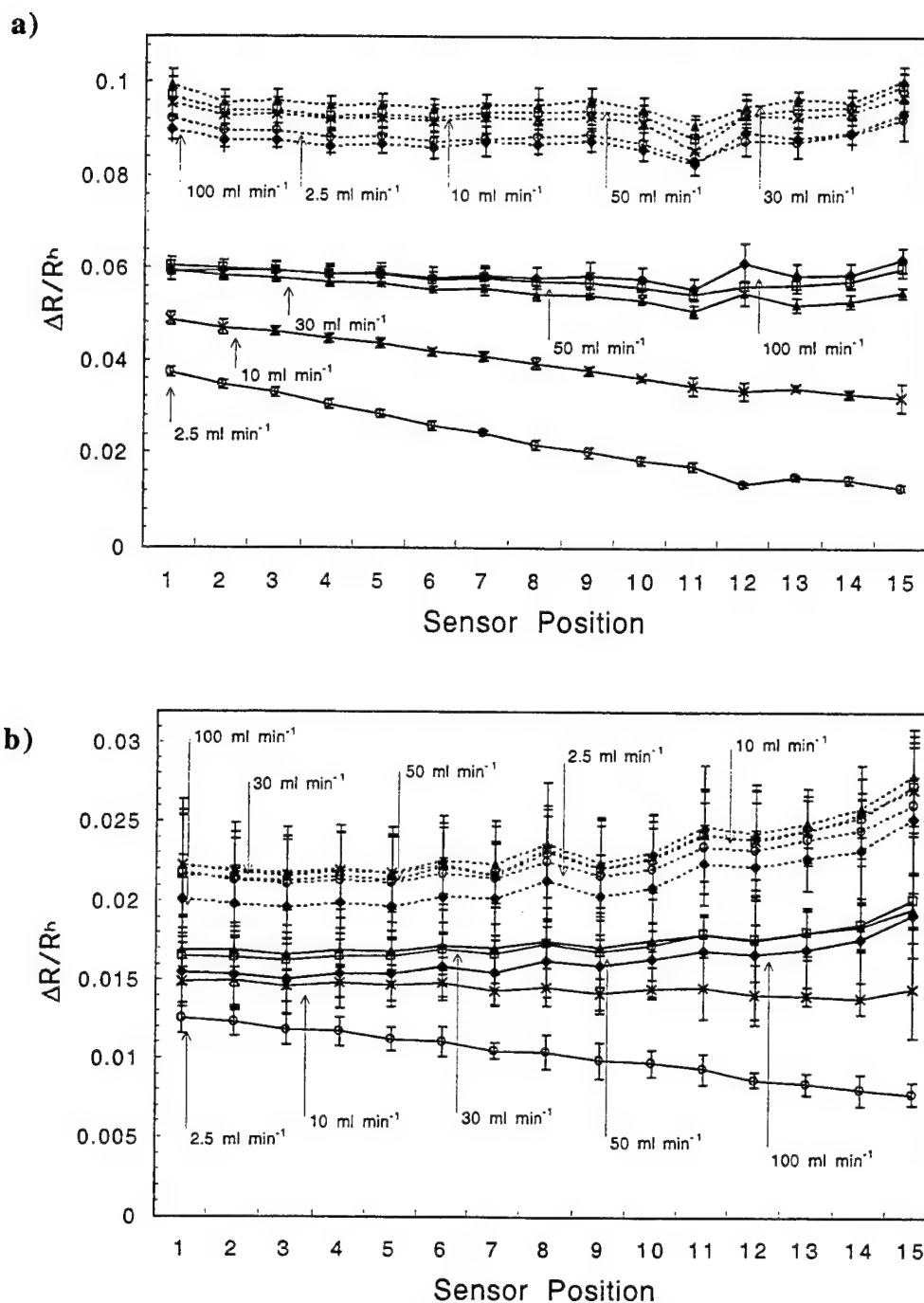
Figure 32. Relative differential resistance responses after 240 s of **a)** carbon black-PEVA composite vapor detectors and **b)** carbon black-PCL detectors to hexane (dashed lines) and dodecane (solid lines) at a constant activity of $P/P^O = 0.10$ in an air background. Data are averages of 5 $\Delta R/R_b$ responses, and the error bars indicate one standard deviation values around the mean. The detectors were arranged in a linear geometry as depicted in Scheme I, and the analyte flowed from the leftmost detector (corresponding to the detector with the lowest numbered position) towards the rightmost detector. The flow rate was varied in five values between 2.5 ml min^{-1} and 100 ml min^{-1}

70

The effect of sorption of low vapor pressure analytes into the composite vapor detector films is also evident in the temporal response of such detectors. Figure 33 shows resistance versus time data for exposure of a PEVA-carbon black composite to hexane (at $P/P^o = 0.10$) followed immediately by exposure to a mixture of hexane and dodecane (each at $P/P^o = 0.10$). These data were obtained at a relatively low carrier flow velocity (2.5 ml min^{-1}) on a PEVA-carbon black detector located at position 7 in Scheme I. Clearly, under these conditions, the different analytes can be distinguished based on their characteristic temporal responses on this detector that arise from the interactions with the analyte flow in the detector chamber.

4.4.3 Flow System Experiments with a S/N Enhancement Targeted Towards an Analyte's Vapor Pressure

The data presented above indicate that the noise decreases approximately as the square root of the detector area, so an increased detector area will produce an increase in S/N for analyte detection under conditions where the mole fraction of analyte sorbed into the polymer film remains constant. However, the analysis presented in eqs 3-11 also indicates that for pulses of low vapor pressure compounds injected at low flow rates, analyte sorption will only effectively occur onto the subset of sensors that are encountered initially by the analyte flow. In this section, we describe the results of experiments designed to exploit both aspects of these properties of detector/analyte/flow interactions.

Figures 34 and 35 display the $\Delta R/R_b$ response of the detector array in the configuration of Scheme II to various analytes of interest. In this configuration, a detector film was deposited onto the edge of a printed circuit board substrate, and a second detector film, of nominally identical composition, was deposited onto the face of the substrate. Several such detectors were then stacked such that the leading edge of each detector first encountered the analyte flow, with the flow subsequently being directed along the face of the substrate. The gaps between adjacent substrates were sufficiently thin to insure that the flow would proceed in the desired direction.

As shown in Figures 34 and 35, the responses of the high vapor pressure analytes (hexane and methanol) on the face detector were $\approx 80\%$ of the magnitude of the response on the edge detector, while the lower vapor pressure analytes (dodecane and hexadecane) produced responses on the face sensor that were less than 4% of the values observed on the edge detectors. The detector films on the leading edge of the substrate had 1/12 the area of the films on the face of the detectors, and therefore exhibited higher noise levels than the detectors on the face of the substrate. Noise values, N_{rms}, in the dc resistance readings measured using the multimeter were on average 2.7 times higher for the PCL edge detectors than for the PCL face detectors, and were on average 1.9 times higher for the PEVA edge detectors than the PEVA face detectors (Table 4). Because the high vapor pressure analytes produced similar $\Delta R/R_b$ values on both detector types when exposed to methanol or hexane, the face detectors exhibited S/N values that were $\approx 60\%$ higher than the S/N values of the corresponding edge detectors. In contrast, for the low vapor pressure analytes (dodecane and n-hexadecane) the S/N values were >20 times higher on the leading edge detectors than on the face detectors. Clearly, the different geometric film form
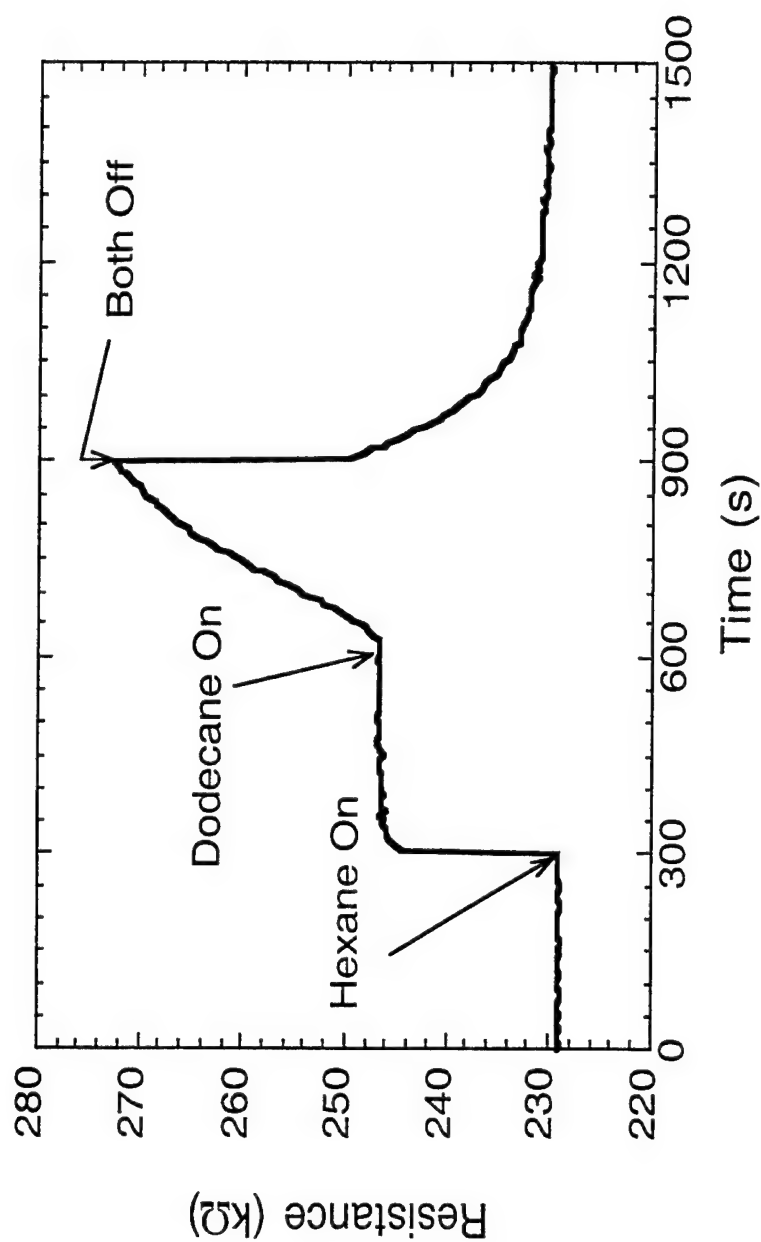
Figure 33. Resistance response vs time for a PEVA-carbon black composite detector (located at position 7 in Scheme I) exposed to hexane at $P/P^o = 0.10$ from 300 to 600 s, and then to a mixture of both hexane at $P/P^o = 0.10$ and dodecane at $P/P^o = 0.10$ from 600 to 900 s.
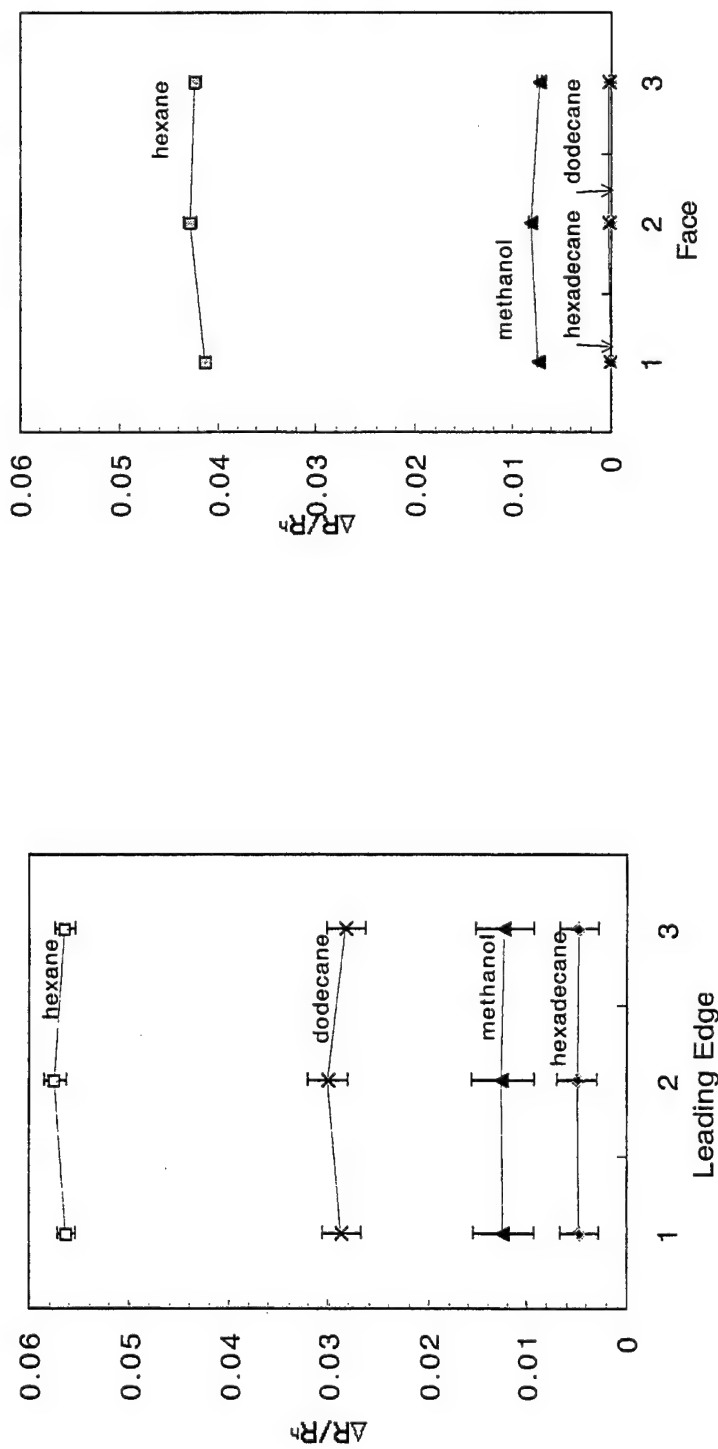
Figure 34. Relative differential resistance responses after 60 seconds for PEVA-carbon black composite detectors on the edge and face positions, respectively, of the substrates arranged in the stacked configuration of Scheme II. Data are averages of 5 $\Delta R/R_b$ responses, and the error bars indicate one standard deviation values around the mean response value for each detector/analyte combination. Each analyte was delivered at $P/P^o = 0.05$ in an air ambient background.
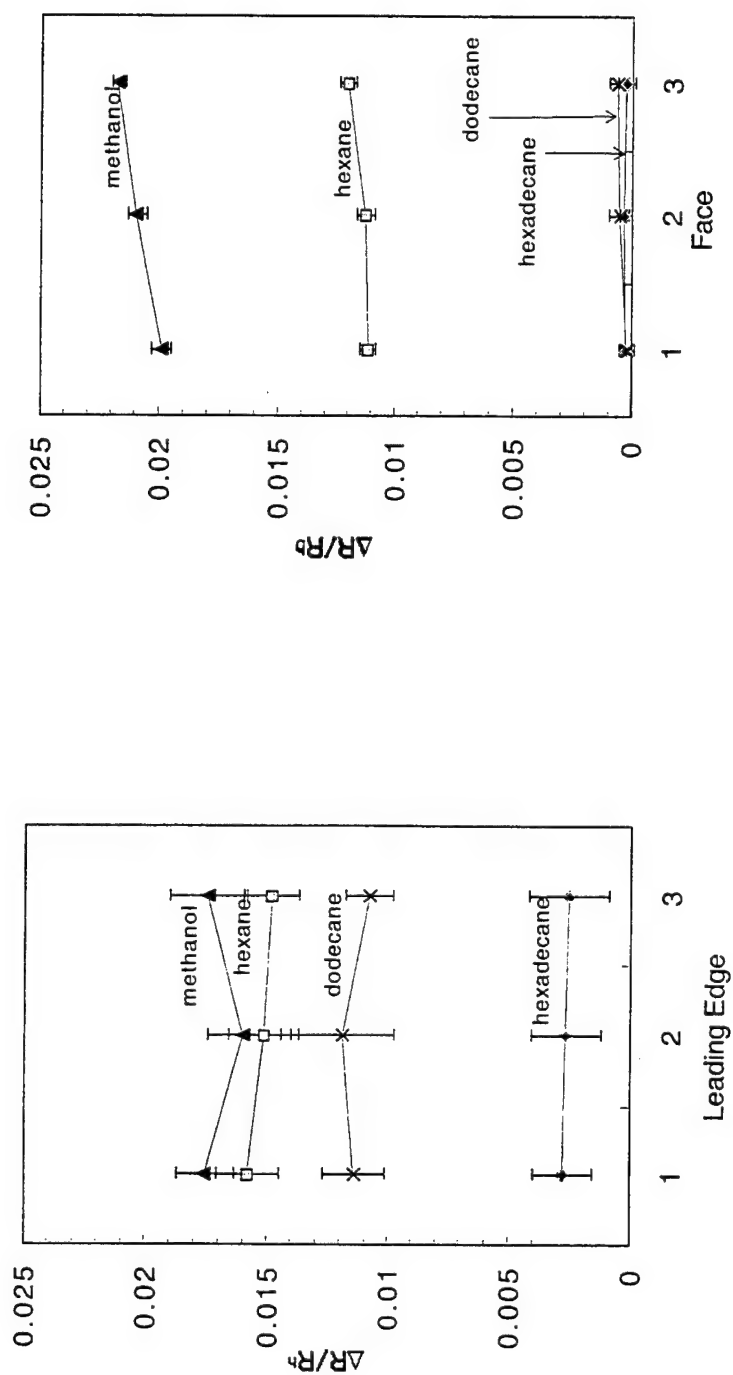
Figure 35. Relative differential resistance responses after 60 seconds of PCL-carbon black composite detectors on the edge and face positions, respectively, of the substrates arranged in the stacked configuration of Scheme II. Data are averages of 5 $\Delta R/R_b$ responses, and the error bars indicate one standard deviation values around the mean response value for each detector/analyte combination. Each analyte was delivered at $P/P^o = 0.05$ in an air ambient background.

Table 4. Responses and S/N for two Types of Polymer-Carbon Black Composite Detectors in the Configuration of Scheme II.

Analyte	Vapor Pressure of Pure Analyte		DR/R$_b$ x 100				S/N			
			PCL		PEVA		PCL		PEVA	
	P° (Torr)	PPM [a]	le [b]	face	le	face	le	face	le	face
hexane	$1.28*10^2$	$1.71*10^5$	1.5	1.2	5.7	4.2	17	28	150	400
methanol	$1.02*10^2$	$1.36*10^5$	1.7	2.1	1.2	0.8	18	60	55	64
dodecane	$9.71*10^{-2}$	$1.29*10^2$	1.1	0.0	2.9	0.0	11	1	130	0
hexadecane	$9.11*10^{-4}$	1.21	0.3	0.0	0.5	0.0	3	1	22	0

Data were averages of 5 randomized presentations of the four vapor at P/P° =0.05 for each vapor, across 3 copies of each detector type. [a] Vapor pressure of analyte in ppm of air at 294 K. [b] le refers to the leading edge sensors and face refers to the face sensors depicted in Scheme II.

factors and interactions with the analyte flow streamlines produced different performance characteristics from a S/N viewpoint for these different types of analytes.

4.4.4 Analyte Classification Information Obtained from Differing Detector Form Factors

An experiment was performed to demonstrate the performance of the detector array of Scheme II in resolving analytes based on spatiotemporal differences in the detector response properties. The concentrations of two analytes, hexane and nonane, were adjusted to generate responses that were similar in magnitude on the PEVA-carbon black composite detectors that were located on the leading edge of the test substrate. Thus, based on these detector responses alone, the analytes could not have been distinguished. However, the responses patterns were clearly differentiable when the ratio of the edge/face detector responses were considered (Figure 36). Analogous additional information on analyte sorption coefficients could of course have been obtained through the use of an array of chemically different composite detectors having additionally an array of differing spatiotemporal and geometric positions relative to the analyte flow path.

4.5. Discussion

4.5.1. Detection Limits of Chemiresistor-Based Vapor Detectors

We have described above studied that indicate that the steady-state $\Delta R/R_b$ values for various carbon black-polymer composite chemiresistors are linearly dependent on analyte concentration.[49] The noise measurements reported herein, in conjunction with the previously-reported dependence of $\Delta R/R_b$ on the partial pressure of analyte[42] and the analyte/polymer sensitivity factors that can be deduced from such plots, allow estimation of the detection limits for various analyte/carbon black composite detector combinations. Two limiting cases will be considered: a) high vapor pressure analytes, which have relatively small partition coefficients for sorption into the carbon black composite detectors, and b) low vapor pressure compounds, which generally sorb strongly and exhibit very large gas/polymer partition coefficients for the polymers of concern.

When the gas/polymer partition coefficient is relatively small, sufficient analyte will in general be present in the sampled volume to produce the equilibrium volume swelling of the entire available detector area. In this situation, too little detector volume is generally present to satisfy the optimum detector area as given by eq 11. At constant film thickness, the $\Delta R/R_b$ value of a given carbon black/polymer composite is directly related to the swelling change of the film. Thus, a given analyte concentration should produce the same $\Delta R/R_b$ signal in the film regardless of the film area of such a detector.

76
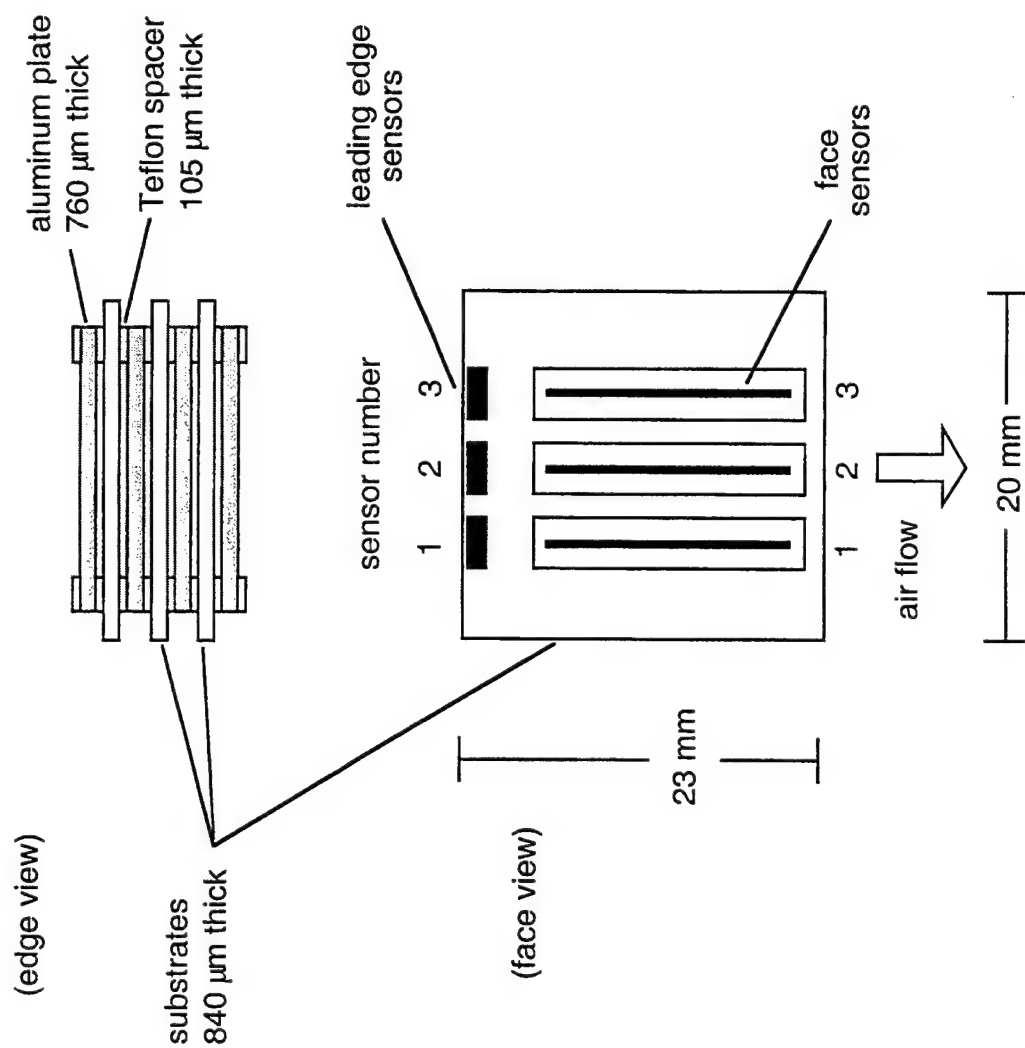
Scheme II. Schematic of the printed circuit boards used to fabricate detectors on the edge and face of a substrate, along with assembly of these substrates into a stack structure to direct the vapor flow.
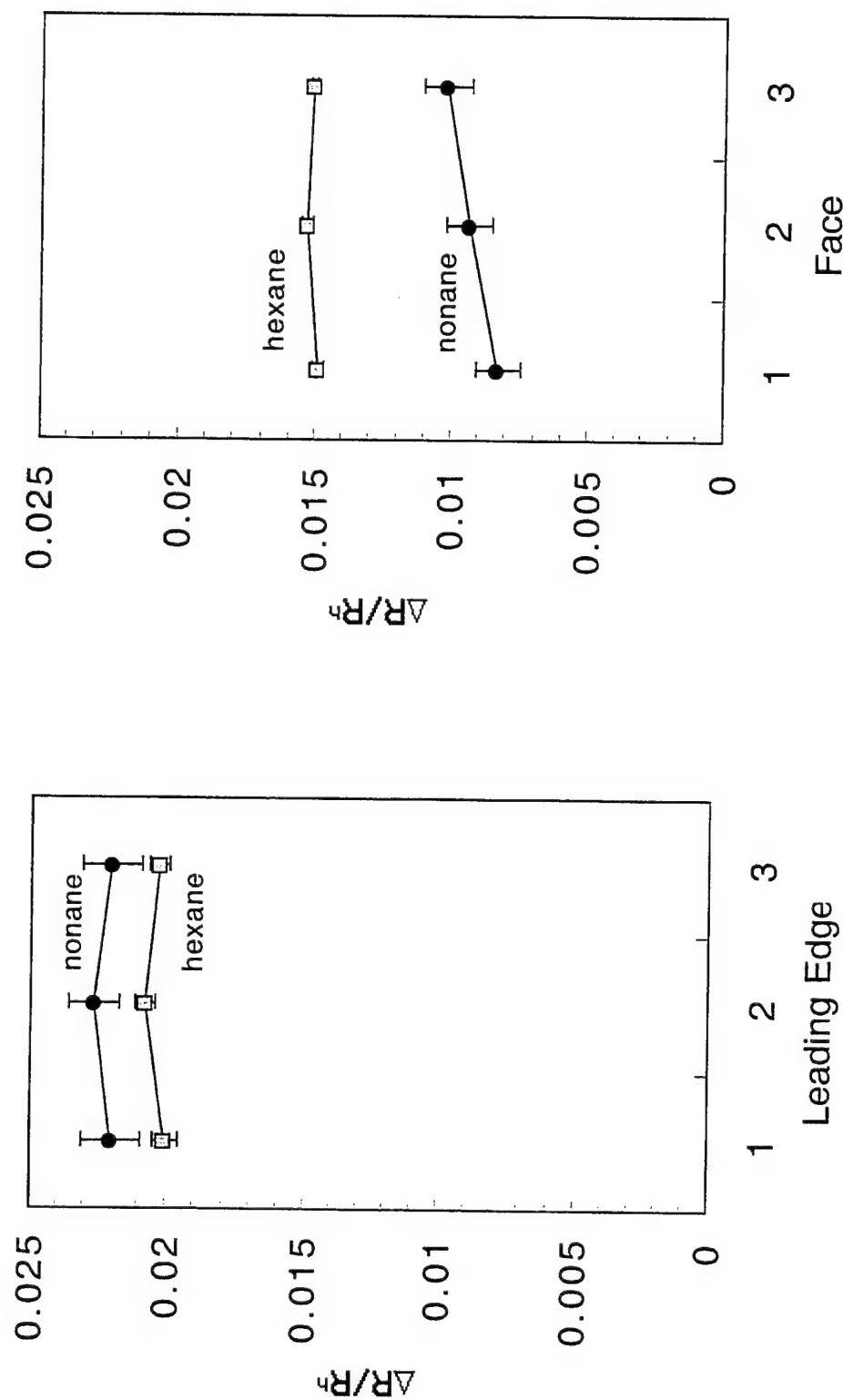
Figure 36. Relative differential resistance values after 60 seconds for PEVA-carbon black composite detectors exposed to a mixture of hexane at $P/P^o = 0.020$ and nonane at $P/P^o = 0.023$ in an air ambient background. The ratio of responses between detectors located on the edge and face, respectively, of a substrate depicted in Scheme II clearly allowed differentiation between these two analytes.

Under these conditions, the scaling of the S/N (in a given measurement bandwidth) with detector area is therefore entirely determined by the dependence of the noise on the detector area. As determined above experimentally, and in accord with theoretical expectations discussed above, the background noise of the carbon black composite chemiresistors at low measurement frequencies scales as $A^{-1/2}$. The S/N, and thus the detection limits of a particular carbon black polymer composite detector towards a given analyte, therefore scale as $A^{1/2}$. The use of a detector film having the largest practical area possible (up to the limit of optimum area given by eq 11, or the area at which the 1/f noise, for the measurement bandwidth, falls below the Johnson noise and the total noise no longer exhibits a dependence on area) is thus the optimum detector design under such conditions.

Table 5 reports the S/N and deduced limits of detection for representative carbon black/polymer composite detectors with various vapor analytes, for 1 cm^2 of detector area. Table 5 also reports representative values taken from the literature for selected polymer-coated SAW vapor detectors.[72] For the given area, the detection limits are comparable for both types of signal transduction, although the carbon black composites exhibit somewhat higher sensitivity than the SAW devices for the analyte/polymer combinations chosen for comparison. We have only reported limits of detection as opposed to limits of classification; the former quantity depends only on the properties of the analyte/detector combination, while the latter quantity also depends on the test set of analytes presented to the array as well as on the algorithms used to perform the classification. In one particular instance, the limit of classification of an analyte was shown to be within a factor of three of the limit of detection of that same analyte, indicating that the limit of classification is likely to be on the same order of magnitude as the limit of detection, at least for some tasks.[73]

In the limit where the analyte exhibits a very strong sorption into the polymer film of the carbon black composite detector, the S/N optimization methodology is quite different. As given by eq 6 above, the sorption process the sorption process under such conditions will be limited by the amount of analyte in the sampled volume. The $\Delta R/R_b$ signal of the detector is proportional to the swelling change of the detector film,[74] so increasing the detector area will reduce the signal (by diluting the fixed amount of analyte into a correspondingly larger volume of polymer). As long as the swelling is linearly dependent on the concentration of analyte sorbed into the polymer,[74] this dilution will produce a linear decrease in the $\Delta R/R_b$ signal with increased detector area. Because the noise scales as $A^{-1/2}$, the S/N under such conditions scales as $A^{-1/2}$. Small detector areas are therefore favored. In fact, the design goal under such conditions is to insure that the most analyte is sorbed into the least area of detector film, and signals should only be acquired from the limited, highly analyte-swollen, portion of the detector. For example, this design principle is appropriate for applications in which 2,4-dinitrotoluene, a vapor component above buried land mines,[62,75,76] or other low vapor pressure analytes, are being detected.

Given the relationships reported previously between the mass loading of analyte and the $\Delta R/R_b$ values for carbon black composite vapor detectors,[74] in conjunction with the background noiselevels reported herein, detection limits can be evaluated in the high sorption/low analyte

79

Table 5. Limits of Detection for Carbon Black-Polymer Composit Vapor Detectors and for Polymer Film-Coated SAW Detectors

		LOD (μg/L)			
	polymer	benzene	cyclohexanone	hexane	nonane
Carbon Black Composite[a]	PEVA	18	1.5	40	1.3
	PCL	525	45	1300	48
SAW[b]	poly[bis(cyanoally)siloxane]	401	15	5300	569
	poly(methylphenylsiloxane)	302	14	1520	111
	poly(phenyl ether)	216	13	991	79
	poly(isobutylene)	259	32	346	19

[a]Carbon black composite limits of detection are calculated from the slopes of $\Delta R/R_b$ vs. P/P^o at 294 K in ref (28) using 3σ noise values in 1 cm^2 of the same film type at average experimental film thickness values of 230 nm for PEVA and 80nm for PCL. [b]SAW values are taken from ref (29) for 158-MHz SAW oscillators at 298 K.

vapor pressure regime. At a noise level of $\approx$10 ppm, and with a $\Delta R/R_b$=0.10 produced at a mass loading of 5.0 μg of analyte sorbed into 1 cm^2 of polymer,[31] the computed 3σ detection limit of a poly(caprolactone)-carbon black composite is 1.5 ng cm^{-2}. This value can only be reached in practice if an efficient sampling and delivery system is available, such that the full amount of the sampled analyte can be delivered effectively to the 1 cm^2 area of the detector film. Of note is that the detection limit scales inversely with the film area and linearly with the efficiency of delivering analyte to the sampled film area.

In the intermediate sorption/partition coefficient regime, an optimum detector area clearly exists for which the S/N, and therefore the detection limit performance, of a particular analyte/polymer combination is maximized. This ratio depends on only the analyte/polymer partition coefficient and the sampled analyte volume, and is readily calculated from eqs 10 and 11 above. The S/N can therefore be optimized for different vapor pressure analytes through control over the form factor of the detector film, as demonstrated herein both theoretically and experimentally.

4.5.2 Geometric Considerations of the Detector for Optimum S/N Performance with a Fixed Sample Volume

The dependence of optimum detector area on the analyte/polymer partition coefficient can also be used advantageously in the classification of analytes and analyte mixtures. In such a system, analytes with a low vapor pressure would be sorbed into the smallest detector area possible, producing the largest signal and therefore the largest S/N ratio for that particular analyte/polymer/sampler combination. Higher vapor pressure analytes are, in turn, detected with higher S/N performance at detectors having larger film areas. In fact, an array of contacts spaced exponentially along a polymer film could be used advantageously to gain information on the sorption coefficients of analytes into polymers, and therefore can provide additional classification information on analytes and analyte mixtures relative only to equilibrium $\Delta R/R_b$ values on a detector film having a single, fixed form factor for all analytes. A relatively simple demonstration of this effect was performed herein, in which two analytes were not distinguishable based on their responses on a single type of detector located on the edges of the substrates, but the analytes were distinguishable when information on the relative response values of detectors located on the edge versus the face of the substrate was used in the data analysis. Additional information is additionally available if the analyte flow rate is varied over the detector array as well.

Variation in the geometric form factor of detectors also could potentially have practical advantages in the implementation of instruments based on arrays of vapor detectors. Although information similar to that produced by a collection of spatiotemporally-arrayed detectors could in principle be obtained from an analysis of the time dependence of the signal. Finally, deliberate variation in the analyte flow rate could be used to encode the analyte signal at higher frequencies, and use of a lock-in amplifier centered at this higher frequency (where the magnitude of the 1/f noise is lower than at dc) would enhance the S/N of these detectors.

Another feature of note is the possible relationship of this type of detector design to the biological olfactory system. Sobel and co-workers have recently reported differences in human

perception of binary odorant mixtures that contained an odorant having a high vapor pressure and an odorant having a low vapor pressure.[77] The perceptual changes were shown to be produced by differences in flow rate between the two nostrils of the human subjects. Although the mixture contained fixed concentrations of each odorant, the subjects perceived the mixture to be enriched in the lower vapor pressure odorant when sampled through the higher flow rate nostril, and the same mixture was perceived to be enriched in the higher vapor pressure odorant when sampled through the lower flow rate nostril. The perceived responses changed when the flow rates in the nostrils were naturally interchanged due to normal physiological processes. The authors concluded that the spatiotemporally-dependent responses of olfactory receptors is useful to humans in resolving certain odor mixtures and in obtaining additional information on the composition of odorants.[34] The relatively primitive system investigated herein demonstrates an analogous principle in a non-biological array of broadly cross-reactive vapor detectors, and thus a differential measurement of the response vs flow rate of two conducting polymer composite detector arrays, sampling the same analyte at different injected flow rates, might provide an interesting platform for evaluating the degree to which spatiotemporal response information can be used to obtain additional classification information in a variety of complex vapor detection scenarios.

4.6   Conclusions

The dependence of the relative power spectral density on the volume of carbon black-polymer composite vapor detectors was of the form $S_n \propto 1/V^n$, with n=1 for PEVA-carbon black detectors and n=0.6 for PCL-carbon black detectors in the frequency range of 1-800 Hz. Analytes with moderate gas/polymer partition coefficients produce the same $\Delta R/R_b$ response values on detectors of different area, so under these conditions the S/N is optimized for detectors of very large area. In contrast, analytes with high gas/polymer partition coefficients produce much larger $\Delta R/R_b$ values on detectors of small area that are positioned to best sample the injected analyte flow. For such detector/analyte combinations, detectors of small area will exhibit significantly better vapor detection sensitivity, in accord with theoretical expectations. Manipulation of the geometric form factor of carbon black-composite vapor detectors thus provides a facile method of optimizing S/N performance for a particular detector/analyte combination of interest. An array of nominally identical polymer-carbon black detectors arranged linearly relative to the analyte flow path produces different spatiotemporal response patterns for analytes having different gas/polymer partition coefficients. Analytes with moderate gas/polymer partition coefficients produce the same signals on all detectors at all available flow rates, whereas analytes with very large gas/polymer partition coefficients produce signals that are highly dependent on the analyte flow rate and the spatial position of the detector in the array. Such a configuration produces useful information on the composition of binary analyte mixtures and adds classification information to an array of compositionally-different conducting polymer composite vapor detectors.

5. Comparison of the Performance of Different Discriminant Algorithms in Analyte Discrimination Tasks Using an Array of Carbon Black-Polymer Composite Vapor Detectors

5.1 Introduction

5.1.1 Background and Goals

The ability of such detector arrays to discriminate between various analytes[58] comprises one figure-of-merit for the sensing system as a whole. This figure-of-merit is analogous to the selectivity ratio of an individual, traditional chemical sensor for the target analyte relative to interferents, because when only one channel of data is available the performance of a sensor system is identical to the performance of the sensor. However, one broadly responsive detector gives no information about an unknown analyte presented at an unknown concentration. In contrast, two differently-responding, only partially correlated, detectors that each respond linearly to analyte concentration will yield a unique quantity, the ratio of their signals, for any given analyte. When an array of n detectors is exposed to an analyte, it generates n responses, which can be plotted as a single point in n-dimensional space. A set of exposures to a given analyte at a given concentration will yield a set of points in detector space, which are separated only by the variations in the detector responses. "Training" the array with many exposures to many known analytes will lead to several clusters, one for each analyte. Various discriminant algorithms can then be used to assign a single exposure of an unknown analyte to one of the clusters obtained from the training set, thus identifying the unknown with a specific probability of success.

Clearly, when an array approach to sensing is used, the system-level discrimination performance is a function not only of the detector performance but is also is related to the performance of the accompanying data processing algorithm. Expressions for the signal-to-noise ratio, sensitivity, and selectivity of a detector array system have been given by Lorber[78] and utilized by Kowalski and coworkers.[79,80] Previous studies have compared the performance of some of these algorithms on both real chemical data and simulated data.[81-83] The goal of this portion of the work was to evaluate the performance of various data processing algorithms on a specific vapor detector array used in some selected, relatively demanding discrimination tasks.

Detector arrays formed from carbon black composite chemiresistors[4] have been shown to exhibit excellent pairwise discrimination between even closely related sets of analytes when a statistically-based, linear discriminant algorithm is used to analyze the responses of 10-20 chemically-diverse conducting polymer composites.[31] To compare the relative performance of various discriminant algorithms in conjunction with these detector array data, the array must be presented with pairs of analytes that will not be perfectly classified by at least some of the discriminant methods. This was not the case with pairs of simple organic vapors, all of whom were essentially perfectly separated from each other, including structural isomers such as *ortho*- and *meta*-xylene.[84] As part of this work, we have challenged a carbon black-polymer composite detector array with a pair of compounds that are very chemically similar, H_2O and D_2O.

In addition, it is of interest to evaluate the array performance on analyte mixtures. The steady state relative differential resistance responses of the carbon black composite detectors, which

serve as the descriptors that form an n-dimensional odor space from an n-member detector array, are linear with analyte concentration, and the response of a binary mixture of analytes is the response of the pure analytes weighted by the mole fraction of analytes in the mixture.[49] For each exposure, the responses of the d detectors can be mapped to d orthogonal axes. In this space, the Euclidean distance of a binary vapor mixture that is 0.5 mole fraction of each constituent and a binary mixture that is a 0.6:0.4 distribution of these same analytes should be one tenth of the Euclidean distance between the array responses of the individual pure analytes. Several different binary mixtures of 1-propanol and 2-propanol, and of n-hexane and n-heptane, were therefore utilized as part of the present work.

Another method to decrease the discriminating ability of a detector array is to decrease the signal-to-noise ratio of the individual detectors. Delivery of low concentrations of analytes will decrease the detector signal and therefore reduce the signal to noise ratio, broadening the clusters relative to their separation. A number of low concentration ($\leq 1\%$ of the vapor pressure) exposures to 1-propanol, 2-propanol, n-hexane, and n-heptane were therefore studied and the performance of different discriminant algorithms was also assessed for these specific sensing tasks.

5.1.2 Description of Selected Discriminant Algorithms

Discriminant algorithms generally fall into two categories: parametric methods, which assume that the data have a certain distribution (usually a normal Gaussian distribution), and non-parametric methods, which make no assumptions about the underlying structure of the data. The classical parametric methods include linear discriminant analysis[85,86] (LDA, also known as Fisher's linear discriminant) and quadratic discriminant analysis (QDA). A hybrid of LDA and QDA, termed regularized discriminant analysis (RDA), has been more recently introduced.[81,87] The classic non-parametric discriminant is k-nearest neighbors (kNN),[86] which has been applied to chemical data as well as to other types of data.[88] Many other classifiers have been developed, including artificial neural networks (ANN),[89] partial least squares methods (PLS),[90] and soft independent modeling of class analogy (SIMCA).[91,92] In this work, the performance of the kNN, LDA, QDA, RDA, PLS, and SIMCA discriminant algorithms was compared for various analyte discrimination tasks using data from the carbon black composite detector array. Brief explanations of the various discriminant algorithms are provided below.

5.1.2.1 k-Nearest Neighbor Discriminant

The kNN algorithm involves calculation of the distance between the response of a test analyte and the responses of all of the examples in the training set.[13] The most commonly used distance metric is the Euclidean distance, which in 2- and 3- dimensions is the familiar spatial distance. For an arbitrary number of dimensions, the Euclidean distance is simply:

$$distance_{ij} = \left[\sum_{n=1}^{d} \left(X_{in} - X_{jn} \right)^2 \right]^{1/2} \tag{12}$$

where X_{in} and X_{jn} are the coordinates of the ith and jth point in the nth dimension, respectively, and d is the number of dimensions. The test sample is then assigned to the class having the largest number of nearest neighbors to the test data. For example, if k = 3, the classes of the three nearest neighbors are compared, and the unknown is assigned to the class with the majority of nearest neighbors. When choosing from more than two classes, any k > 1 allows the possibility of a tie. For this reason, and because it has been shown that k = 1 is the best method for a wide variety of distributions,[93] k = 1 has been used in our study. It has also been shown that any classification rule, including those with information about the statistical distribution of the data, can perform at best twice as well as kNN (k = 1) in the asymptotic case in which the training set includes a very large number of examples from each class.[93] The straightforward kNN classifier is therefore a good benchmark against which to measure other, more sophisticated, discriminants.

5.1.2.2 *Linear Discriminant Analysis*

Linear discriminant analysis is typically taken to mean Fisher's linear discriminant.[85] The orthogonal projection of points in a d-dimensional space onto a line reduces the classification problem from d dimensions to one dimension. When the data are projected onto one dimension, it is desirable to maximize the distance between the means of the two classes being separated, while minimizing their within-class variation. Such a ratio can be expressed as a resolution factor, RF (eq 13), where δ is the distance between the two class means, and σ_1 and σ_2 are the standard deviations of the two classes, respectively:

$$RF = \frac{\delta}{\sqrt{\sigma_1^2 + \sigma_2^2}} \tag{13}$$

Fisher's discriminant finds the vector $\mathbf{w}$ onto which the data are projected that maximizes the RF. The Fisher method does not prescribe how the resulting one-dimensional data should be separated into classes. In our work, we have used a simple threshold that is derived using the assumption that the projected (one-dimensional) distributions for each class are Gaussian.

5.1.2.3 *Quadratic discriminant analysis*

Quadratic discriminant analysis (QDA) assumes a multivariate normal distribution of the data for each class.[86] A data point x is placed in the class ω_k that minimizes the value of $D_k(x_i)$, as given by.

$$D_k(x) = (x - \mu_k)^T \Sigma_k^{-1} (x - \mu_k) + \ln|\Sigma_k| - 2\ln[P(\omega_k)] \tag{14}$$

85

In this equation, μ_k is the mean vector of class ω_k, Σ_k is the covariance matrix of class ω_k, and $P(\omega_k)$ is the *a priori* probability of membership in class ω_k. The value of $P(\omega_k)$ was taken to be equal to the quantity 1/(number of classes) for all of the classes. QDA effectively measures the distance from the unknown point to the mean of a class, while normalizing for the variance in the individual measurements (dimensions). The unknown is assigned to the class with the minimum "normalized" distance, $D_k(x)$. In practice, the class-conditional mean vectors and covariance matrices are not known in advance, so these parameters are typically estimated from training data using the conventional maximum likelihood (ML) estimators.[86]

5.1.2.4   *Regularized discriminant analysis*

Regularized discriminant analysis (RDA) minimizes the same $D_k(x)$ as is done in QDA (eq 3), but the ML estimates of the class-conditional covariance matrices are replaced with regularized estimates, $\Sigma_k(\lambda,\gamma)$.[87] The first regularizing parameter, λ, converts the class covariance matrix to a linear combination of the class covariance matrix and the pooled covariance matrix (i.e., that of all training samples) (eq 15-17). The second regularizing parameter, γ, shrinks the class covariance matrix toward a multiple of the identity matrix (eq 18). These regularizations correct for known discrepancies between the estimates of class distributions obtained from finite samples and the true population densities. The optimal values of λ and γ are determined by minimizing the misclassification in a leave-one-out cross-validation of all samples. The RDA discriminant will therefore always perform at least as well as the better-performing of LDA and QDA. The terms of eq 15-18 are defined as follows: Q_k is the ML-estimated class-conditional covariance matrix of class ω_k, Q_p is the pooled covariance matrix, N_k is the number of objects in class ω_k, N is the total number of objects, K is the number of classes, $x_i^{(k)}$ is the vector of the ith object in class ω_k, μ_K is the mean vector of class k, d is the number of variables (dimensions), $tr[\Sigma_k(\lambda)]$ is the trace of $\Sigma_k(\lambda)$, and I is the identity matrix.

$$Q_k = \frac{1}{N_k} \sum_{i=1}^{N_k} (x_i^{(k)} - \mu_k)(x_i^{(k)} - \mu_k)^T \tag{15}$$

$$Q_p = \sum_{k=1}^{K} \frac{N_k}{N} Q_k \tag{16}$$

$$\Sigma_k(\lambda) = \frac{(1-\lambda)N_k Q_k + \lambda N Q_p}{(1-\lambda)N_k + \lambda N}, \qquad 0 \le \lambda \le 1 \tag{17}$$

$$\Sigma_k(\lambda, \gamma) = (1-\lambda)\Sigma_k(\lambda) + \frac{\gamma}{d} tr[\Sigma_k(\lambda)]\mathbf{I}, \quad 0 \le \gamma \le 1 \tag{18}$$

5.1.2.5   *Partial least squares*

A slightly different approach to classification is through the use of regression. Given a set of examples, we seek a weight vector **w** that will map each example to a desired target value. The target value is termed t_1 for class 1 and t_2 for class 2; t_1 is typically +1 and t_2 is typically -1. The parameter n_1 is defined as the number of examples in class 1, n_2 is defined as the number of examples in class 2, and n is defined as n_1+n_2. If the examples from class 1 are arranged as rows in a matrix **X1** (each column is a detector) and the examples from class 2 are arranged as rows in a matrix **X2**, then **w** can be determined by solving the following multiple linear regression (MLR) problem:

$$\mathbf{t} = \mathbf{Xw} + \mathbf{e} \tag{19}$$

where **t** is a column vector containing n_1 rows of t_1 followed by n_2 rows of t_2. **X** is the vertical concatenation of the matrices **X1** and **X2**. The magnitude of the error vector, **e**, is minimized to solve the regression problem. Typically, the target vector and the measurements are mean-centered (and in some cases auto-scaled as well). The minimum mean-squared error solution to the MLR problem is well known,[86] and is given by:

$$\mathbf{w} = (\mathbf{X'X})^{-1}\mathbf{X't} \tag{20}$$

The effectiveness of **w** for classification can be determined by evaluating its predictive ability on new data (e.g., on a sequestered test set or on holdout examples in a leave-one-out cross-validation). If the target values are chosen as follows: $t_1 = n/n_1$ and $t_2 = -n/n_2$, then it can be shown that this approach reduces exactly to Fisher's linear discriminant.[86]

In some situations, such as when the measurements from different sensors are highly correlated or are noisy, obtaining a good weight vector through standard multiple linear regression is difficult due to the inverse appearing in eq 20. One method to resolve this problem is to perform a principal components analysis on **X** to determine the directions that have the most variance. The data are projected onto this reduced dimensional subspace and directions with smaller variance are presumed to correspond to noise and discarded. The target values are then predicted from the projected subspace rather than from the original data. In the chemometrics literature, this approach is known as principal components regression (PCR).[94] The projected data are commonly referred to as the "score matrix".

Principal components regression provides an alternative solution to the regression equation (eq 19) that may be better-behaved than the standard MLR solution. Partial least squares regression (PLS) is another method that provides an alternative solution to the regression equation.[90,94] The PLS method is similar to PCR, except that both the target vector and the measurements are

used to determine a lower dimensional subspace from which the predictions will be made. Determination of the subspace is accomplished through an iterative procedure.[90]

5.1.2.6   SIMCA

The SIMCA algorithm, which was developed by Wold in the 1970's,[91,92] is based on representing each class with its own principal components model. If a class is viewed as a cloud of points in a d-dimensional space, principal components analysis (PCA) finds an orthonormal basis for the cloud. (Here we assume that the PCA is applied to mean-centered data.) The first principal component is the direction of maximum variance of the data. The second principal component is the direction of maximum variance in the subspace orthogonal to the first component, and so on. If the cloud is "thin" in some directions, the class can be accurately approximated as a linear combination of $k < d$ principal components.

In the original SIMCA formulation,[91] the distance of a point from a class was determined by the out-of-space distance, i.e., by the Euclidean distance of the point from the subspace spanned by the k principal components used to model the class. The underlying assumption was that the variances in the directions orthogonal to the PCA subspace were all equal (e.g., due to white noise). By considering the out-of-space distance relative to the average out-of-space distance observed for the training set (the training examples do not all lie exactly on the PCA subspace), the SIMCA algorithm determined whether an unknown point was well-modeled by a particular class.

In more recent formulations,[91] the SIMCA distance includes an in-space-distance, as well as an out-of-space distance. The in-space distance is a measure of how well the projection of the point into the principal components subspace agrees with the projections of the known class data. The maximum and minimum values of the projected training data along each dimension of the subspace define a bounding box. SIMCA uses a slightly larger box (one standard deviation wider along each principal component direction) to represent the in-space distribution. If the projected point falls within the SIMCA box, i.e., within the "normal bounds", the in-space distance is 0; otherwise, the in-space distance is given by the weighted Euclidean distance of the point from the SIMCA box, where the weights correspond to the inverse variance along each dimension. The in-space and out-of-space distances are then combined and the unknown test point is assigned to the nearest class.

With a different definition of the in-space distance that is not based on a bounding box, but is based instead on a Gaussian model of the in-space distribution, it is readily shown that SIMCA is similar to a form of regularized QDA known in the chemometrics literature as DASCO (discriminant analysis with shrunken covariances).[83] The maximum likelihood estimates of the class covariance matrices used in standard QDA are replaced by a principal components estimate in which variances along the directions of highest variance are retained, while variances along directions of lowest variance are replaced with a constant value (related to the average out-of-space distance of the training set, which is used as a normalizing factor in SIMCA). Frank and Friedman discuss the connection between LDA, QDA, RDA, SIMCA, and DASCO in more detail.[83]

5.2 *Experimental*

5.2.1 Materials

Poly(ethylene-*co*-vinyl acetate) (70% vinyl acetate), polycaprolactone, cellulose acetate, hydroxypropylcellulose, poly(4-vinylpyridine), poly(vinyl acetate), ethyl cellulose, poly(ethylene-*co*-acrylic acid) (86% ethylene), 1,2-polybutadiene, poly(methyloctadecylsiloxane), and poly(styrene-*co*-acrylonitrile) were purchased from Scientific Polymer Products. Poly(4-vinylphenol), poly(vinyl butyral), and poly(ethylene glycol) were purchased from Polysciences. Poly(ethylene oxide), poly(ethylene-*co*-vinyl acetate) (18% vinyl acetate), poly(styrene-*co*-maleic anhydride) (50:50), polyvinylpyrrolidone, polystyrene, and poly(methyl methacrylate) were purchased from Aldrich. The carbon black was Black Pearls 2000 from Cabot Corporation. Bis(2-ethylhexyl)phthalate was purchased from Aldrich. n-Hexane was 99+% from Aldrich, heptane was supplied by Mallinckrodt, and 1-propanol and 2-propanol were obtained from EM Science. The H_2O was filtered through a Barnstead 18 MΩ–cm resistivity filter. D_2O was 99.9 atom % deuterium, purchased from Aldrich and used as received.

5.2.2 Detectors and Instrumentation

Polymers were generally dissolved in tetrahydrofuran, except for poly(4-vinylpyridine) and poly(vinylpyrrolidone), which were dissolved in ethanol, and poly(ethylene-*co*-vinyl acetate) (18% vinyl acetate), and 1,2-poly(butadiene), which were dissolved in toluene. Each polymer (160 mg) was dissolved in 20 mL of its respective solvent either at room temperature or by heating to 35-40° C for several hours. Carbon black (40 mg) was then added and the suspension was then sonicated for at least 20 min.

Corning microscope slides were cut into 10 mm x 25 mm pieces to provide substrates for the detectors. A 7-8 mm gap across the middle of each slide was masked and 300 nm of chromium and 500 nm of gold were then evaporated onto the ends of the slides to form the electrical contacts. Detectors were formed by spin-coating polymer-carbon black suspensions onto the prepared substrates. The resulting films were then allowed to dry overnight.

5.2.3 Measurements

The instrumentation and apparatus for resistance measurements and for the delivery of vapors has been described previously.[31] The array of 20 polymers listed in Table 6 was used for the measurements. All exposures were performed for a duration of 300 s, and were separated by periods of 600 s of flowing laboratory air. The first several exposures in a long series tended to give responses that were different from those of the remainder of the exposures, so the initial 40 exposures were excluded from analysis for every data set evaluated in this work. The background

TABLE 6. Polymers in the 20-detector array used for discrimination algorithm evaluation

Detector	Polymer
1	poly(ethylene-*co*-vinylacetate) (70% vinyl acetate)
2	poly(ethylene oxide)
3	polyvinylpyrrolidone *P*
4	1,2-polybutadiene
5	polycaprolactone
6	poly(4-vinylphenol) *P*
7	poly(vinyl acetate) *P*
8	cellulose acetate
9	poly(4-vinylpyridine) *P*
10	poly(methyl methacrylate) *P*
11	poly(styrene-*co*-maleic anhydride) *P*
12	poly(vinyl butyral) *P*
13	hydroxypropylcellulose
14	ethyl cellulose
15	poly(ethylene-*co*-acrylic acid) (86% ethylene)
16	poly(methyloctadecylsiloxane)
17	poly(ethylene glycol)
18	poly(ethylene-*co*-vinylacetate) (18% vinyl acetate)
19	polystyrene *P*
20	poly(styrene-*co*-acrylonitrile) *P*

P indicates plasticization with
8% by mass bis(2-ethylhexyl)phthalate

air contained 1.10 ± 0.15 part per thousand of water vapor, but no active auxiliary control over the humidity of the solvents or over the ambient temperature of the bubblers or the detectors (generally 21.5 ± 1.5 °C) was performed during data collection

5.2.3.1 *H₂O vs. D₂O*

Two bubblers were filled with D_2O (labeled #1 and #3) and two with H_2O (labeled #2 and #4). For all exposures, vapors were diluted to $P/P^o = 0.050$, where P is the partial pressure of the analyte and P^o is the vapor pressure of the analyte at room temperature. Forty exposures alternating between H_2O and D_2O were performed, and then two hundred additional exposures were performed, cycling fifty times sequentially through bubblers 1, 2, 3, and 4.

5.2.3.2 *Pairwise Resolution of Similar Analytes at Low Fractions of their Vapor Pressure*

A series of 120 exposures to 1-propanol and 2-propanol were performed, with exposures alternating sequentially between each member of the pair of analytes. All exposures were initially performed at a partial pressure, P, such that $P/P^o = 0.01$ for the analyte in a background of laboratory air. Similar data were collected at partial pressures of $P/P^o = 7.5 \times 10^{-3}$, 5.0×10^{-3}, and 2.5×10^{-3}, with 100 alternating exposures to each member of the solvent pair performed at each analyte concentration. An identical exposure sequence and protocol was performed for collection of the detector response data for n-hexane vs. n-heptane.

5.2.3.3 *Mixtures of Analytes*

Vapor was delivered from 2 bubblers, one containing 2-propanol and the other containing 1-propanol. The 40 initial exposures (which were not used in the data analysis) consisted of a combination of 2-propanol at $P/P^o = 2.5 \times 10^{-2}$ and 1-propanol at $P/P^o = 2.5 \times 10^{-2}$. For data collection, exposure 1 consisted of a combination of 2-propanol at $P/P^o = 2.5 \times 10^{-2}$ and 1-propanol at $P/P^o = 2.5 \times 10^{-2}$. Exposure 2 consisted of 2-propanol $P/P^o = 2.7 \times 10^{-2}$ and 1-propanol $P/P^o = 2.3 \times 10^{-2}$; exposure 3, 2-propanol $P/P^o = 2.1 \times 10^{-2}$ and 1-propanol $P/P^o = 2.9 \times 10^{-2}$; exposure 4, 2-propanol $P/P^o = 3.5 \times 10^{-2}$ and 1-propanol $P/P^o = 1.5 \times 10^{-2}$. The series of exposures 1, 2, 3 and 4 was repeated 100 times, for a total of 400 exposures. An identical data set was collected for n-hexane and n-heptane.

5.2.4 Data Reduction

The average of resistance readings for the 60 s immediately prior to the beginning of the exposure was used as the baseline resistance, R_b, and the average of the resistance readings for the last 60 s of the exposure was taken as the equilibrium response, R_{eq}. The quantity used in data analysis was the steady state relative differential resistance change, $\Delta R/R_b$, where $\Delta R = R_{eq} - R_b$. Data were converted to $\Delta R/R_b$ form in Microsoft Excel, while all subsequent manipulations were performed using Matlab. Original Matlab code was written to analyze the data, but the SIMCA

routine was based upon one by Donald B. Dahlberg, available on the internet at ftp://ftp.cdrom.com/pub/MacSciTech/chem/ chemometrics/Dahlberg SIMCA.text.

The $\Delta R/R_b$ data were evaluated in three different forms--unnormalized, and normalized by two different methods. In the first normalization (n_a), for each exposure the signal ($X_i = \Delta R/R_b$) of the ith detector was divided by the sum of the X_i signals of all 20 detectors in the array (eq 21). In the second normalization (n_g), signals were divided by the square root of the sum of the squares of the signals across the array (eq 22). In three dimensions, the first normalization method maps the data onto a plane, whereas the second normalization method maps the data onto the unit sphere. Because the responses of the carbon black composite detectors to various analytes have been observed to vary linearly with concentration of the analyte in the vapor phase,[9] either normalization results in a unique, concentration-insensitive signature for an analyte of interest. The two normalizations had a very similar effect on the classification accuracy of the discriminants studied herein; therefore, only the results from n_a are presented.

$$X^{(n_a)} = X \bigg/ \sum_{n=1}^{d} X_n \tag{21}$$

$$X^{(n_g)} = X \bigg/ \left[\sum_{n=1}^{d} \left(X_n \right)^2 \right]^{1/2} \tag{22}$$

Except where otherwise specified, all the discriminants were evaluated using a leave-one-out cross validation methodology. In this procedure, one exposure (data vector) is left out of the data set and the remaining exposures are used as a training set to create the classification boundary. The left-out exposure is then classified by this rule and the classification is checked against the analyte's true class. The procedure is repeated for each member of the data set, and the rate of correct classification is a useful measure of a particular discriminant's efficiency.

5.3   *Results*

5.3.1 Discrimination Between H_2O and D_2O

Figure 37 presents the average responses and standard deviations of the detectors in response to 100 exposures of H_2O and 100 exposures of D_2O. Despite the similarities in response that were expected, and observed, for these two compounds, it was possible to discriminate robustly between the light and heavy water exposures based on the differences in response patterns that they produced on the carbon black-polymer composite chemiresistor array.
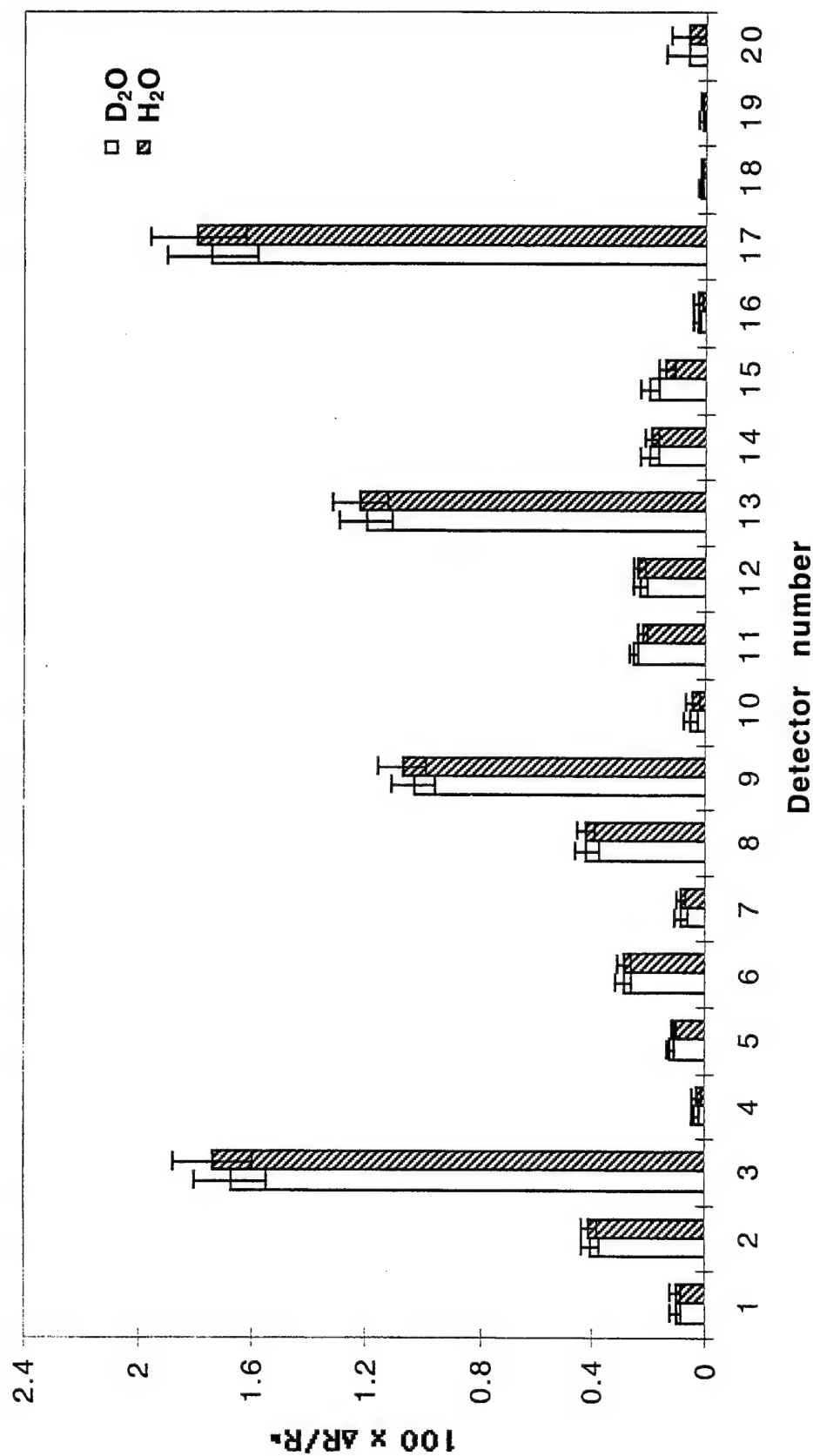
FIGURE 37. Steady-state relative differential resistance response, $\Delta R/R_b$, of carbon black-polymer composite vapor detectors to H_2O and D_2O (error bars are plus and minus one standard deviation). All exposures were at $P/P^o=0.050$. Data represent means and standard deviations for 100 exposures to each analyte. The detector number indicates the polymer used to form the composite, with the detector numbering corresponding to the polymer composition listed in Table 6.

Table 7 presents the resolution factors between D_2O and H_2O obtained from Fisher's linear discriminant when each bubbler is treated as a separate class. Bubblers containing H_2O were well-differentiated from bubblers containing D_2O, with resolution factors between 8.1 and 10.1.

Interestingly, the analyte exposures from bubbler 1 were resolved from analyte exposures from bubbler 3 by a factor of 2.1, even though both contained D_2O. Similarly, analytes from bubblers 2 and 4 were both nominally H_2O, yet were resolved by a factor of 1.8. Resolution factors obtained using the LDA algorithm will never be zero with a finite sample size. Additionally, small amounts of contamination in the bubblers and lines could possibly contribute to the differences in patterns from nominally identical analytes placed in different bubblers. As a test for differences between bubblers, the exposures were divided into four sets, two each of H_2O and D_2O, but with each set containing data from a combination of two bubblers. As shown in Table 3, resolution factors between H_2O and H_2O and between D_2O and D_2O were then only 0.8 and 0.9, clearly indicating that some of the original discrmination was due to differences in what was delivered from the bubblers. The RF values for discrimination between these grouped exposures of H_2O and D_2O were still quite significant, and fell in the range of RF = 8.3 - 8.6 (Table 8).

To further test that discrimination was occurring because of differences between H_2O and D_2O, and not because of various impurities in the bubblers or some other cause, the data were divided into 2 halves, one of which was used as a training set and the other was used a test set. The array was trained on the exposures from bubbler 1 (D_2O) and 2 (H_2O) and LDA was then used to classify the exposures from bubblers 3 (D_2O) and 4 (H_2O). All 100 of these exposures from bubblers 3 or 4 were correctly identified as either H_2O or D_2O using this procedure. Similarly, training on bubblers 3 and 4 and testing on 1 and 2 yielded 100 correct identifications. Training on 100 randomly selected exposures taken from all 4 bubblers and then testing on the other 100 exposures also produced perfect classification.

Table 9 presents the leave-one-out cross-validation error rates for all of the data obtained on this system. All the discriminants except for kNN and SIMCA (when a fixed number of principal components were used) were perfect in their classification. Normalization decreased the performance of the kNN algorithm, whereas it enhanced the performance of SIMCA. The degradation in performance of the kNN algorithm upon normalization of the response data occurred because the normalization produced less overall amplitude differences between the patterns, and the kNN algorithm utilized such differences in classifying the analytes.

5.3.2 Resolution of Analytes at Low Fractions of Their Vapor Pressure

5.3.2.1 Form of the Data

Figure 38 shows the unnormalized response data for each detector in the array to hexane and to heptane, with each analyte at $P/P^o = 7.5 \times 10^{-3}$. Figure 39 displays similar data at an analyte partial pressure of $P/P^o = 2.5 \times 10^{-3}$. At a fixed fraction of the analyte's vapor pressure, the response patterns for hexane and heptane are quite similar, as would be expected from their similar chemical structure and properties. The magnitude of the response from detectors that showed significant signals with hexane (detectors 1, 2, 4, 5, 8, 12-19) decreased by a factor of 3.0 when the hexane partial pressure was decreased from $P/P^o = 7.5 \times 10^{-3}$ to $P/P^o = 2.5 \times 10^{-3}$,

TABLE 7. Resolution factors for H_2O versus D_2O using LDA when data from each bubbler is treated as a separate class.

Bubbler	1, D_2O	2, H_2O	3, D_2O	4, H_2O
1, D_2O	0.0			
2, H_2O	8.2	0.0		
3, D_2O	2.1	8.1	0.0	
4, H_2O	9.3	1.8	10.1	0.0

TABLE 8. Resolution factors for H_2O versus D_2O LDA when data are grouped into 4 classes, with the 2 H_2O classes each a random combination of half the H_2O exposures, and the 2 D_2O classes each a random combination of half the D_2O exposures.

Analyte	D_2O	H_2O	D_2O	H_2O
D_2O	0.0			
H_2O	8.6	0.0		
D_2O	0.9	8.5	0.0	
H_2O	8.4	0.8	8.3	0.0

TABLE 9. Leave-one-out cross-validation error rates for H_2O versus D_2O (complete data set).

	k-NN	LDA	QDA	RDA	PLS	SIMCA	SIMCA
unnormalized	0.125	0	0	0	0	0.015	0 (17)
na	0.37	0	0	0	0	0.005	0 (16)

FIGURE 38. $\Delta R/R_b$ response of an array of carbon black-polymer composite vapor detectors to n-hexane and n-heptane at $P/P° = 0.0075$. Means and standard deviations are for 120 exposures to each analyte.
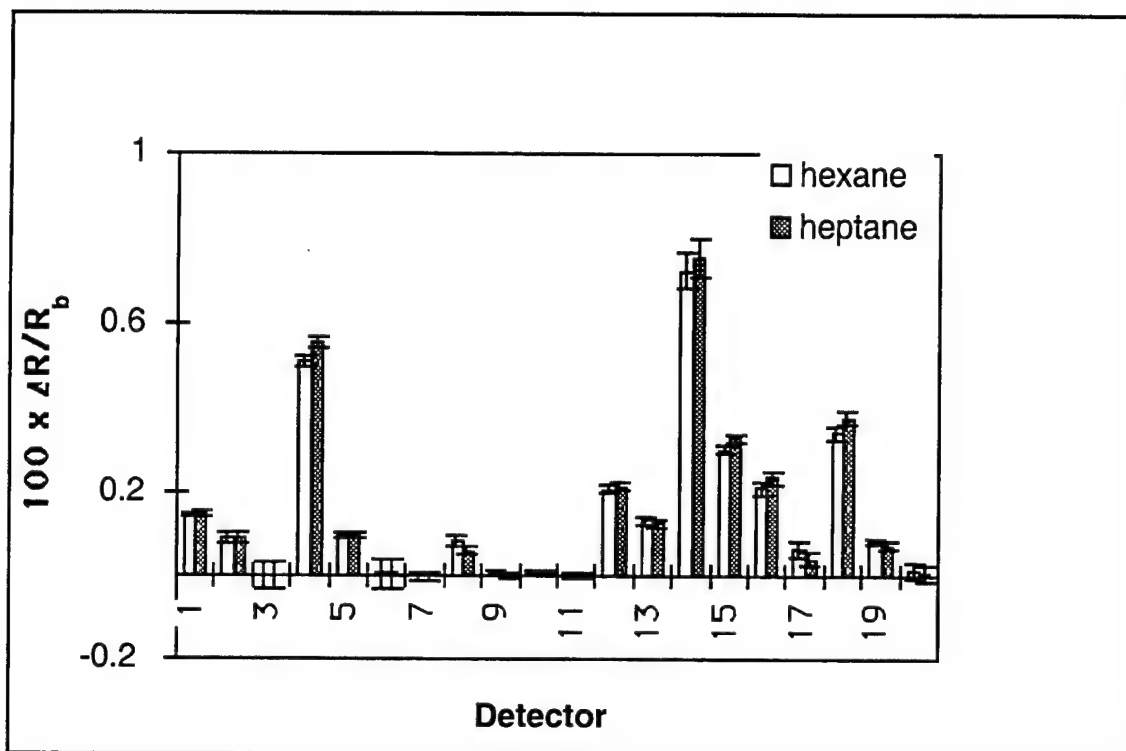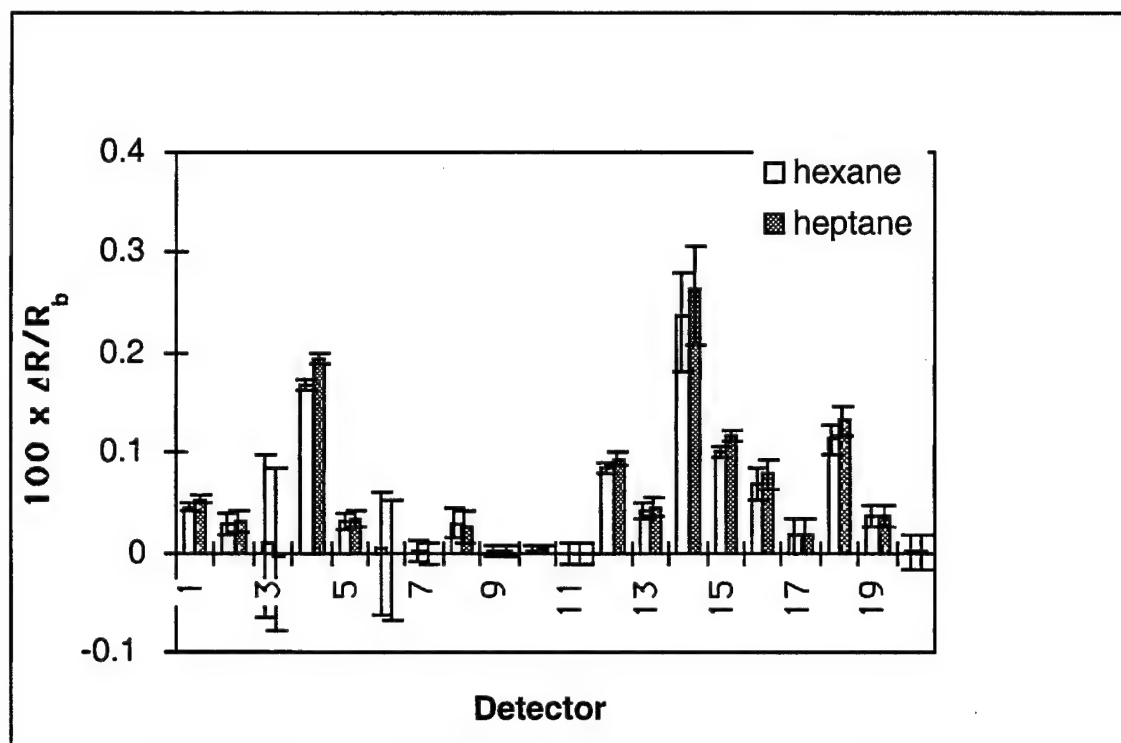
FIGURE 39. $\Delta R/R_b$ response of an array of carbon black-polymer composite vapor detectors to n-hexane and n-heptane at $P/P° = 0.0025$. Means and standard deviations are for 120 exposures to each analyte, with exposures alternating sequentially between each member of the pair of analytes.

99

whereas the same decrease in heptane partial pressure produced a mean signal decrease of 2.7 across the same set of detectors. These data are in accord with the linearity of response of carbon black composite detectors to analyte concentration that has been observed previously.[9]

In contrast, the absolute standard deviation of the responses across the set of 100 exposures was essentially constant as the analyte concentration was varied. For example, the ratio of the standard deviation of a detector's responses to hexane at $P/P^o=7.5 \times 10^{-3}$ to that at $P/P^o=2.5 \times 10^{-3}$ had an average of 1.15 across the set of detectors that responded well to hexane (1, 2, 4, 5, 8, 12-19), whereas this ratio had a value of 1.12 for heptane. Thus, the absolute signal strength decreased as the analyte partial pressure declined, but the absolute variance remained essentially constant, so the discrimination ability of the array is expected to become worse at lower analyte partial pressures.

A quite different situation was, however, observed for 1-propanol and 2-propanol. The absolute standard deviations decreased by an average of 3.91 for 1-propanol and by an average of 3.54 for 2-propanol when the partial pressure of these analytes was reduced from $P/P^o = 1.0 \times 10^{-2}$ to 2.5×10^{-3} (Figures 40 and 41). The main cause for the difference was not a change in random noise, but a steady drift in some of the detector responses over the course of this particular interval of data collection. The effect was more pronounced at $P/P^o = 1.0 \times 10^{-2}$ than at $P/P^o = 2.5 \times 10^{-3}$, accounting for the larger absolute standard deviation values observed at the higher analyte concentration. For illustration, Figure 42 shows the data for 100 responses of detector 8 to 1-propanol at $P/P^o = 1.0 \times 10^{-2}$ and $P/P^o = 2.5 \times 10^{-3}$, respectively. At the higher concentration, the signal drifted by 32% over 50 hours, while at the lower concentration it drifted by only 10%. When a simple linear correction was applied to the data (Figure 42), the standard deviation of the higher concentration data decreased by a factor of 3.3, while that of the lower concentration data decreased by a factor of 1.3.

5.3.2.2 *Performance of Various Discriminant Algorithms*

Table 10 presents the leave-one-out cross-validation error rates for the different discriminant algorithms for the 1-propanol /2-propanol and hexane/heptane data sets. For both the 1-propanol/2-propanol and n-hexane/n-heptane classifications, the error rate increased for all discriminants at lower partial pressures of analyte. For the unnormalized data, LDA and RDA were the best discriminants (average error rates of 0.079 for hexane vs heptane) with RDA offering only a very slight improvement upon LDA. The PLS algorithm had an average error rate of 0.089, followed by QDA and optimized SIMCA at ≈ 0.10. The kNN discriminant had an average error rate of 0.117, and the worst-performing discriminant was SIMCA, with an average error rate of 0.13.

The discriminants were more uniform in their leave-one-out cross validated performance on normalized data. Once again, SIMCA and kNN were the worst classifiers. LDA and QDA were similar overall in their classification accuracy, but their classification performance differed somewhat in different tasks. Because RDA can vary between LDA and QDA, and necessarily chooses the best of these two limiting algorithms based upon cross-validation, RDA was the best discriminant for these normalized data.

100

TABLE 10. Leave-one-out cross-validation error rates for 1-propanol versus 2-propanol and n-hexane versus n-heptane at low concentration.

Error Rates[a]

1-propanol vs. 2-propanol

$100 \times P/P°$	k-NN		LDA		QDA		RDA		PLS		12 PC's SIMCA		best #PC's SIMCA	
0.01	0	(0.01)	0	(0)	0	(0)	0	(0)	0	(0)	0	(0.025)	0	(0.005)
0.0075	0.01	(0.015)	0.005	(0)	0.005	(0.01)	0.005	(0)	0.015	(0)	0.02	(0.005)	0.01	(0)
0.005	0.41	(0.495)	0.26	(0.48)	0.335	(0.41)	0.255	(0.39)	0.3	(0.495)	0.47	(0.445)	0.36	(0.395)
0.0025	0.385	(0.465)	0.35	(0.495)	0.435	(0.47)	0.35	(0.415)	0.38	(0.55)	0.44	(0.515)	0.4	(0.42)
						n-hexane vs. n-heptane								
0.01	0.03	(0.01)	0.005	(0.005)	0.005	(0.005)	0.005	(0.005)	0.005	(0.005)	0.01	(0.005)	0	(0.005)
0.0075	0.035	(0.065)	0.005	(0.01)	0.01	(0.045)	0.005	(0.01)	0.005	(0.01)	0.065	(0.11)	0.03	(0.075)
0.005	0.02	(0.285)	0.005	(0.18)	0.005	(0.245)	0.005	(0.165)	0.005	(0.16)	0.01	(0.29)	0.005	(0.285)
0.0025	0.045	(0.41)	0.005	(0.35)	0.01	(0.32)	0.005	(0.29)	0.005	(0.305)	0.025	(0.36)	0.01	(0.345)
averages:	**0.134**	**(0.219)**	**0.079**	**(0.190)**	**0.101**	**(0.188)**	**0.079**	**(0.159)**	**0.089**	**(0.191)**	**0.130**	**(0.219)**	**0.102**	**(0.191)**

[a] Error rate for Unnormalized Data; Error rates for Normalized Data given in parenthesis

101
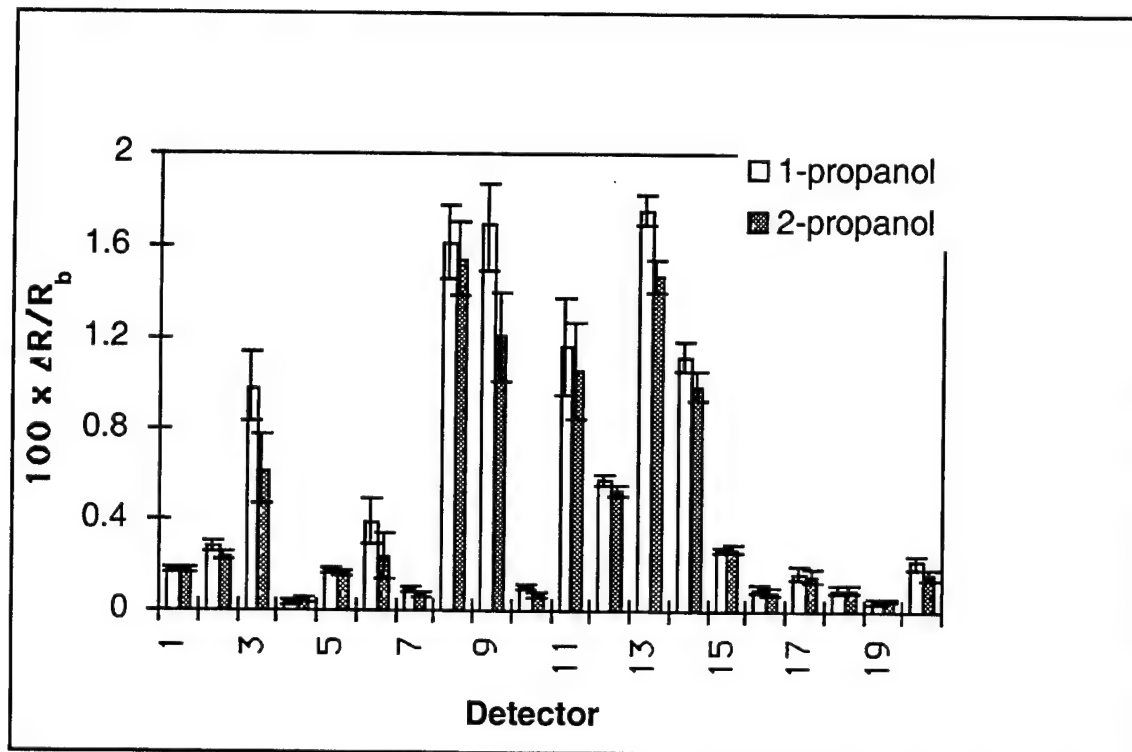
FIGURE 40. $\Delta R/R_b$ response of an array of carbon black-polymer composite vapor detectors to 1-propanol and 2-propanol at $P/P° = 0.010$. Means and standard deviations are for 120 exposures to each analyte, with exposures alternating sequentially between each member of the pair of analytes.
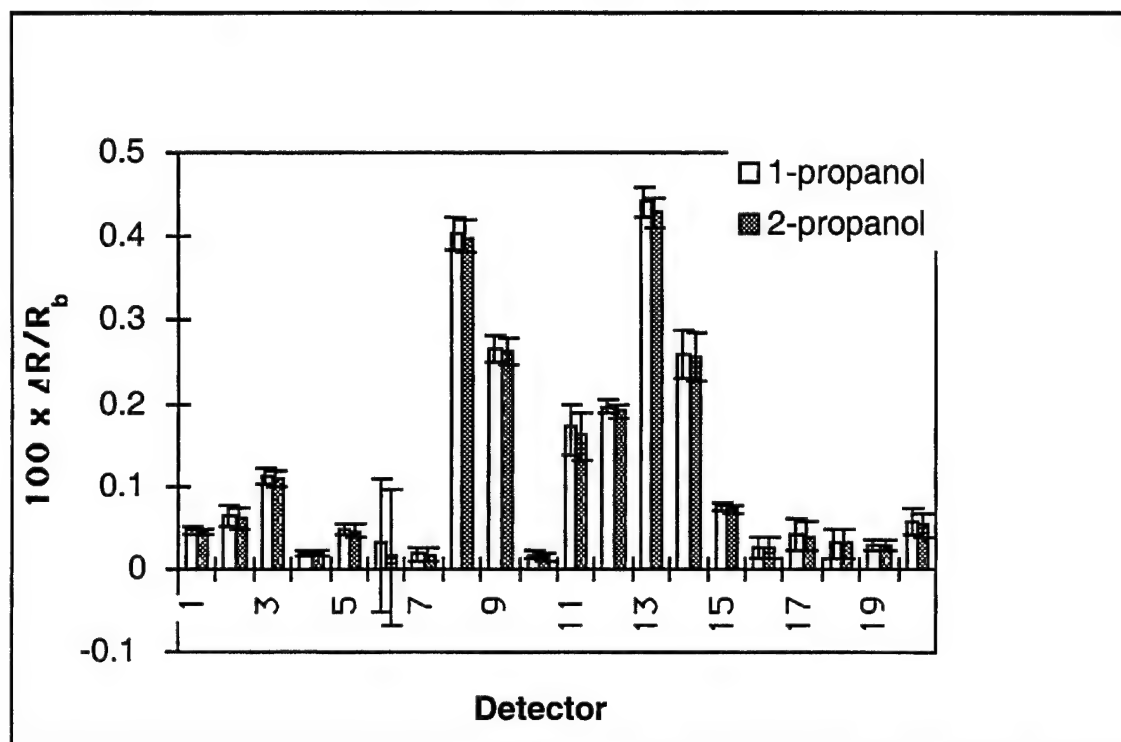
FIGURE 41. $\Delta R/R_b$ response of an array of carbon black-polymer composite vapor detectors to 1-propanol and 2-propanol at $P/P° = 0.0025$. Means and standard deviations are for 120 exposures to each analyte, with exposures alternating sequentially between each member of the pair of analytes.

103

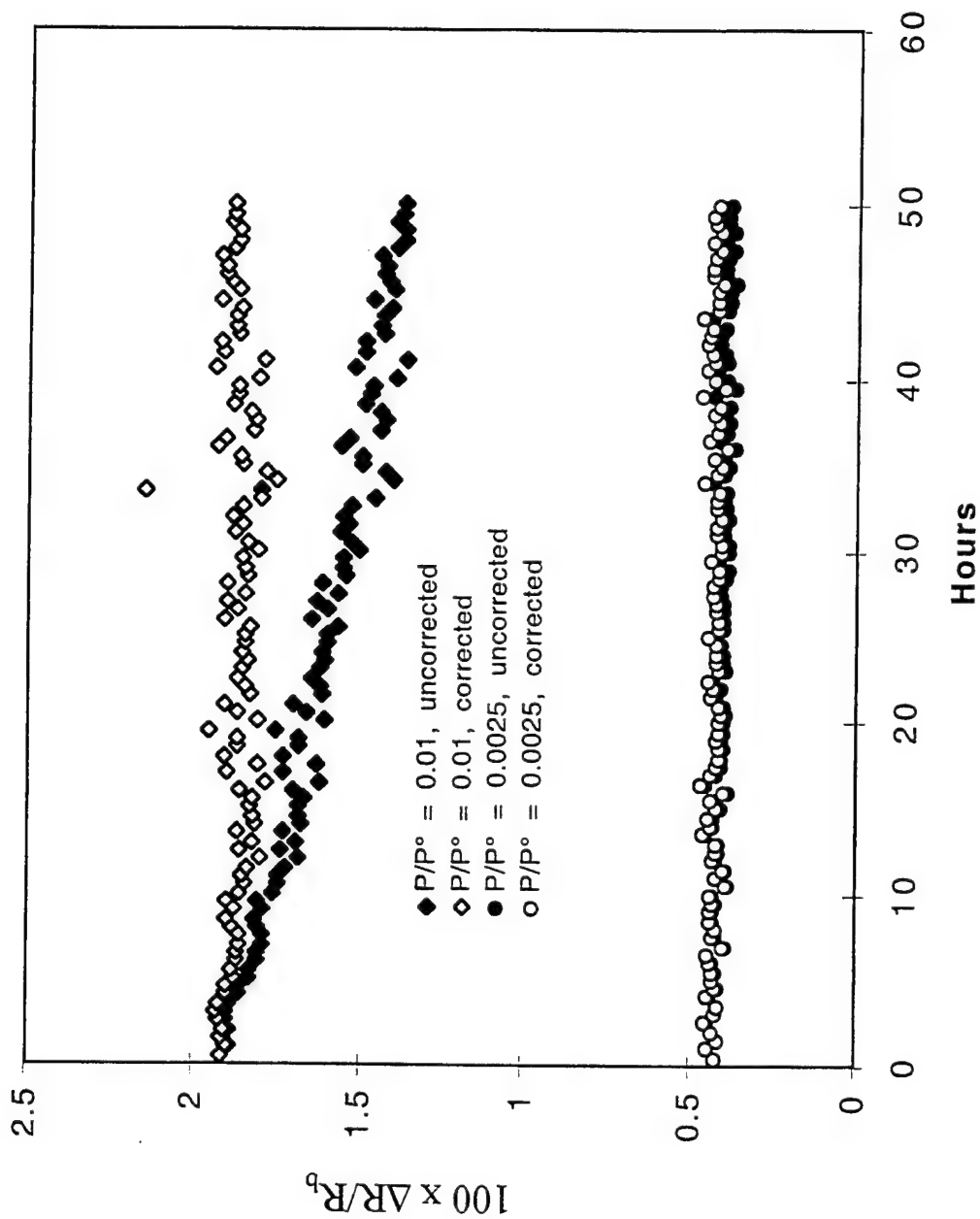**Figure 42.** $\Delta R/R_b$ response of detector 8 to 1-propanol and 2-propanol at $P/P^\circ = 0.010$ (diamonds) and at $P/P^\circ = 0.0025$ (circles). Uncorrected, raw data are indicated by filled symbols, and data produced through the use of a linear correction to yield a regression line with slope of zero are indicated by unfilled symbols.

104

5.3.3 Discrimination Between Compositionally Similar Binary Analyte Mixtures

5.3.3.1   Structure of Data

Figure 43 displays the average responses of each detector to the four different hexane/heptane binary mixtures. The detector responses exhibited a monotonic trend as a the mole fraction of hexane was increased, as expected. In contrast, the response of some detectors was not monotonic for the 1-propanol / 2-propanol vapor mixtures (Figure 44). Standard deviations of the detector responses for the 1-propanol / 2-propanol vapor mixtures were also generally larger than those for the hexane/heptane mixtures. The larger standard deviations can be attributed to a steady change (usually a decrease) in the response of a detector observed over the course of that particular data collection interval, and the error introduced by the drift may account for the fact that the change across a series is not always monotonic, especially when comparing the very similar 50/50 and 54/46 binary mixtures of 1-propanol and 2-propanol.

5.3.3.2   Performance of Discriminant Algorithms

The leave-one-out cross-validation error rates for this data set are given in Table 11. For both the 1-propanol/2-propanol and n-hexane/n-heptane classifications, the error rate decreased for all discriminants as the separation in mole fraction between the analytes increased. Normalization did not have a large effect on discriminant performance. The LDA and RDA algorithms were the best-performing discriminants, with average error rates near 0.024. The RDA algorithm was nearly identical in performance to LDA, and usually converged to the grid point $(\lambda,\gamma) = (1,0)$, equivalent to LDA. The PLS discriminant was almost as proficient as LDA and RDA, with average error rates of about 0.025. The other discriminants followed in the order, best to worst: QDA, optimized SIMCA, SIMCA, and kNN.

5.4   Discussion

5.4.1 Discrimination Between H_2O and D_2O

Although H_2O and D_2O have very similar physical properties, there are many quite measurable differences, including, for example, boiling point (100 °C vs. 101.4 °C) and melting point (0 °C vs. 3.8 °C).[95] Note that in Figure 37 the detectors with the largest responses (those that are most polar and hydrogen-bonding) tended to respond more strongly to H_2O than D_2O, while the converse is true of the relative responses of the less-polar polymers.

An examination of Figure 37 (and specifically the indicated standard deviations) reveals that most detectors would individually perform very poorly in distinguishing H_2O from D_2O. Detector 11 is the most discriminating individual detector, as reflected by the fact that the **w** vectors found between H_2O and D_2O always had their largest coefficients for 11. Even so, when 11 was removed from the data set; RFs of 8-10 were still obtained, and identification tests were perfect.

105

TABLE 11. Leave-one-out cross-validation error rates for compositionally-similar analyte mixtures of 1-propanol/2-propanol and n-hexane/n-heptane.

Error Rates[a]

1-propanol and 2-propanol

Δ mixture (100 x P/P°)	k-NN		LDA		QDA		RDA		PLS		12 PC's SIMCA		best #PC's SIMCA	
4	0.325	(0.165)	0.03	(0.025)	0.075	(0.08)	0.03	(0.025)	0.03	(0.025)	0.205	(0.145)	0.13	(0.12)
8	0.12	(0.105)	0.005	(0.01)	0.015	(0.02)	0.005	(0.01)	0.005	(0.01)	0.19	(0.21)	0.045	(0.065)
12	0.065	(0.045)	0	(0)	0	(0)	0	(0)	0	(0)	0.1	(0.05)	0.005	(0.005)
16	0.01	(0.01)	0	(0)	0	(0)	0	(0)	0	(0)	0.01	(0)	0	(0)
20	0.005	(0)	0	(0)	0	(0)	0	(0)	0	(0)	0.005	(0.005)	0	(0)
28	0	(0)	0	(0)	0	(0)	0	(0)	0	(0)	0	(0)	0	(0)

n-hexane and n-heptane

Δ mixture (100 x P/P°)	k-NN		LDA		QDA		RDA		PLS		12 PC's SIMCA		best #PC's SIMCA	
4	0.42	(0.45)	0.225	(0.21)	0.31	(0.285)	0.225	(0.21)	0.23	(0.21)	0.34	(0.365)	0.28	(0.305)
8	0.365	(0.295)	0.025	(0.04)	0.04	(0.06)	0.025	(0.01)	0.025	(0.025)	0.085	(0.13)	0.06	(0.105)
12	0.3	(0.27)	0.005	(0)	0.01	(0.05)	0.005	(0)	0.005	(0.005)	0.025	(0.045)	0.015	(0.025)
16	0.31	(0.265)	0.005	(0.005)	0.005	(0)	0.005	(0)	0.005	(0.005)	0.035	(0.025)	0.015	(0.025)
20	0.215	(0.135)	0	(0)	0	(0)	0	(0)	0	(0)	0.005	(0)	0	(0)
28	0.065	(0.01)	0	(0)	0	(0)	0	(0)	0	(0)	0	(0)	0	(0)
averages:	**0.183**	**(0.146)**	**0.025**	**(0.024)**	**0.038**	**(0.038)**	**0.025**	**(0.024)**	**0.025**	**(0.025)**	**0.083**	**(0.081)**	**0.046**	**(0.054)**

a Error rate for Unnormalized Data; Error rates for Normalized Data given in parenthesis

106

Figure 43. $\Delta R/R_b$ response of an array of carbon black-polymer composite vapor detectors to mixtures of hexane and heptane. The total partial pressure of the two analytes was $P/P^o = 0.050$; the fraction of the total analyte partial presure that was due to hexane and heptane, respectively, is indicated in the legend.
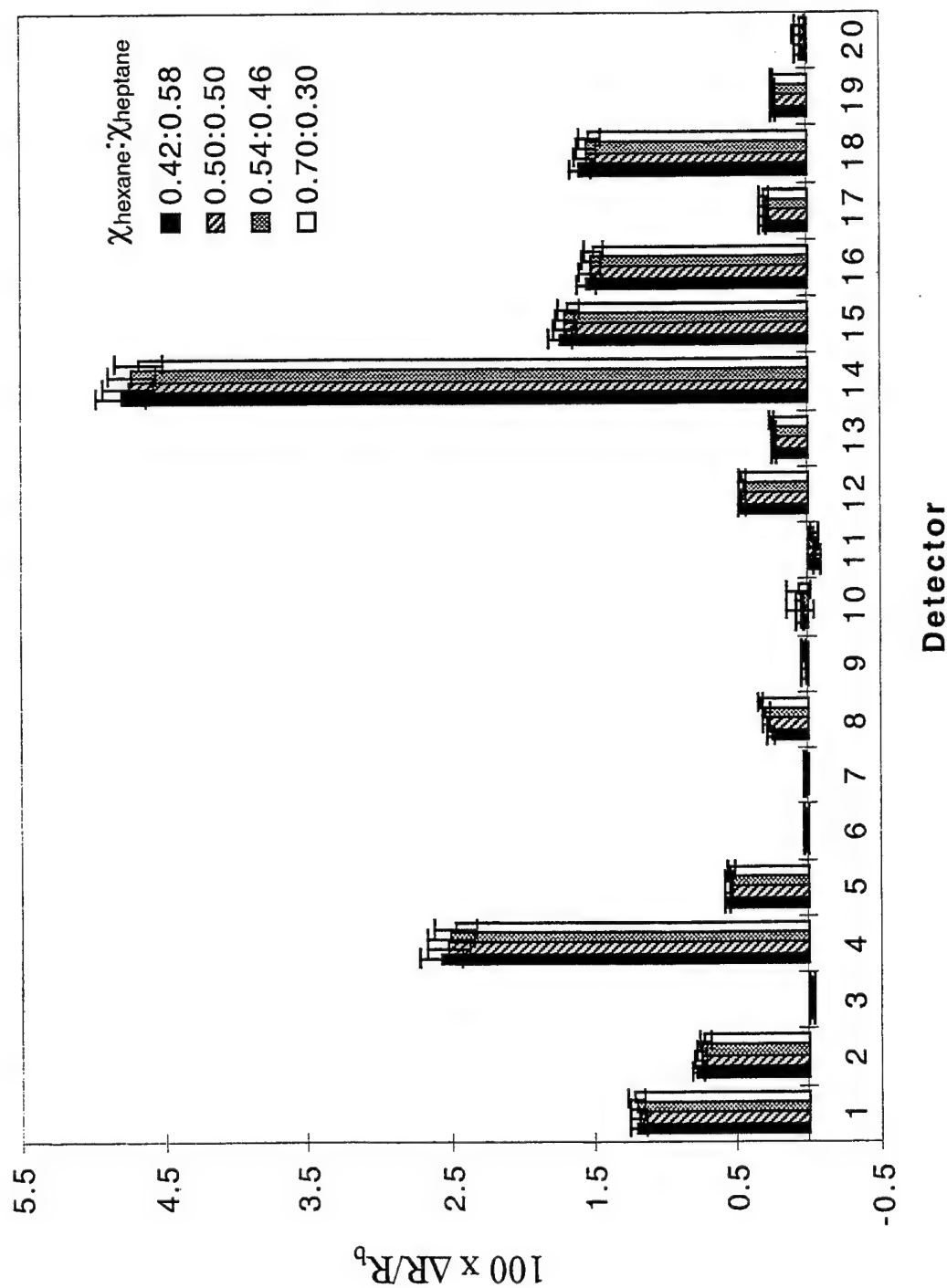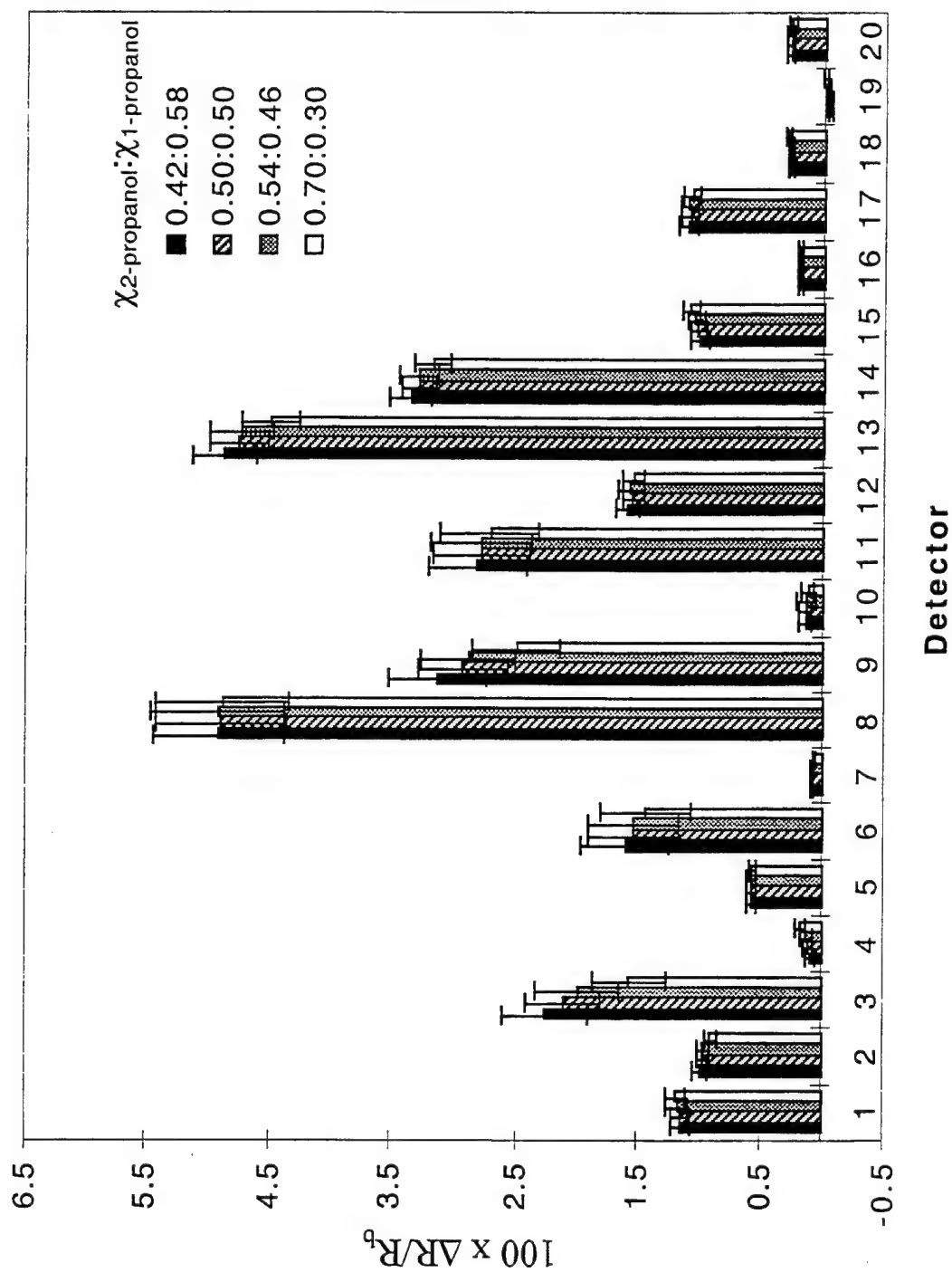
Figure 44. $\Delta R/R_b$ response of an array of carbon black-polymer composite vapor detectors to mixtures of 1-propanol and 2-propanol. The total partial pressure of the two analytes was $P/P° = 0.050$; the fraction of the total analyte partial pressure that was due to 1-propanol and 2-propanol, respectively, is indicated in the legend.

108

5.4.2 Performance of LDA and QDA

The H_2O and D_2O data do not provide an appropriate challenge for evaluating the performance of discriminant algorithms, because perfect classification was achieved for most of the algorithms investigated. Such comparisons could be made, however, for both of the experiments involving analytes at low fractions of their vapor pressure and for those involving compositionally-similar binary analyte mixtures. In these tasks, LDA performed better than QDA. In RDA, where the floating parameter λ allows hybridization between LDA and RDA, a λ value near 1, corresponding to LDA, was generally found to be optimal. These results may at first seem surprising, because QDA is a more general classifier and because QDA reduces to LDA in the specific case when the class covariance matrices are equal. LDA simply uses the pooled covariance matrix, effectively assuming that all the class covariance matrices are equal.

If the true class covariance matrices are the same, then the two classifiers should perform identically in the asymptotic situation in which an infinite number of training examples are available and the class statistics are known exactly. However, in the present situation, the statistics must be estimated from a finite number of training examples. The QDA algorithm estimates a (d x d) covariance matrix for each class, whereas LDA estimates a (d x d) covariance matrix for the pooled data. The covariance estimates produced by QDA will be based on half as much data as in the LDA case and therefore are less likely to reflect the 'true' covariance matrix. Also, as shown below, QDA emphasizes the differences in covariance structure between the two classes. From eq 14, we have

$$D_1(x) = (x - \mu_1)^T \Sigma_1^{-1}(x - \mu_1) + \ln|\Sigma_1| - 2\ln[P(\omega_1)] \tag{23}$$

$$D_2(x) = (x - \mu_2)^T \Sigma_2^{-1}(x - \mu_2) + \ln|\Sigma_2| - 2\ln[P(\omega_2)] \tag{24}$$

After some manipulation one obtains:

$$D_2(x) - D_1(x) = x^T(\Sigma_1^{-1} - \Sigma_2^{-1})x + 2(\Sigma_2^{-1}\mu_2 - \Sigma_1^{-1}\mu_1)^T x + c \tag{25}$$

When Σ_1 and Σ_2 are identical, the first term drops out and the LDA classifier is obtained. However, when Σ_1 and Σ_2 are replaced with their estimated versions, which are not likely to be exactly equal, the first term remains, leading to suboptimal classification.

5.4.3 Performance of PLS and SIMCA

The performance of PLS tracked very closely with that of LDA. The PLS discriminant is fundamentally a form of multiple linear regression, and, as explained in above, linear regression is equivalent to LDA. It is therefore not surprising that, through different algorithms for optimization, PLS and LDA give similar results. The LDA algorithm might be preferred method because it is somewhat simpler to implement.

When compared to the other discriminants evaluated, SIMCA performed rather poorly on the discrimination tasks investigated in this work. When the model with the optimal number of principal components was chosen, 16 or 17 principal components were often found to give near-optimal (or optimal) classification accuracy. At these higher limits, SIMCA becomes somewhat similar to QDA, because it is using almost the full dimensionality of the data. Both SIMCA and QDA create a separate model for each class. In situations where the covariance matrices (size, shape, and orientation of the data "cloud") of the two classes under study are very different, it is advantageous to have these separate models. However, as observed in the comparison of LDA with QDA, the data in our tasks generally consists of pairs of classes that have similar covariance matrices. There is therefore little advantage in forming two separate models.

When comparing SIMCA to the other discriminants, it is important to keep in mind the manner in which the models were formed. For LDA, QDA, and PLS, the model is created using the training data, and then unknown "test" data is then classified according to the model. The situation is similar for SIMCA when 12 principal components was chosen as an approximately optimal number and used for both classes in all the tasks. In contrast, the optimized SIMCA model was customized for each classification by performing a leave-one-out cross-validation for models that used from 6 to 18 principal components. It is therefore most appropriate to compare the optimized SIMCA to RDA, which also built many models that were tested by cross-validation, and from which the best-performing model was chosen for each classification task.

Overall, QDA and RDA both outperformed SIMCA, whether it was optimized or not. Frank and Friedman discuss some shortcomings of SIMCA that may explain its relatively poor performance.[83]

5.4.4 Effects of Normalization

5.4.4.1 Analytes at Low Fractions of Their Vapor Pressure

Because all pairs of vapors were delivered at the same fraction of their vapor pressure, to a first approximation the total response across the array should be similar for different analytes.[42] This is the case in our experiments, especially because the pairs of analytes investigated are so chemically similar. There are differences, however, with heptane giving a slightly larger total response than hexane, and 1-propanol producing a larger total response than 2-propanol. Normalization using eq 21 forces the total response across the array to be the same for every single exposure. If the response patterns of two analytes are similar but differ in magnitude, normalization will make their discrimination more difficult, and this was indeed found to be the

110

case for both analyte pairs across all the discriminants (Table 10). However, normalization is necessary when one has no auxiliary information about the concentration of the analyte and is attempting to perform a classification/identification task for members of these analyte pairs.

5.4.4.2 *Compositionally Similar Binary Analyte Mixtures*

In contrast to the situation for pure analyte discrimination described above, for the binary mixture data both normalization procedures led to an improvement in the performance of kNN, while the performance of the other discriminants was essentially unaffected by data normalization. This behavior occurs because each exposure is normalized individually, so the effects of variations in external parameters that influence all the detectors in the same way is eliminated though the normalization process. For example, if variations are present in the amount of analyte that is delivered to the array among nominally identical exposures, normalization will ideally correct all the response patterns to the same normalized pattern. Variance in detector response due to other external parameters (perhaps the temperature or the humidity of the background air) that affect the detector signals in the same direction, albeit by different relative magnitudes, will also be canceled to some extent by normalization. One large effect of this type is the drift of the detector signals over the course of the experiment. If the drift is in the same direction for all the detectors, it will be partially ameliorated by normalization. The standard deviations for individual detectors across a set of responses will decrease, but it is not clear how the classification accuracy of the discriminants will be affected.

The drift was much larger for the propanols than for the alkanes, and decreased significantly for the propanols between $P/P° = 0.01$ and 0.0025. The largest baseline resistance drifts of any of the sensors over the course of data collection was ~10%, and this appeared to have no correlation with the largest drifts in $\Delta R/R$. The largest downward drifts in $\Delta R/R_b$ (for propanols) were observed for hydrogen-bonding polymers, including polyvinylpyrrolidone, poly(4-vinylphenol), cellulose acetate, poly(4-vinylpyridine), and poly(styrene-co-maleic anhydride), whereas the one polymer in which a significant upward drift in $\Delta R/R_b$ (for propanols) was observed was 1,2-polybutadiene.

5.4.5 Extension to Other Vapor Sensor Array Data Sets

Our experiments were carried out under controlled laboratory conditions using carbon black composite chemiresistors, thus the conclusions regarding which discriminant performed optimally will not necessarily apply to other situations in which variations in detector responses can be produced by a variety of additional factors. For example, a hand-held detector array system that is utilized outdoors may encounter a variety of ambient temperatures, humidities, and background vapors. The resulting class covariance matrices may have a different form and relation to each other than those encountered in our experiments. We point out, however, that a 20-member array of polymer-carbon black detectors has little difficulty in distinguishing two analytes at significant fractions of their vapor pressure unless they are extremely similar (i.e., more similar than H_2O and D_2O). Therefore, the cases in which a choice of discriminant is important will occur only in classification of very similar vapors or at relatively low analyte concentrations. Training of such an array under the variety of conditions under which it will be expected to perform classifications of unknowns will presumably result in similar variances (and

relationships between variances on different detectors, i.e. covariances) because the analytes themselves are so similar. The LDA algorithm, which assumes identical covariance matrices for both classes, will therefore likely perform well relative to the other discriminant algorithms evaluated in this work in any high analyte concentration situation in which the discrimination ability of such an array is challenged. Polymer-coated quartz resonators of either quartz crystal microbalance (QCM, also called thickness-shear mode resonators) or surface acoustic wave (SAW) devices[58] also utilize sorption of a vapor by the polymer film to effect detection of an analyte, so the conclusions described herein may well also apply to other polymer-based sensor arrays.

5.5   *Summary and Conclusions*

In summary, an array of 20 compositionally different carbon black polymer composite chemiresistor vapor detectors was challenged under laboratory conditions to discriminate between a pair of extremely similar pure analytes (H_2O and D_2O), compositionally similar mixtures of pairs of compounds, and low concentrations of vapors of similar chemicals. H_2O and D_2O were perfectly separated from each other, and all 100 examples in a test set were correctly classified based on 100 examples in a training set. Discrimination performance decreased as the analyte concentration decreased, and for n-hexane and n-heptane, classification error rates on normalized data using a leave-one-out cross validation method exceeded 18% when the analyte concentration was less than 0.005 P/P^o. Mixtures of chemically similar analytes were also robustly discriminated (error of 1% or less) when the analyte compositions differed by more than 0.006 P/P^o (and the total analyte concentration was 0.05 P/P^o), with classification error rates using the leave-one-out cross validation method exceeding 20% only when the mole fractions of the hexane and heptane differed by less than 0.002 P/P^o in composition (and the total analyte concentration was 0.05 P/P^o). Excluding regularized discriminant analysis, which required the building and cross-validation of many models and which tended to become linear discriminant analysis under optimization, Fisher's classic linear discriminant was the best-performing method under the conditions evaluated in this work.

6. An Integrated Chemical Vapor Detector Array using Carbon Black Polymers and a Standard CMOS Process

6.1 Introduction

This paper describes the development of an array of chemical vapor detectors based on employing carbon black and non-conducting polymers.[3,96] Because the detector elements can be fabricated at room temperature and because a change in resistance is easily measured, this technology is attractive for integration with active circuitry. This array is capable of chemical discrimination that does not require external excitation or complicated signal processing like optical sensing.[57] Unlike SAW devices, we can integrate large arrays onto the same chip.[54] Applications including environmental monitoring, narcotic and explosives detection have demanding chemical sensing requirements. The goal is to create small, inexpensive, low power and even wearable chemical detector arrays that rival the detection and discrimination capabilities of mammalian olfaction.

6.2 Design And Fabrication

The detector consists of an array of individually addressable electrical contacts onto which a polymer/carbon black mixture is deposited. The detector technology is well suited to integration with on-chip circuitry. The array allows each detector to be addressed individually.

Figure 45 shows the schematic of the unit detector cell. The cell consists of a switch transistor and decoding logic. The availability of only two metals layers in the IC process required transistors at each detector cell to perform decoding. This circuitry (M1-M4) decodes X and Y selection signals generated by shift registers on the periphery of the array. This selection signal controls a switch (M7) that toggles a current (I_{in}) through the resistive sensor. In this design only one detector is energized at a time to reduce power consumption. To reduce noise and the switch resistance, transistor M7 occupies most of the detector area. The decoding circuitry also selects a transmission gate (M5,M6,M8,M9) which passes the detector voltage to a column output bus. This signal is amplified and transmitted off-chip for processing. The decoding circuitry is complicated because the detector occupies one of two available metal layers in the fabrication process we used for this chip, precluding the use of a simplified bus scheme.

Figure 46 shows the 0.5 cm X 0.25 cm chip, with 492 detectors arranged as an array of 41 X 12 sites, fabricated in a 2.0 micron process through the MOSIS design service. The dark vertical bars on the chip are deposited chemical detectors, discussed later in the text.

A close-up of the individual detector sites its shown in Figure 47. There are two contacts to the sensor: one with the drive switch M7, and another connecting the detector to signal ground. The ground terminal is laid out as a ring around the perimeter of the cell and is common to all sensors. The interior of each cell contains the drive contact for the detector. The ring structure was motivated by difficulties encountered in early detector deposition trials – the carbon black particles would aggregate along the perimeter of a deposited sensor, creating a low resistance path. Moreover, the ring structure allows us to experiment with depositing mixtures of detector
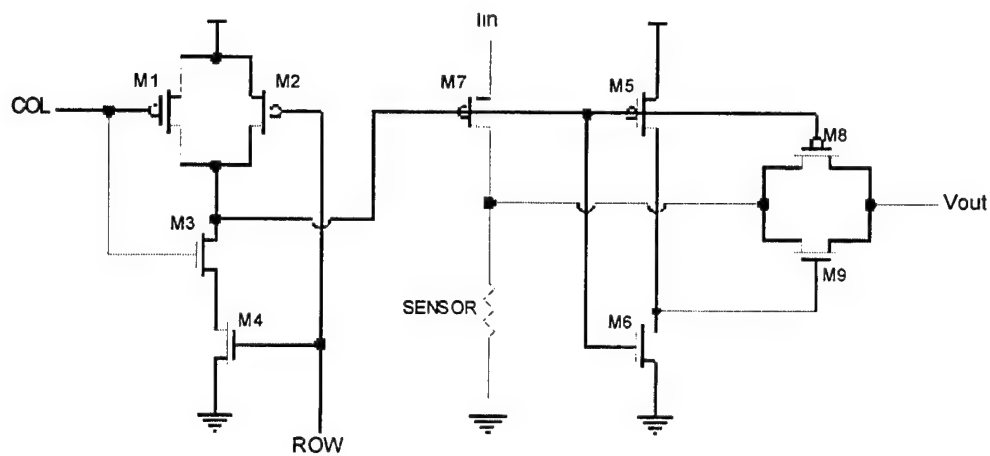
113

Figure 45. Schematic of three wire sensing cell. Transistors M1-M4 form a NAND gate to select the cell, M7 switches the current source on sensor resistor, and M5,M6,M8,M9 form a transmission gate to select the output on a column output line. The column output is buffered and passed off-chip.
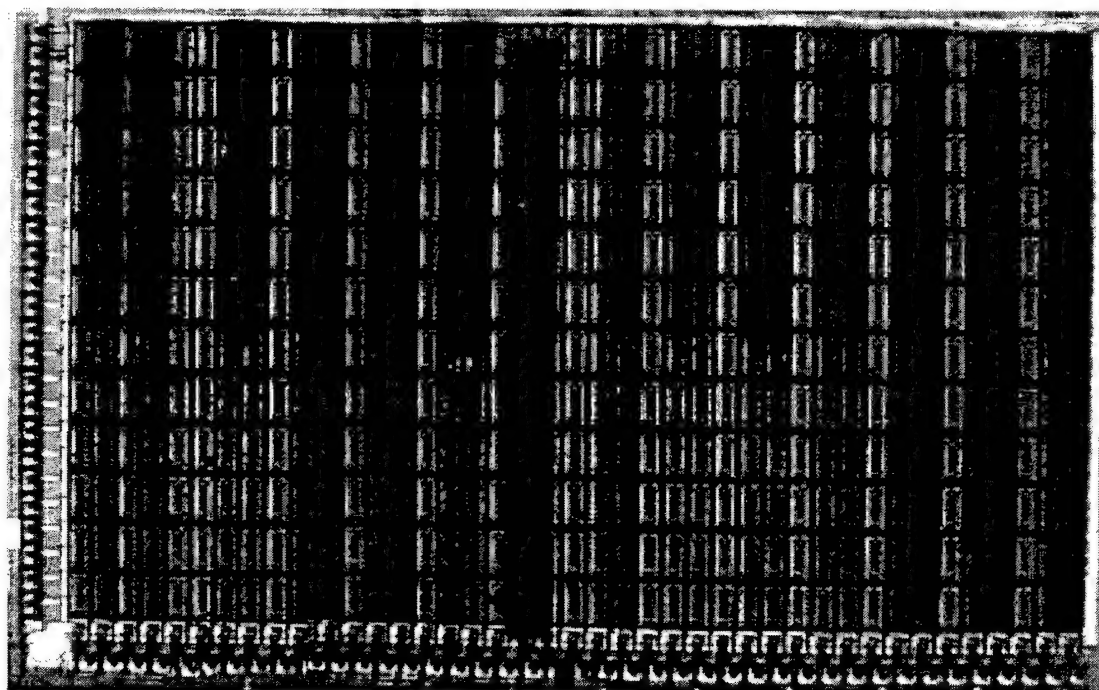
Figure 46. Photograph of the integrated vapor detector chip, after post fabrication electroless gold plating and polymer deposition by airbrush. The chip contains 492 detector sites arranged in a 41X12 array. On this test chip 209 detector sites have been covered with one of eight different polymer based chemiresistors. Shift registers located along the left and bottom of the array select an individual sensor site, whose output is amplified and passed off chip. The chip is 0.5 cm by 0.25 cm.

115

materials across the chip.[59] We deposit the sensor polymer between these two contacts, directly on top of the active circuitry. We make the sensors rectangular to increase the contact area for the interior contact, as well as to reduce contact noise and 1/f noise due to the non-uniform electrical field.[97]

We use a standard commercial foundry for the fabrication of the integrated circuits. The top layer of aluminum is used for the detector contact. Unfortunately, the native aluminum oxide that forms on the contacts prevents depositing the detectors without a post-processing step. Since dedicated wafer runs are cost prohibitive for small prototyping runs, this step must be performed on the individual chip die returned from the foundry. This precludes the use of a conventional mask based approach, since it is difficult to use a resist mask on an individual die.

To create suitable contacts we have used an electroless Ni/Au process from Stapleton Technologies (Long Beach, California)that requires no masking. This process can be performed easily on individual die with simple equipment and requires only seven procedures: four involving cleaning and surface preparation and three plating steps. The surface preparation involves an acid zincate process to remove the native oxide and activate the aluminum surface. This is followed by the three plating steps. Nickel is plated first, followed by a two stages of gold plating: a monolayer process that plates the nickel and then a build up stage that finishes the plating. Figure 47 shows three sensors, plated with 9 microns of Ni and 1 micron of Au. In addition to creating a nonreactive surface for the sensor contacts, the plating also creates wells that help constrain the sensor material during deposition.

The detectors are a combination of a particular polymer and carbon black particles. To prepare the detector material 20 mg of carbon black and 80 mg of the polymer in powder form are combined, as described above. The polymers and solvents are shown in Table 12. The mixture is placed in an ultrasonic bath for a minimum of five minutes to suspend the carbon black particles before depositing the detector films.

To deposit the detector material on the surface of the integrated circuit we employed an airbrush. A sheet of polyamide 50 microns thick is used as a physical mask to define the sensors. Apertures are cut in the polyamide using a computer-controlled laser. While other materials and processes are available to make this mask, the polyamide gaskets well to the surface of the chip. In addition, the ability to see through the polyamide allows us to position the mask accurately. We are able to create apertures as small as 50 microns using this technique, enabling us to spray individual sensor sites. We sprayed eight different polymers (Table 12) in columns two sensors (270 m) wide. Figure 48 shows a close-up of the sprayed chip, demonstrating the ability to fabricate small sensors on the chip. The spraying of the polymer allows us to create thin, uniform films of sensor material. Previously we used a direct deposition technique using a fine tip that resulted in uneven deposition and thick films.
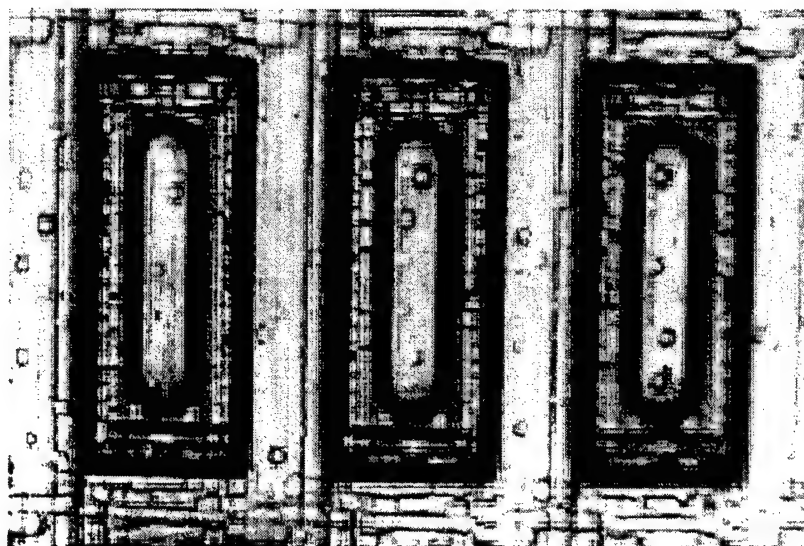
116

Figure 47. Picture of three sensor sites after the electroless gold plating. The central bars are the switched output node of each individual sensor. The surrounding conductor is a common ground. The sensor material is deposited on top of the chip, forming the sensor between the central contact and the surrounding ground
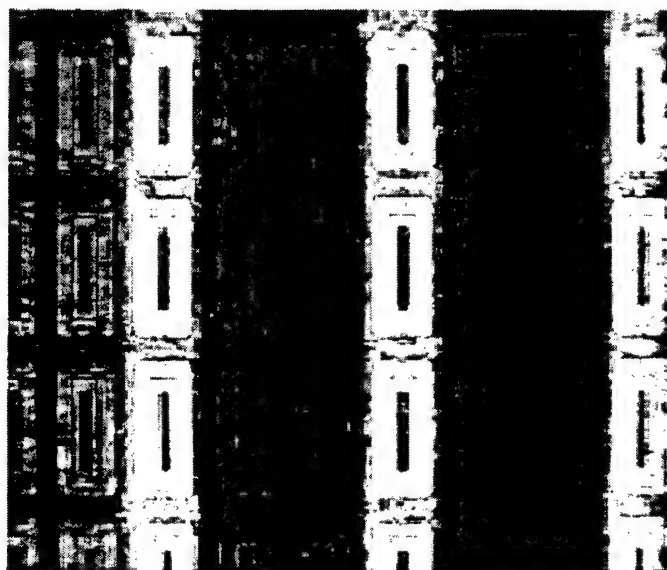
Figure 48. Deposition of sensor materials. The sensors are sprayed with an airbrush, using a laser cut polyamide mask. We sprayed the chip in columns of two sensors wide (270 m), with a row left blank to demonstrate the ability to selectively spray the sensors at this resolution

Table 12. Listing of the eight polymers and the corresponding solvents used in the fabrication of the chemiresistors.

Polymer	Solvent
PEO	Toluene
PEVA	Toluene
p-Butadiene	Toluene
p-vinyl carbazole	THF
p-vinyl acetate	Acetone
p-capraclactone	THF
p-vinyl pyrrolidone	Ethanol
p-4-vinyl phenol	THF

6.3   Testing

The current vs. voltage characteristic for an individual sensor node is shown in Figure 49. This demonstrates that we are able to successfully fabricate an individually addressable sensor pixel. The nonlinearity of the response is due to the on-chip amplifier, which is not optimized to be linear over the entire voltage range. In practice, the sensors are biased to operate at a single operating point to minimize the error due to the nonlinearity of the amplifier.

To test the sensors we use an automated flow system to generate solvent vapors at a specific vapor pressure. Mass flow controllers regulate a laboratory air supply through ceramic frits in glass bubblers filled with the desired solvent.

Figure 50 shows the temporal response of a p-vinyl acetate/carbon black detector to a series of analyte exposures at 5% of the analyte's vapor pressure. After the analyte is removed the detector returns to its nominal value. The maximum percentage change in resistance during an exposure was used as the output response.

While we have only reported data on eight different polymers in this configuration, classification is still possible robustly for certain tasks. The array of detectors produces a characteristic fingerprint for a particular analyte, shown in Figure 51 for eight unique detectors exposed to eight analytes at 5% of the analyte's vapor pressure at room temperature. One method of performing classification is using principal component analysis. Figure 52 shows the second and third principal components applied to the output responses of the 209 detectors on the chip. The response of the sensors to the eight different analytes clearly permits classification and discrimination of these test analytes.

6.4   Conclusions

We have demonstrated the successful integration of a chemical vapor detector array with a standard CMOS process. Following a simple post-processing operation we have been able to deposit the detector film material onto the surface on an integrated circuit. Deposition of different detector film materials allows formation of an array of vapor detectors that is capable of discriminating analytes. Larger arrays with a large number of different polymers, and arrays with additional active circuitry such as amplification and adaptation, will be important follow-up steps in the development of this technology.
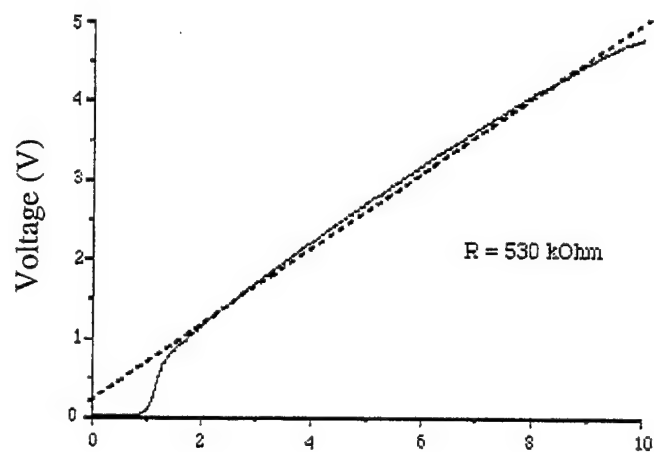
Figure 49. Voltage vs Current sweep of an individual sensor node, demonstrating its linear resistive nature. At<1 V output the column amplifier does not operate, and the deviation from linear is due to errors inn the amplifier over its operating range.
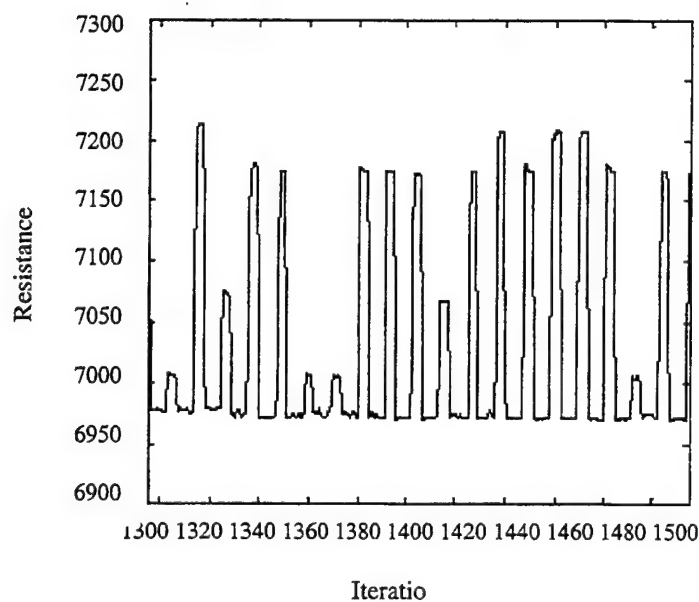
Figure 50. Temporal response of a typical polymer carbon black chemiresistor to a series of analyte exposures. This detector was composed of a p-vinyl acetate/carbon black composite, and the response shown is the change in resistance to a solvent exposure at 5% of the analyte's vapor pressure.
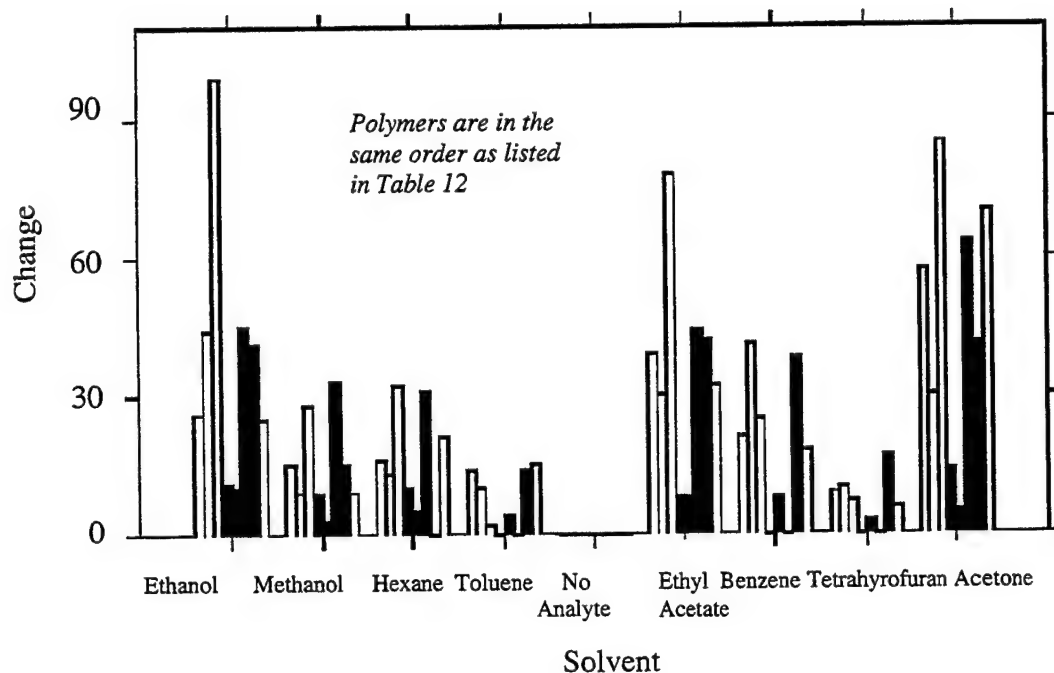
Figure 51. A characteristic fingerprint for a particular analyte for eight unique detectors exposed to eight analytes at 5% of the analyte's vapor pressure at room temperature.
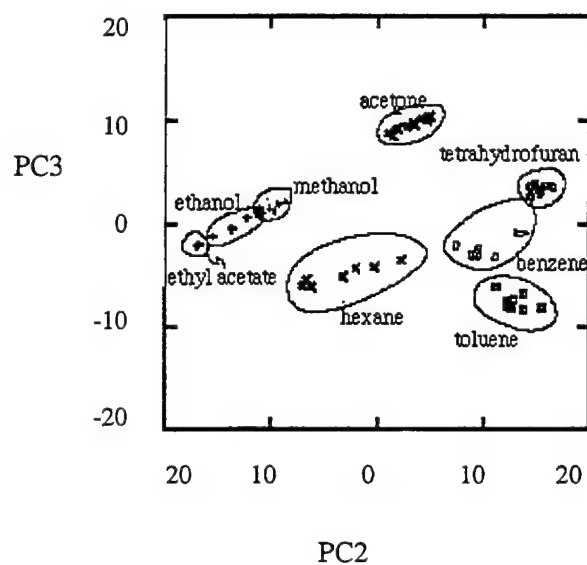
Figure 52. Principal component analysis of the chip response. The second (PC2) and third (PC3) principal components of the maximum resistance change per exposure are shown in two dimensions. Use of these two components alone allows discrimination and classification of the selected test analytes.

124

7.   Progress in Use of Carbon Black-Polymer Composite Vapor Detector Arrays for Land Mine Detection

7.1   Introduction

In this section of the project, we have focused on the performance of carbon black-polymer composite detector arrays[98-107] towards 2,4-dinitrotoluene (DNT). This compound has been reported to comprise the predominant vapor phase signature above land mines,[74] and the presence of DNT has been associated with the success of canines as well as with the success of novel vapor detection schemes for locating buried mines in the field.[108] We describe measurements of the sensitivity of a particular representative detector towards DNT as a function of exposure time, flow rate, and DNT concentration. In addition, we describe progress in developing a sampler for efficiently transporting DNT packets in air to the detector films of interest and describe the underlying engineering principles that have guided our sampler design.

7.2   Experimental

Two separate types of experiments were performed. The procedures for each set are described briefly in this section.

7.2.1 Response at Constant Flow Rate to 5 s Pulses of DNT in Air

5% of the vapor pressure of DNT at 20 °C was selected as a dilution of DNT that would deliver less than 10 ppb of the compound to the detectors. The DNT source was a tube approximately a meter in length that held about 180 g of loosely packed, granulated DNT. The air flow through the tube was 0.5 L-min^{-1}. This air flow was mixed with, and therefore diluted by a flow of 9.5 L-min^{-1} of air (from the same source) that did not flow through the DNT tube. Flows were controlled by mass flow controllers in a computer controlled system that has been described in detail previously.[49] A union-T was used to mix the background and analyte-containing gases, and a short Teflon tube was connected to the output of the union to direct the gas toward the bank of detectors. At this dilution, the upper limit of the DNT concentration is 7 ppb, because the vapor pressure of DNT at room temperature is approximately 140 ppb. If saturation of the background air through the DNT tube occurred, and if no DNT stuck to the walls of the tubing after mixing with the pure background analyte flow, this dilution would produce a concentration of 7 ppb of DNT. However, analyses performed by sorbing the analyte flow onto Tenax for a 10 minute period (to obtain enough DNT with which to perform analysis) and then analyzing the desorbed products with a GC-ECD system indicated that the actual DNT concentration exiting the tubing and available to be detected was approximately 0.2-0.4 ppb.

Eight nominally identical poly(methyloctadecylsiloxane)-carbon black composite detectors were used in this experiment. The detectors were spray-coated onto a ceramic substrate that had pairs of leads spaced 1.0 mm apart. The leads were 3.5 mm in length and 0.1 mm in width and were interdigitated such that the total width contacting a given detector film was 3.0 mm. The outputs of every pair of leads from each detector were connected to a printed circuit board that was equipped with electronics that read the resistance signals to a precision of <5 ppm every 0.5 s on

the entire bank of detectors. The detectors were placed perpendicular to the output of the DNT flow and were approximately 0.5 cm from the end of the tubing.

The experimental protocol consisted of one hour of exposure to air only, followed by ten control exposures to 5 s DNT pulses spaced every 605 s, followed by a randomized sequence of 20 exposures/nonexposures to DNT spaced every 605 s. The data were then analyzed independently without knowledge of the actual order of the randomized sequence of exposures/nonexposures.

A run was also performed to investigate whether responses would be obtained due to small changes in the flow rate of gas to the detectors. For this experiment, the existing lines were unhooked at the outlets of both mass flow controllers (the one feeding the DNT generator and the one providing diluent air). The lines were then replaced with lines and a union-T that had never been exposed to DNT or to solvents. The lengths of the flow paths with the new lines in place approximated those in the DNT dilution system. A run of four 60 s exposures, each separated by 10 min, was performed. In this run, 5% of the air during each exposure came via the mass flow controller that was normally used to feed the DNT generator. The total flow rate at all times was 10 L-min^{-1}.

7.2.2 Dependence of Detector Response on DNT Flow Rate at Constant DNT Concentration

A separate set of experiments was performed to evaluate the dependence of DNT detection on the flow rate of DNT to the detectors. For this run, a poly(methyloctadecylsiloxane)-carbon black mixture was spray-coated onto the edges of glass slides. Prior to the deposition of the sensor film, conductive coatings had been deposited onto both surfaces of the slides. Spacers were then placed between these edge-coated slides. The result was a detector with a width of ≈ 6 mm that had slits 0.13-0.25 mm in width spanning the length of the detector. This ventilated detector assembly was then cemented into one end of a section of vacuum hose. The other end of the hose was connected to a vacuum pump. A flow meter was placed in the line to monitor the flow rate through the slits in the detector. The rectangular detector face was fitted into a similarly-sized aperture in a Teflon block, the fit being loose enough that gas flow onto the detector could escape around the edges. The output tube of the gas mixer was fitted to a second teflon block that was bolted to the block holding the detector assembly, creating a small chamber with a volume of about 0.3 cm^3. The resulting distance between the gas mixture outlet and the detector was ≈ 5 mm. The resistance of the detector was measured by connecting the leads to one channel in a data acquisition board that recorded the resistance versus time data. The data were then transferred to a laptop computer.

Four trials were performed, with each trial using vapor emerging from the DNT-containing analyte tube diluted to 5% by volume with background air. In experiment 1, 10 exposures were made following a 20 min purge with air at 10 L-min^{-1}. Each DNT exposure was 10 s in length. The total flow rates into the detector chamber were varied progressively, starting at 1 L-min^{-1} for the first exposure and ending with an exposure at 10 L-min. Each exposure was followed by a purge at 10 L-min^{-1} of background air. Prior to each exposure, the flow through the vacuum line drawing gas through the detector was set to produce a flow rate that was 1 L-min^{-1} less than the

flow rate impinging onto the detector chamber. This positive differential flow rate arrangement was used to avoid drawing in ambient air through the remaining gap between the detector and the walls of the chamber.

In experiment 2, 10 exposures were made using the same ascending series of total flow rates into the chamber (i.e. 1-10 L-min^{-1}), but no vacuum was applied during any of the exposures.

In experiment 3, the same ascending series of flow rates into the chamber was used, and the same ascending series of vacuum-induced flow rates through the detector as in experiment 1 was employed, but no analyte (DNT) was present.

In experiment 4, the flow rate of DNT (at 5% of its vapor pressure at 20 °C) into the chamber as not varied, being maintained at 10 L-min^{-1} for all 10 exposures. Vacuum-induced flow rates through the detector were, however, varied in the same way as in experiments 1 and 3, beginning with no flow for the first exposure and ending with 9 L-min^{-1} during the 10th and final exposure.

7.3. Results

7.3.1 Response to 5 s Pulses of DNT Vapor at Constant Flow Rate

Figure 53 shows the resistance versus time profile computed by averaging over the bank of eight nominally identical poly(methyloctadecylsiloxane)-carbon black detectors that were placed perpendicular to the outlet of the DNT flow. The red vertical lines show the ground truth of when the DNT puffs were applied. The first ten lines represent the control set. Note that the time axis spans over 6 hours (22, 000 s). The series of "bumps" that are visible on this long time scale plot are not related to the DNT pulses, and in fact represent environmentally-induced oscillations in the baseline resistance of the detector. The DNT-induced behavior occurs on a 5 second time scale that is not discernible on this plot.

Using essentially a matched filter algorithm with adaptive background subtraction, all DNT exposures and non-exposures were correctly identified within the randomized sequence. The black circles show local maxima of the detector output that exceeded a given threshold. Based on this selection criterion, all of the DNT exposures were detected with no false alarms. In fact, a much stronger result was obtained: the separability at the detector output was sufficient for all DNT exposures (in the control set and the randomized set) to be correctly identified with zero false alarms over the entire > 6 hour duration of the experiment (Figure 54).

The highest detector output value (15.3) occurred at the 6th control sample. The resistance versus time profile for this sample is shown in detail in Figure 55a. The detector output versus time is shown in Figure 55b.

An intermediate case (roughly the median in detector output fidelity) occurred at the 4th control sample. The resistance versus time profile for this sample is shown in detail in Figure 56a. The detector output versus time is shown in Figure 56b.
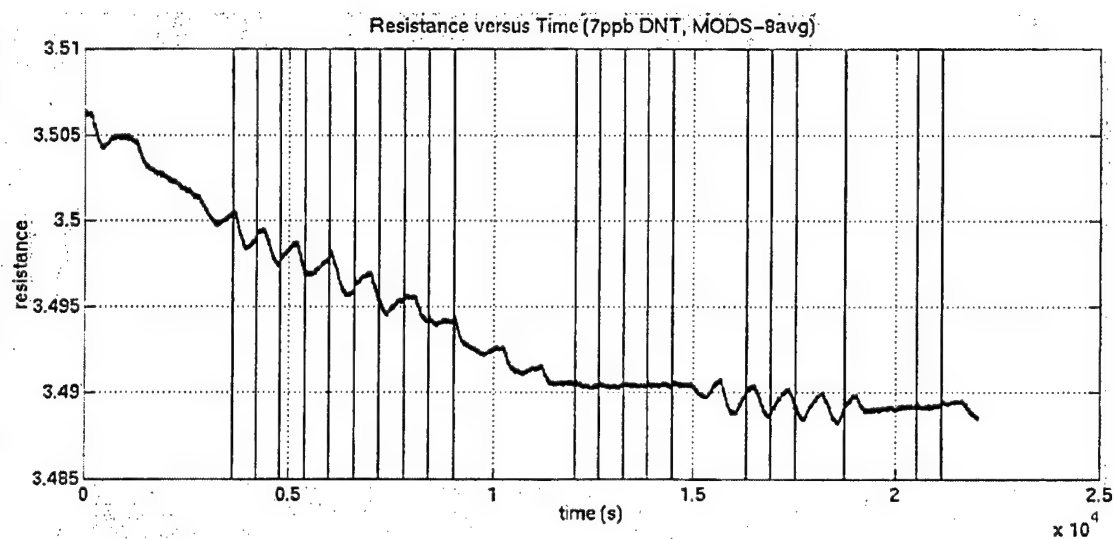
Figure 53. Resistance versus time profile computed by averaging over the bank of eight nominally identical poly(methyloctadecylsiloxane)-carbon black composite detectors. (The y-axis is in units of 10 kΩ.)
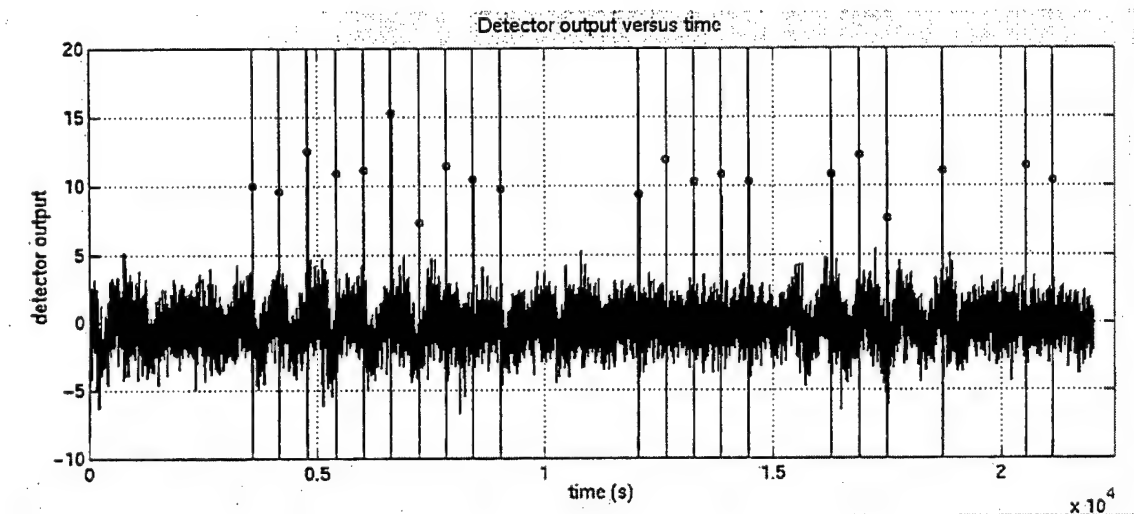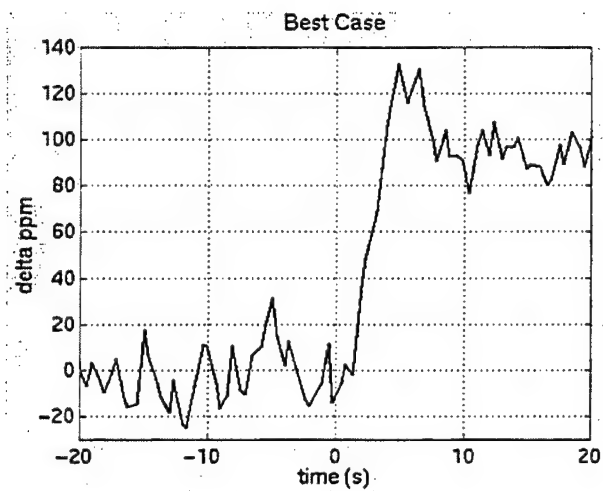
128

Figure 54. Detector output versus time over the >6 hours of the experiment. The vertical lines show the ground truth of when DNT puffs were applied. The units on the y-axis are in standard deviations of the signal relative to the local background of the detector.
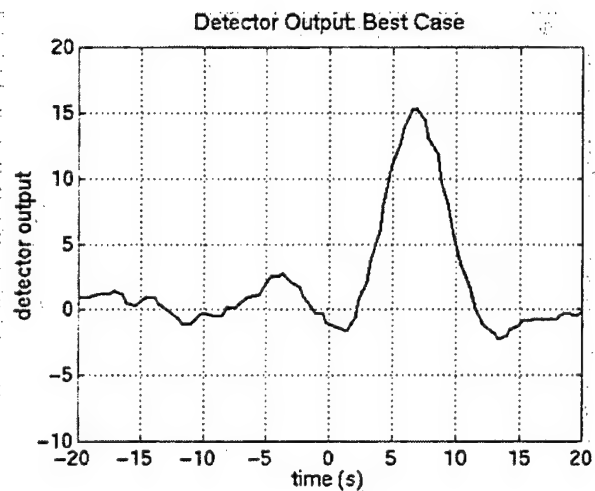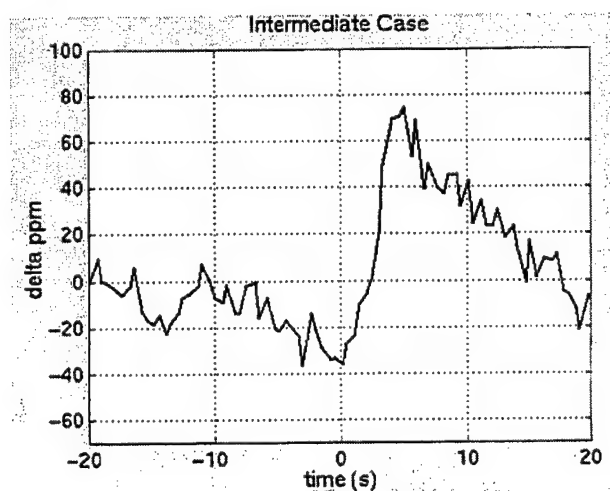
129

a)

b)

Figure 55. a) Resistance (delta ppm) behavior of the DNT exposure that produced the largest detector output value (control sample 6). **b)** Detector output value (unitless) versus time.
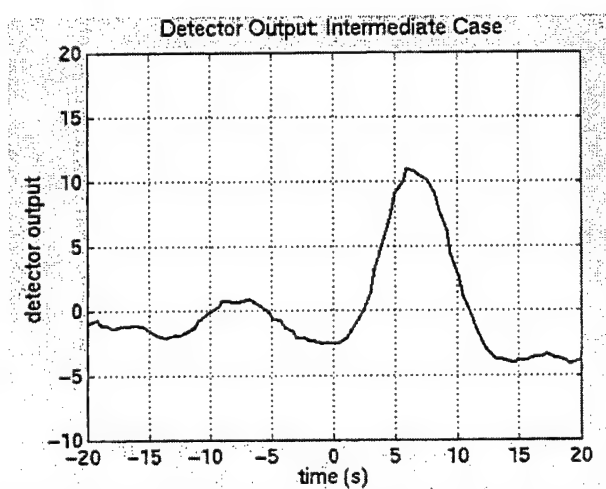
130

Figure 56. a) Resistance (delta ppm) behavior of the DNT exposure that produced an intermediate detector output value (control sample 4). **b)** Detector output value (unitless) versus time.

The lowest detector output value (7.35) occurred at the 7th control sample. The resistance versus time profile for this sample is shown in detail in Figure 57a. The detector output versus time is shown in Figure 57b.

Although all the DNT exposures were perfectly separated from the background with zero false alarms, it is interesting to look at the "close calls" or "near false alarms". In Figure 54 there are 4 places where the detector output on the background exceeds a threshold of 5 but is still well below the minimum target value of 7.35. The detailed resistance versus time profiles for these 4 "near false alarms" are shown in Figure 58a-d.

7.3.2 Dependence of Detector Response on DNT Flow Rate at Constant DNT Concentration

Because the vapor pressure of DNT is so low, the detectors are operating far from their equilibrium response values. In this situation, increasing the mass of DNT that impinges upon the detector in a given time period will produce an increase in the measured resistance response. A set of experiments was performed in order to evaluate whether there was an experimentally accessible flow rate that provided saturation of the detector, or whether improved signals could be obtained at increased flow rates up to the available limit in our laboratory system.

These experiments were performed as described in the experimental section above, with the flow rate impinging upon the detector assembly slightly exceeding the flow rate being pulled through the ventilated detector assembly. This simulated conditions of a "real world" sampling unit that would actively transport analyte vapor to the detectors. As indicated in Figure 59, pulling analyte through the detector at a rate about 1 L-min^{-1} less than the flow rate of gas into the chamber generally resulted in an increase in detector response of a factor of 2. This was particularly noticeable at higher flow rates.

When flow into the detector chamber was kept at a constant, high rate (10 L-min^{-1}), the detector response increased, apparently due to increased flow through the detector slits. These data clearly imply a critical role for sampling design in achieving rapid and high sensitivity detection of DNT and other low vapor pressure analytes (Figure 60).

7. 3.3 Sampler Design

In response to these results, AeroVironment, Inc. designed and fabricated several prototype circuit board detector concepts (Figure 61) and a detector test-fixture (Figure 62).

The detectors of Figure 61b are stacked so that their leading edges are normal to the flow, so in essence the linear gaps between detector plates of the Figure 61 design are a 1-dimensional analog of the detector hole flow path in the design of Figure 61a. Both of these have their advantages and disadvantages, but they should perform quite similarly to each other based on the results of simulations of the flow and analyte capture properties of these systems.

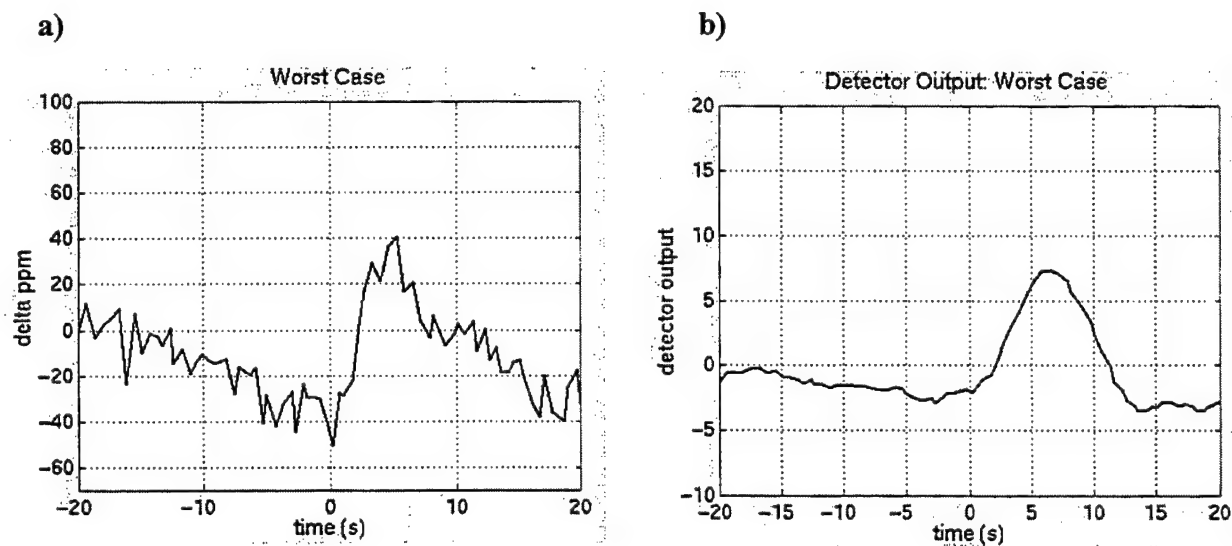The design principles of these detector heads are summarized in the remainder of this section.

Figure 57. **a)** Resistance (delta ppm) behavior of the DNT exposure that produced the smallest detector output value (control sample 7). **b)** Detector output value (unitless) versus time.
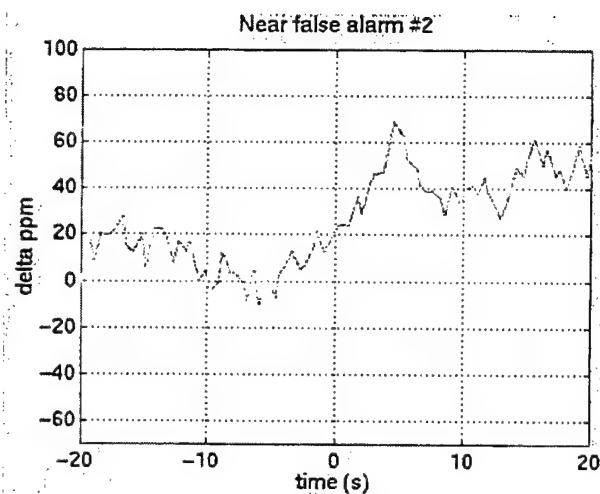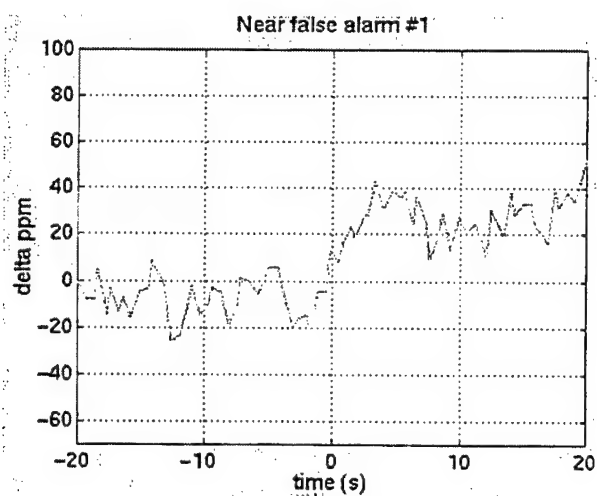
Figure 58. Resistance (delta ppm) behavior in the four background windows that slightly above 5, while the lowest value produced the largest detector output values. The maximum detector output produced over these background samples was produced for a real DNT exposure was 7.35.

134

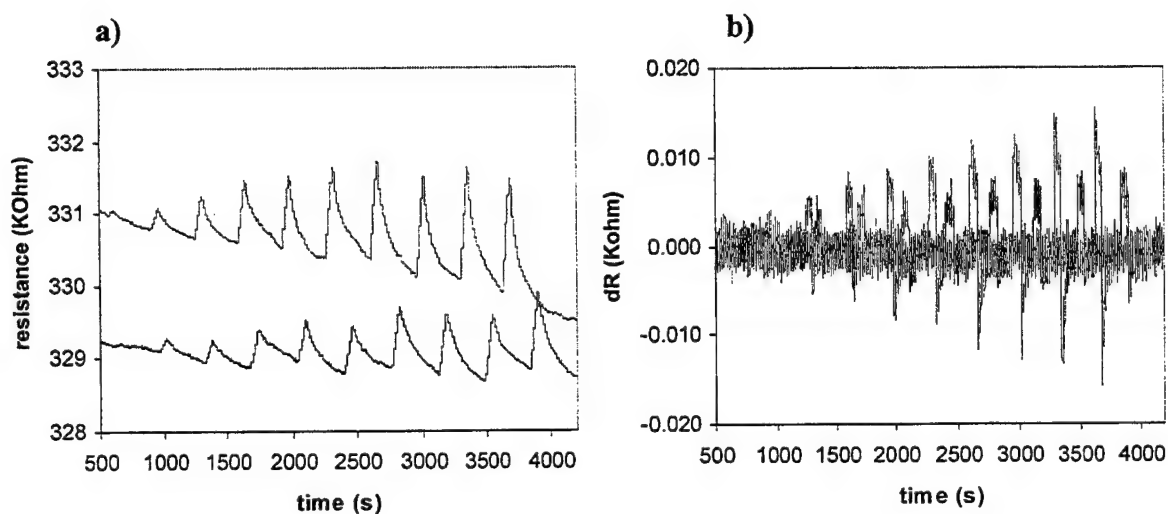**Figure 59.** Dependence of signal from a ventilated sensor on flow rate where the total flow rate through the chamber ranged from 1 to 10 L-min^{-1}. **a)** Resistance transients for 1 minute exposure to DNT at 5% of its vapor pressure (top: vacuum on; bottom: vacuum off). **b)** Change in resistance as a function of time indicating magnitude of slope during exposure.
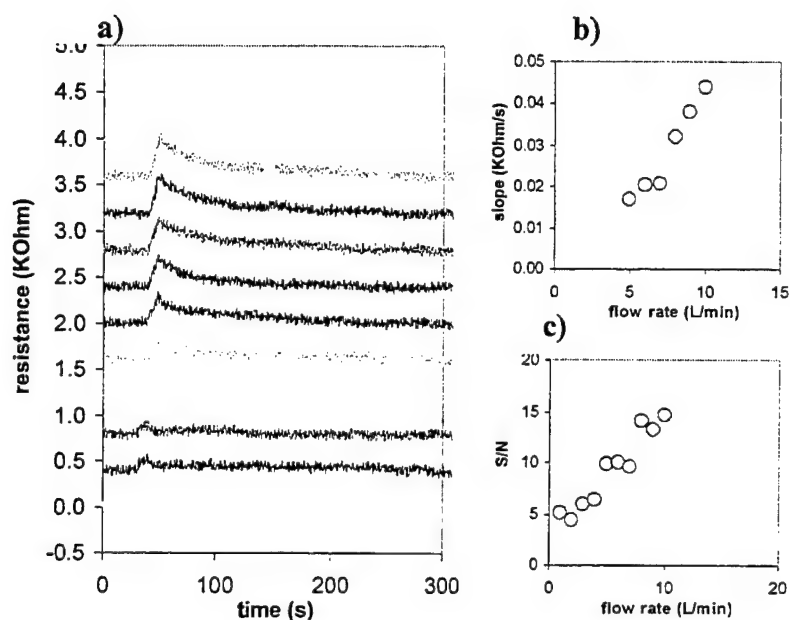
Figure 60. Ventilated sensor response characteristics for 5 s exposures to 10 L-min⁻¹ total flow rates of 5% DNT as a function of flow rate through the sensor. **a)** Response transients ranging from no flow through the sensor (second from the bottom) to 9 L-min⁻¹ through the sensor (top). **b)** Response slope as a function of flow rate through the sensor. **c)** Signal to noise after 5 s exposure as a function of flow rate.

136

Figure 61. Detector circuit boards. Left: 21-element "flow-through" detector. Right: High-low vapor pressure stacking detector.

Figure 62. Detector head test fixture for flow-through detector.

The smallest allowable detector open (through-flow) area is dictated by the specified flow rate, $\dot{V}$, and the speed of sound in air, a. Using representative numbers, the airflow *open area* must be on the order of,
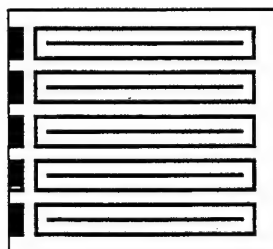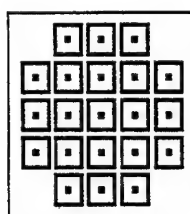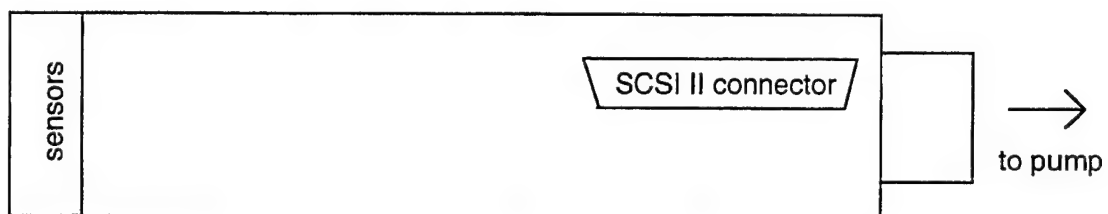
$$\ell^2 \sim \frac{\dot{V}}{aM} = \frac{10 \ cm^3 \ / \ s}{(34000 \ cm \ / \ s)(0.6)} \sim (0.2 \ mm)^2, \qquad (26)$$

where M is the Mach number, or fraction of sound speed in the holes. Note that sonic flow through the holes can usually be achieved by pulling a vacuum on the backside of the perforated plate.

Another consideration is that the optimum signal to noise requirements suggest a detector area, A_p, of,

$$A_p = \frac{\varepsilon}{f} \frac{1}{K} \frac{V_a}{t_p} \sim \frac{0.5}{0.25} \frac{1}{10^8 \, \blacklozenge \, 10^9} \frac{10 \ cm^3}{10^{-5} \ cm} \sim (1.4 \ mm)^2 \, \blacklozenge \, (0.4 \ mm)^2, \qquad (27)$$

where V_a is analyte air volume, t_p is the detector polymer thickness, ε is the collection efficiency, and f is the analyte fraction of saturation. This occurs because larger detector areas will simply produce a dilution of the available DNT into larger detector volumes, thereby producing less resistance change in such detector films. Because the signal scales linearly with the concentration of sorbed analyte, whereas the noise scales like the square root of the detector film area (for constant film thickness), this favors smaller detector areas, as indicated in eq 27.

The analysis above suggests that use of a flow-through detector configuration of roughly 2-25% open area (98%-75% solidity, with the exact value depending on the assumed partition coefficient of DNT into the polymer film) would be optimal for DNT detection.

Simulations of detectors having 1% open area suggest that the capture effectiveness of the perforated plate arrangement scales with the flow Reynolds number. However, the capture effectiveness can be bounded from below by 50% (the value used in eq 27 above) for Reynolds numbers up to 100 which, for the current exercise, is the limiting case of a detector with one or two holes and an open area of 1-2%. It is probably sufficient to have enough holes to ensure even flow into the detector.

Significant improvements over this design (up to ~90% analyte capture) can be expected when the Reynolds number is on the order of 1 (very many small holes ~ 1 μm in diameter). Micro-machining methods are required to satisfy the dimensions of Equation (2) above. However, a 10x version of the flow-through detector concept is achievable using standard circuit and flex-board processes. Having a length scale 10 times larger than optimal, these can be expected to have roughly 1/10 the signal to noise of the example above.

These designs described above take advantage of our understanding to date of how to best accomplish several key features simultaneously:

139

Significant improvements over this design (up to ~90% analyte capture) can be expected when the Reynolds number is on the order of 1 (very many small holes ~ 1 μm in diameter). Micro-machining methods are required to satisfy the dimensions of eq 27 above. However, a 10x version of the flow-through detector concept is achievable using standard circuit and flex-board processes. Having a length scale 10 times larger than optimal, these can be expected to have roughly 1/10 the signal to noise of the example above.

These designs described above take advantage of our understanding to date of how to best accomplish several key features simultaneously:

1)   they insure that the low vapor pressure material in the analyte puff being sampled encounters a minimum volume of detector film, consistent with the volume of detector needed based on the equilibrium partition coefficient data (obtained previously for these particular films) to sorb all of the DNT in this analyte plug into the detector film;

2)   they insure that the maximum quantity of analyte impinges upon and can be sorbed by the film, leaving only clean air to pass through the holes/slots when encountering a puff of DNT-containing analyte approximately 10 cm^3 in volume;

3)   the design of Figure 61b also allows sorption of high vapor pressure analytes where they will have the greatest signal/noise, along the faces of the detectors. This not only allows differential removal of high vapor pressure analyte signals but also insures that the low vapor pressure analytes are captured where their S/N ratio is the highest and the high vapor pressure analytes are captured where their S/N ratio is the highest.

These designs are based on the validated performance of simple mockups and in dye tests, in conjunction with DNT flow rate vs sensitivity tests of mock-ups in analogous designs. These designs are also supported by both analytical flow dynamics solutions and by CFD simulations. The hole diameter (or gap width in the 1-D case) is bigger than one would ultimately wish to fabricate, but these designs should provide a very good rapid prototype test bed for assessing the performance of the detector/sampling system in real-world laboratory and field environments.

The above samplers are being tested with a single polymer to verify their predicted performance. Next we will make arrays of detectors instead of a single detector film covering all of the available sensing area. The improved fluidics and sampler design will produce the most mass on the least detector area, maximizing the S/N presumably values below the ppb level. They will also allow for improved rejection of signals due to high vapor pressure analytes, which are not well-detected at the small area detectors. In addition, these systems are designed to operate optimally at flow rates that correspond to sampling 1-10 cm^3 of analyte per second, which is in accord with estimates of the volume desired to be sampled spatiotemporally above a land mine in order to perform efficient area searches by a walking deminer.

REFERENCES

(1) Taubes, G. *Discover* , **1996**, *17*, 40.

(2) Lewis, N. *Eng. & Sci.* **1996**, *59*, 3.

(3) Freund, M. S.; Lewis, N. S. *Proc.Natl.Acad. Sci, U.S.A.* **1995**, *92*, 2652.

(4) Lonergan, M. C.; Severin, E. J.; Doleman, B. J.; Beaber, S. A.; Grubbs, R. H.; Lewis, N. S. *Chem. Mater.* **1996**, *8*, 2298.

(5) Gupta, B.; Goodman, R.; Jiang, F.; Tai, Y.-C.; Tung, S.; Ho, C.-M. *IEEE Micro* **1996**, *16*, 53.

(6) Grate, J. W.; Rosepehrsson, S. L.; Venezky, D. L.; Klusty, M.; Wohltjen, H. *Anal.Chem.* **1993**, *65*, 1868.

(7) Gardner, J. W.; Shurmer, H. V.; Corcoran, P. *Sens. Actu. B* **1991**, *4*, 117.

(8) Gardner, J. W.; Bartlett, P. N. *Synt. Met.* **1993**, *57*, 3665.

(9) White, J.; Kauer, J. S.; Dickinson, T. A.; Walt, D. R. *Anal. Chem.***1996**, *68*, 2191.

(10) Shurmer, H. V.; Corcoran, P.; Gardner, J. W. *Sens. Actu. B* **1991**, *4*, 29.

(11) Pearce, T. C.; Gardner, J. W.; Friel, S.; Bartlett, P. N.; Blair, N. *Analyst* **1993**, *118*, 371.

(12) Grate, J. W.; Patrash, S. J.; Abraham, M. H. *Anal. Chem.***1995**, *67*, 2162.

(13)   Grate, J. W.; Klusty, M.; McGill, R. A.; Abraham, M. H.; Whiting, G.; Andonian-Haftvan, J. *Anal. Chem.* **1992**, *64*, 610-624.

(14) Gardner, J. W.; Bartlett, P. N. *Sens. Actuator B Chem* **1994**, *18*, 211-220.

(15) Walt, D. R.; Dickinson, T.; White, J.; Kauer, J.; Johnson, S.; Engelhardt, H.; Sutter, J.; Jurs, P. *Biosensors Bioelect.***1998**, *13*, 697.

(16) Nakamoto, T.; Fukuda, A.; Moriizumi, T. *Sens. Actuator B* **1993**, *10*, 85-90.

(17) Ballantine, D. S.; Rose, S. L.; Grate, J. W.; Wohltjen, H. *Anal. Chem.* **1986**, *58*, 3058-3066.

(18) Grate, J. W.; Abraham, M. H. *Sens. Actuator B* **1991**, *3*, 85-111.

(19) Grate, J. W.; Martin, S. J.; White, R. M. *Anal. Chem.* **1993**, *65*, A987-A996.

(20) Gardner, J. W.; Bartlett, P. N. *Sensors and Sensory Systems for an Electronic Nose*; Kluwer Academic Publishers: Dordrecht, 1992.

(21) Corcoran, P.; Shurmer, H. V.; Gardner, J. W. *Sens. Actuator B Chem* **1993**, *15*, 32-37.

(22) Butler, M. A.; Ricco, A. J.; Buss, R. *J. Electrochem. Soc.* **1990**, *137*, 1325-1326.

(23) Hughes, R. C.; Ricco, A. J.; Butler, M. A.; Pfeifer, K. B. *J. of Biochem.Biotech.* **1993**, *41*, 77-85.

(24) Slater, J. M.; Paynter, J. *Analyst* **1994**, *119*, 191-195.

(25) Slater, J. M.; Watt, E. J. *Analyst* **1991**, *116*, 1125-1130.

(26) Schweizerberberich, P. M.; Vaihinger, S.; Gopel, W. *Sens. Actuator B Chem* **1994**, *18*, 282-290.

(27) Gardner, J. W.; Shurmer, H. V.; Tan, T. T. *Sens. Actuator B Chem* **1992**, *6*, 71-75.

(28) Shurmer, H. V.; Gardner, J. W.; Chan, H. T. *Sens. Actuator* **1989**, *18*, 361-371.

(29) Charlesworth, J. M.; Riddell, S. Z.; Mathews, R. J. *J Appl Polym Sci* **1993**, *47*, 653.

(30) Nieuwenhuizen, M. S.; Harteveld, J. L. N. *Sens. Actuator A-Phys* **1994**, *44*, 219.

(31) Doleman, B. J.; Lonergan, M. C.; Severin, E. J.; Vaid, T. P.; Lewis, N. S. *Anal. Chem.* **1998**, *70*, 4177-4190.

(32) Severin, E. J. *Ph.D. Thesis*; California Institute of Technology: Pasadena, CA, 1999.

(33) Atkins, P. W. *Physical Chemistry*; W.H. Freeman and Co.: New York, NY, 1994.

(34) Hecht, H. G. *Mathematics in Chemistry: An Introduction to Modern Methods*; Prentice Hall: Englewood Cliffs, NJ, 1990.

(35) Anderson, J. E.; Adams, K. M.; Troyk, P. R. *J. of Non-Cryst.Sol.* **1991**, *131*, 587-592.

(36) Godovski, D. Y.; Koltypin, E. A.; Volkov, A. V.; Moskvina, M. A. *Analyst* **1993**, *118*, 997-999.

(37) Kirkpatrick, S. *Rev. Mod. Phys.* **1973**, *45*, 574-588.

(38) Persaud, K. C.; Travers, P. J. *Arrays of Broad Specificity Films for Sensing Volatile Chemicals*; Kress-Rogers, E., Ed.; CRC Press, Inc.: New York, NY, 1997, pp 563-592.

(39) Ralston, A. R.; Tobin, J. A.; Bajikar, S. A.; Denton, D. D. *Sens. Actuator B-Chem* **1994**, *22*, 139.

(40) Boltshauser, T.; Leme, C. A.; Baltes, H. *Sens. Actuator B-Chem* **1993**, *15*, 75.

(41) Denton, D. D.; Senturia, S. D.; Anolik, E. S.; Scheider, D. *Digest of Technical Papers, 3rd Int. Conf. on Solid-State Sensors and Actuators (Transducers '85)* **1985**, 202-205.

(42) Doleman, B. J.; Severin, E. J.; Lewis, N. S. *Proc. Natl. Acad. Sci., USA* **1998**, *95*, 5442-5447.

(43) Harsanyi, G. *Polymer Films in Sensor Applications*; Technomic Pub. Co., Inc.: Basel, Switzerland, 1995.

(44) Ast, D. G. *Phys. Rev. Lett.* **1974**, *33*, 1042-1045.

(45) Lu, C. in "Applications of Piezoelectric Quartz Crystal Microbalances", Lu, C.C., Ed., Elsevier, New York, 1984, Vol., 7, pp. 19-61.

(46) Buttry, D.A., in "Electroanalytical Chemistry; A Series of Advances:, Bard, A.J., Ed., Marcel Dekker, New York, 1991, Vol. 17, pp 1-85.

(47) Comfort, J. C.; Urban, F. K.; Barton, D. *Thin Solid Films* **1996**, *291*, 51.

(48) Urban, F. K. *App. Surf. Sci.* **1988**, *33*, 934.

(49) Severin, E. J.; Doleman, B. J.; Lewis, N. S. *Anal. Chem.*, **2000**, *72*, 658-668.

(50) Swann, M. J.; Glidle, A.; Cui, L.; Barker, J. R.; Cooper, J. M. *Chem. Commun.* **1998**, 2753-2754.

(51) Ali, M. H.; AboHashem, A. *J.Mater. Proc.Tech.* **1997**, *68*, 163.

(52) Ali, M. H.; AboHashem, A. *J.Mater. Proc.Tech.* **1997**, *68*, 168.

(53) Ali, M. H.; Abohashem, A. *Plastics Rubber and Composites Processing and Applications* **1995**, *24*, 47.

(54) Grate, J. W.; Martin, S. J.; White, R. M. *Anal. Chem.* **1993**, *65*, A940-A948.

(55) Cornila, C.; Hierlemann, A.; Lenggenhager, R.; Malcovati, P.; Baltes, H.; Noetzel, G.; Weimar, U.; Gopel, W. *Sens. Actuator B-Chem.* **1995**, *25*, 357-361.

(56) Johnson, S. R.; Sutter, J. M.; Engelhardt, H. L.; Jurs, P. C.; White, J.; Kauer, J. S.; Dickinson, T. A.; Walt, D. R. *Anal. Chem.* **1997**, *69*, 4641-4648.

(57) Dickinson, T. A.; White, J.; Kauer, J. S.; Walt, D. R. *Nature* **1996**, *382*, 697-700.

(58) Albert, K. J.; Lewis, N. S.; Schauer, C. L.; Sotzing, G. A.; Stitzel, S. E.; Vaid, T. P.; Walt, D. R. *Chem. Rev.* **2000**, *100*, 2595-2626.

(59) Doleman, B. J.; Sanner, R. D.; Severin, E. J.; Grubbs, R. H.; Lewis, N. S. *Anal. Chem.* **1998**, *70*, 2560-2564.

143

(60) Benes, E.; Groschl, M.; Burger, W.; Schmid, M. *Sens. Actuator A-Phys.* **1995,** *48,* 1-21.

(61) Grate, J. W.; Klusty, M. *Anal. Chem.* **1991,** *63,* 1719-1727.

(62) Briglin, S. M.; Burl, C. M.; Freund, M. S.; Lewis, N. S.; Matzger, A.; Ortiz, D. N.; Tokumaru, P. *Proc. SPIE-Int. Opt. Eng.* **2000,** *4038.*

(63) Wilmshurst, T. H. *Signal Recovery from Noise in Electronic Instrumentation;* Adam Hilger Ltd: Boston, 1985.

(64) Larry, J. R.; Rosenberg, R. M.; Uhler, R. O. *IEEE Trans. Comp. Hybrids, Manufact. Technol.* **1980,** *CHMT-3,* 211-225.

(65) Weissman, M. B. *Rev. Mod. Phys.* **1988,** *60,* 537-571.

(66) Dziedzic, A.; Kolek, A. *J. Phys. D-Appl. Phys.* **1998,** *31,* 2091-2097.

(67) Scofield, J. H.; Darling, D. H.; Webb, W. W. *Phys. Rev. B* **1981,** *24,* 7450-7453.

(68) Fu, S. L.; Liang, M. S.; Shiramatsu, T.; Wu, T. S. *IEEE Trans. Comp. Hybrids Manufact. Technol.* **1981,** *4,* 283-288.

(69) Deen, M. J.; Rumyantsev, S.; Orchard-Webb, J. *J. Vac. Sci. Technol. B* **1998,** *16,* 1881-1884.

(70) Peled, A.; Johanson, R. E.; Zloof, Y.; Kasap, S. O. *IEEE Trans Compon. Packag. Manuf. Technol. Part A* **1997,** *20,* 355-360.

(71) Horowitz, P.; Hill, W. *The Art of Electronics,* 2nd ed.; Cambridge University Press: New York, 1989.

(72) Patrash, S. J.; Zellers, E. T. *Anal. Chem.* **1993,** *65,* 2055-2066.

(73) Zellers, E. T.; Park, J.; Hsu, T.; Groves, W. A. *Anal. Chem.* **1998,** *70,* 4191-4201.

(74) Severin, E. J.; Lewis, N. S. *Anal. Chem.* **2000,** *72,* 2008-2015.

(75) la Grone, M.; Cumming, C.; Fisher, M.; Reust, D.; Taylor, R. *Proc. SPIE-Int. Opt. Eng.* **1999,** *3710,* 409-420.

(76) George, V.; Jenkins, T. F.; Leggett, D. C.; Cragin, J. H.; Phelan, J.; Oxley, J.; Pennington, J. *Proc. SPIE-Int. Opt. Eng.* **1999,** *3710,* 258-269.

(77) Sobel, N.; Khan, R. M.; Saltman, A.; Sullivan, E. V.; Gabrieli, J. D. E. *Nature* **1999,** *402,* 35-35.

(78) Lorber, A. *Anal. Chem.* **1986,** *58,* 1167.

(79) Carey, W. P.; Kowalski, B. R. *Anal. Chem.* **1986**, *58*, 3077.

(80) Carey, W. P.; Beebe, K. R.; Kowalski, B. R. *Anal. Chem.* **1987**, *59*, 1529.

(81) Aeberhard, S.; Coomans, D.; de Vel, O. *J. Chemometrics* **1993**, *7*, 99.

(82) Wu, W.; Mallet, Y.; Walczak, B.; Penninckx, W.; Massart, D. L.; Heuerding, S.; Erni, F. *Anal. Chim. Acta* **1996**, *329*, 257.

(83) Frank, I. E.; Friedman, J. H. *J. Chemometrics* **1989**, *3*, 463.

(84) Vaid, T. P.; Lewis, N. S., unpublished results.

(85) Fisher, R. A. *Ann. Eugneics* **1936**, *7, Part II*, 179.

(86) Duda, R. O.; Hart, P. E. *Pattern Classification and Scene Analysis*; John Wiley & Sons: New York, 1973.

(87) Friedman, J. H. *J. Am. Stat. Assoc.* **1989**, *84*, 165.

(88) Kowalski, B. R.; Bender, C. F. *Anal. Chem.* **1972**, *44*, 1405.

(89) Burns, J. A.; Whitesides, G. M. *Chem. Rev.* **1993**, *93*, 2583.

(90) Geladi, P.; Kowalski, B. R. *Anal. Chim. Acta* **1986**, *185*, 1.

(91) Wold, S. *Pattern Recognition* **1976**, *8*, 127.

(92) Wold, S.; Sjöström, M. In *Chemometrics: Theory and Application*; B. R. Kowalski, Ed.; American Chemical Society: Washington, D. C., 1977; Vol. 52; pp 243.

(93) Cover, T. M.; Hart, P. E. *IEEE Trans. on Info. Theory* **1967**, *IT-13*, 21.

(94) Livingstone, D. *Data Analysis for Chemists: Applications to QSAR and Chemical Product Design*; Oxford University Press: New York, 1995.

(95) *CRC Handbook of Chemistry and Physics*; 67th ed.; Weast, R. C., Ed.; CRC Press: Boca Raton, FL, 1986.

(96) E. J. Severin, R. D. Sanner, B. J. Doleman, and N. S. Lewis, "Differential detection of enantiomeric gaseous analytes using carbon black-chiral polymer composite, chemically sensitive resistors," *Analytical Chemistry*, vol. 70, pp. 1440-1443, 1998.

(97) H. Yoshida, "The Effect of Resistor Geometry On Current Noise," *IEEE Transactions On Components Hybrids and Manufacturing Technology*, vol. 16, pp. 344-349, 1993.

(98) Norman, R. H. *Conductive Rubbers and Plastics*; Elsevier: Amsterdam, 1970.

(99) *Carbon Black-Polymer Composites*; Sichel, E. K., Ed.; Marcel Dekker, Inc.: New York, 1982.

(100) Medalia, A. I. *Rubber Chem. Tech.* 1986, *59*, 432.

(101) Ford, C. J. In U.S. Patent 2,691,134, 1951.

(102) Newton, R. G. *J. Rubber Res.* 1946, *15*, 35.

(103) Sands, A. G.; McDowell, M. V. *Rubber Age, New York* 1956, *80*, 500.

(104) Boyd, J.; Bulgin, D. *J. Text. Inst. Proc.* 1957, *48*, 66.

(105) Lundberg, B.; Sundqvist, B. *J. Appl. Phys.* 1986, *60*, 1074.

(106) Ruschau, G. R.; Newnham, R. E.; Runt, J.; Smith, B. E. *Sens. Actuators* 1989, *20*, 269.

(107) Talik, P.; Zabkowskawaclawek, M.; Waclawek, W. *J. Mater. Sci.* 1992, *27*, 6807.

(108) Cummings, C., private communication.